The effect of torso mass in direct head impacts using a Hybrid III neck and a novel surrogate neck model

by

Lindsey Dawn Agnew

A thesis submitted in partial fulfillment of the requirements for the degree of

Master of Science

Department of Mechanical Engineering
University of Alberta

Abstract

Concussions are one of the most common injuries in sport and can result in detrimental long-term health effects. To reduce the severity of concussion and head injury, protective headgear has been implemented and is continually evaluated to minimize head kinematics after impact. For investigation of head dynamic behavior in impact and to conduct helmet certification testing, surrogate anthropomorphic test device head and neck models are used. Although there is evidence of head-neck-body coupling in impacts, most testing methods use isolated surrogate head-neck assemblies that ignore or provide no justification for the simulated torso mass on resultant head behavior in impacts. The objective of this thesis was to quantify the head kinematic and upper neck kinetic differences in head impacts using an isolated head-neck system fixed to a translating linear rail and a head-neck assembly fixed to a dummy torso. A secondary objective was to overview the repeatability of a novel surrogate neck model when fixed to a translating linear rail.

One Hybrid III neck and three copies of a novel surrogate neck (Phase III neck) were fixed to a Hybrid III headform fit with a NOCSAE certified football helmet and subjected to two sets of impacts; 1) fixed to a translating platform on a linear rail and, 2) fixed to a Hybrid III dummy torso. Direct head impacts were conducted with a pendulum impactor at 4.0 m/s to frontal, lateral, and front boss locations. The impact metrics investigated were head center of gravity linear acceleration, angular acceleration, angular velocity, and upper neck impact and peak force, and upper neck impact and peak moment.

The Phase III neck showed acceptable within-neck and between-neck repeatability based on the coefficient of variation of repeatability, coefficient of variation of reproducibility, and normalized

absolute difference values. Normalized absolute difference values of >20% between the surrogate necks and the Hybrid III neck and significantly different ANOVA results indicate the surrogate neck and the Hybrid III neck produce differing head kinematics during impact.

Significant differences were found in almost all impact metrics between the system with the head-neck assembly fixed to a translating linear rail (head-neck-rail system) and a head-neck assembly fixed to a Hybrid III dummy torso (head-neck-torso system). An independent samples, two-tailed t-test, a Welch t-test, or a Mann-Whitney U Test were used to analyze the seven impact metrics from impacts with four surrogate necks. Out of a combination of 28 impact metric comparisons, 75% (21 of 28), 71.4% (20 of 28), and 50% (14 of 28) of impact metrics were higher for the head-neck-torso system compared to the head-neck-rail system in frontal, lateral, and front boss impact locations, respectively. Linear acceleration was the only impact metric that was higher for the head-neck-torso system for all four surrogate necks in all three impact locations.

The results from this investigation suggest that torso mass influences the head center of gravity kinematics and the upper neck kinetics. However, it remains unknown which approach is the better approximation of human head dynamics from a head impact in sport, and further investigation is needed to determine which method is more appropriate for use in helmet testing to ensure the most accurate methods are used to increase player safety. Additionally, significant differences between the head kinematics and upper neck kinetics from the Hybrid III neck and the Phase III neck emphasizes the demand for the continued development and biofidelity assessment of surrogate neck models such as the Phase III neck to compare against the Hybrid III neck, to ultimately assist researchers in improving injury assessment effectiveness.

Preface

This research is an original work by Lindsey Agnew. Parts of this thesis will be submitted to be published in the Journal of Biomechanical Engineering.

Agnew, L., Dennison, C. R., Li, X., (to be submitted), "The Effect of Torso Mass in Direct Head Impacts". ASME. *J Biomech Eng.*

Agnew, L., Brice, A., Wynn, G., Dennison, C. R., Li, X., (to be submitted), "The Repeatability of a Modified Surrogate Neck Model in Direct Head Impacts Fixed to a Hybrid III Head". ASME. *J Biomech Eng.*

Acknowledgements

I would like to thank Dr. Christopher Dennison and Dr. Xinming Li for their guidance, support, and encouragement throughout my graduate program as they facilitated the culmination of my interdisciplinary education. I appreciate their help as I navigated my graduate school experience despite their own personal and professional transitions, against the backdrop of a global pandemic.

I would also like to thank Gabriella Wynn, a colleague and friend, for being a constant support. I've enjoyed every discussion we found ourselves engaged in, on topics across all subjects. I am humbled by the depth of her knowledge, and am excited to see how her current ideas and future work will benefit the academic community, and beyond.

Thank you to all current and past members of the Biomedical Instrumentation Laboratory and the Occupational Ergonomics Research Laboratory for your help throughout my degree. I'd like to give a special thank you to Aaron Brice and Ashton Martin for helping with my experiments, brainstorming ideas and troubleshooting solutions, and making two years of virtual grad school enjoyable. I appreciate their friendships and collegiality in scaffolding my development as a scientist.

It is with deep admiration that I follow in the scientific footsteps of Megan Ogle, Samantha MacGillivray, and Gabriella Wynn, in their scholarly contributions to the development of the surrogate neck. I would like to thank these three intelligent women for the foundational contributions they made to the field that paved the way for me to build upon their ideas.

Dr. Dennison, Dr. Li, and I would also like to kindly acknowledge that select instrumentation was used on-loan from Defense Research and Development Canada as part of an ongoing collaborative relationship.

Finally, thank you to my family, for making it possible for me to pursue my studies. You've always encouraged my academic interests and have supported me unconditionally throughout my entire post-secondary education, and all life endeavors. I wouldn't have accomplished this without you.

Table of Contents

List of Tables

List of Figures

List of Abbreviations and Symbols

a	Linear acceleration
α	Angular acceleration
ω	Angular velocity
ATD	Anthropomorphic test device
BIOSID	Biofidelic Side Impact Dummy
CFC	Channel frequency class
COG	Center of gravity
CTE	Chronic traumatic encephalopathy
CV_B	Coefficient of variation of reproducibility
CV_W	Coefficient of variation of repeatability
ES-2re	European Side Impact Dummy 2
F	Force
M	Moment
MEP	Modular elastomer programmers
mTBI	Mild traumatic brain injury
NAD	Normalized absolute difference
NFL	National Football League
NOCSAE	National Operating Committee on Standards for Athletic Equipment
PMHS	Post mortem human subjects
SD	Standard deviation
SI	Severity index
TBI	Traumatic brain injury
THOR	Test device for Human Occupant Restraint
WorldSID	Worldwide Harmonized Side Impact Dummy
WSTC	Wayne State Tolerance Curve

1 INTRODUCTION

This chapter introduces the prevalence, severity, and costs associated with traumatic brain injury and the impact TBI has on athletes in football. The role that surrogate torso mass plays in laboratory settings is introduced, and finally, the research objectives and thesis organization are summarized.

1.1 Motivation

In recent years, traumatic brain injury (TBI) has become a silent epidemic as it is a leading cause of disability worldwide, critically affecting public health, socio-economic condition, and human capital resources [1]. The precise global incidence of TBI is unknown, but estimations fall between 64-74 million new cases each year [2]. In 2012, TBI was the leading cause of death for people under the age of 45 in the western world [3]. In the United States alone, approximately 220,000 TBI-related hospitalizations occurred in 2019, with nearly 30% resulting in death, indicating approximately 176 TBI-related deaths per day [4]. A recent study detailed the economic costs of TBI in the United States in 2016 and reported that the estimated overall health care cost attributable to nonfatal TBI covered by a private health insurance, Medicaid, or Medicare health plan was $40.6 billion [5]. Including costs of treatment, rehabilitation, and loss of human capital, the economic impact of TBI in the United States was estimated to be $75 billion, approximately $396,000 per patient, which is nearly $560,000 in 2022 due to inflation [2]. Further, individuals who suffered a TBI experience a negative effect on quality of life. Measured from years of life

lived with disability, it is estimated that people with mild and severe TBI experienced health losses of 11.0% and 21.4%, respectively, compared to an individual in full health [6].

1.2 TBI in Football

Traumatic brain injuries are categorized as mild (mTBI), moderate, or severe, encompassing not only physical impairments, but cognitive dysfunction and behavioral disturbance as well. Concussions are considered a subset of mTBI and account for 21% of all TBIs [7]. Sports-related concussions are very common, with football being one of the most at-risk sports for head injury and concussion. A recent study tracked 658 NCAA football players over five years and recorded 528,684 head impacts, a median of 415 impacts per player per season [7]. As interest in the sport over the last two decades has increased, so has player's athletic capabilities. The development of stronger, more aggressive players has resulted in the average players' momentum increasing by 2% from the year 2000 to 2010 [8].

With increased interest in the sport and stronger players has also come increased attention to concussion. Concussion has been a focal point of conversation and research in the National Football League (NFL) for decades. In recent years, this attention has spiked, stemming from the NFL's recognition of the correlation of participation in the NFL to chronic traumatic encephalopathy (CTE), a fatal brain disease resulting from repeated head impacts and TBIs. Because of this, intervention methods have been implemented to try to minimize the severity and frequency of collisions. Some methods include rule changes to protect defenseless players (Table

1.1), increasing players' neck strength, and the requirement and evolution of protective equipment, such as helmets.

Table 1.1: A non-exhaustive list of rule changes in the National Football League (NFL) to reduce concussion in athletes [9].

Year	Category	Rule Change
1982	Defenseless player	Use of crown prohibited as primary point of contact against passer, receiver while catching, or rusher already being tackled by another player.
1995	Defenseless player: Expanded	Rule expanded to include kickoff/punt returners, and players already on the ground. Rule modified to also prohibit use of forehead as primary point of contact to defenseless player's head, neck, or face.
2009	Defenseless player: Expanded	Prohibited head impacts from defenders for all defenseless players. Prohibited impacts to kickers and punters by opponent's helmet, forearm, and shoulder.
2009-2011	Reduction of head impacts	Prohibited impacts to the head from tackler's or blocker's helmet, forearm, and shoulder.
2011	Kickoffs	Reduction of player's running head start in attempt to reduce player's speed and increase touchbacks.
2012, 2013, 2015	Defenseless player: Expanded	Defenseless players now include blocking players, long snappers on field goals and point-after attempts, and intended wide receivers.
2016	Horse collar rule	Prohibits defenders from grabbing a jersey at the name plate or above and pulling a runner toward the ground.
2017	Defenseless player: Expanded	Prohibits leaping block attempts on field goal and extra point plays; extended defenseless player protection to receiver running pass routes; reduction of game time of overtime.
2018	Defenseless player: Expanded	Rule change to make lowering head to initiate contact a foul.

For the safety of players across all levels of play, the National Operating Committee on Standards for Athletic Equipment (NOCSAE) was established in 1969 to set performance standards for American football helmets and protective equipment. Since then, helmet design, technology, and research has improved rapidly, and is constantly being updated and modified.

1.3 Surrogate Torso Mass in Laboratory Testing

To investigate sports-related head injury and evaluate the performance standards of football helmets, laboratory reconstructions and testing methods are implemented; including linear drop tests, pendulum impactors, and linear impactors (Figure 1.1).

Figure 1.1: Linear drop test (left), pendulum impactor (center), and linear impactor (right) testing methods [10–12].

Simplified head and neck systems are most often used in these laboratory settings, as seen above, and the biomechanical effects of head-neck-body coupling that result from the inclusion of a surrogate torso mass are ignored or estimated without sufficient explanation. Many researchers

have attempted to quantify these biomechanical effects in a variety of experimental setups and computational models to determine if a surrogate torso mass is necessary in laboratory testing; however, there is no consensus on the conclusion of this research. For NOCSAE helmet testing specifically, a head-neck assembly is fixed to a translating linear rail. The helmeted headform is directly impacted by a linear impactor, and pre-determined resultant head center of gravity parameters are evaluated to determine a passing helmet. In these impacts, the head-neck assembly is fixed to a linear bearing table with a mass of 15.75kg. The mass of this table, however, is not referenced to any body mass and no biomechanical rationale is known to the author or documented in the NOCSAE standards. To the author's knowledge, a paucity of research exists directly comparing the resultant head dynamics of impacts when an isolated head-neck is fixed to a translating linear rail and when a head-neck assembly is fixed to an upright surrogate torso, to determine the differences in head response.

1.4 Research Objectives

The increase of stronger, more aggressive football players continues to emphasize the need for accurate and reliable laboratory testing methods to produce sufficient protective equipment. Therefore, the main objective of this thesis is to investigate the differences of head response during direct helmeted head impacts between a head-neck system fixed to a linear rail (head-neck-rail system) and a head-neck assembly fixed to a dummy torso (head-neck-torso). The head response investigated in this work includes the head center of gravity (COG) kinematics and upper neck kinetics.

A secondary objective is to overview the repeatability and reproducibility of a novel surrogate neck model (Phase III neck) when fixed to a translating linear rail. Three copies of the Phase III surrogate neck were tested in identical experimental conditions as mentioned above. A comparison of the Phase III surrogate neck to the Hybrid III neck is summarized in this thesis and is presented in detail in a separate original work.

1.5 Thesis Organization

Chapter 2 provides background information about the importance of the neck in head injury biomechanics research and introduces current anthropomorphic test device (ATD) neck models used in impact research. Additionally, the development and subsequent modifications to a novel surrogate neck model are presented. Finally, laboratory reconstruction and helmet certification testing methods are introduced and gaps in the research are identified, giving rise to the objectives of this thesis.

Chapter 3 summarizes the design and material properties of the Phase III surrogate neck and details the experimental methods and protocol performed in this thesis. Also presented is an explanation of the data analyses used to compare head COG kinematic and upper neck kinetic impact metrics.

Chapter 4 reports the results of the repeatability and reproducibility analysis of the Phase III surrogate neck and the Phase III neck is compared to the Hybrid III neck. Next, results of the comparison of head COG impact metrics between the linear rail system and the Hybrid III torso system are detailed.

Chapter 5 provides an overview of the repeatability and reproducibility of the Phase III neck and comments on a comparison to the previous Phase II model and the Hybrid III neck. Next, the comparison of the head-neck-torso and head-neck-rail systems are presented with a discussion of the implications of the experimental results. Limitations of the current work and recommendations for future work are identified.

Chapter 6 gives a summary of the present work's motivation and main results and outlines the contributions of this thesis.

2 BACKGROUND

This chapter describes the mechanics of TBI and details the role of the neck in concussion. Current ATD neck models used in impact research are identified, and the design, development, and modifications of a novel surrogate neck are outlined. Finally, a summary of laboratory reconstruction and helmet certification testing methods are presented.

2.1 Mechanics of TBI

Traumatic brain injury is caused by a mechanical force to the head that generates a sudden displacement of the brain and disrupts neurological function. A mechanical force can be broadly defined by one of two types: focal (contact) or diffuse (inertial). Focal forces are focused over a small area of the skull, often resulting in skull fracture and a compression of the tissue underneath causing subsequent injury such as epidural bleeding. This type of force is typically associated with moderate to severe TBI. Diffuse forces, which are linked to mTBI, are typically caused by an abrupt acceleration-deceleration of the head and produce tensile, compressive, and shear forces in the brain tissue [13]. In every concussive impact, there are two acceleration components that occur based on the behavior of the head and neck during impact: linear and rotational acceleration. There is evidence from animal studies that limited brain distortion occurs in impacts that are purely linear directed through the brain's center of mass and the impact does not result in concussion [14]. More commonly and realistically, however, a blow to the head will result in a combination of linear and rotational acceleration of the head. Many studies have shown there is a positive correlation between rotational velocities and accelerations and severity of brain deformation and injury,

demonstrating that head injury is dependent on magnitude of rotational kinematics [14–19]. Therefore, these kinematics are central to the analysis of head impact biomechanics.

2.2 The Role of the Neck

Increased attention to concussion in sports has introduced a discussion surrounding the role of neck structure and musculature in head impact response. Findings have shown that cervical spine biomechanics, such as neck strength, neck strength imbalance, neck girth, and cervical spine posture affect the stabilization of the head and influence the peak head dynamics upon impact [20–24]. More specifically, greater linear accelerations, angular velocities, and angular accelerations are seen in individuals with weaker, smaller, and more compliant necks [23]. One study involving 46 subjects (female and male, ages 8-30 years) investigated impacts in the sagittal and coronal plane separately. These anatomical planes are depicted in Figure 2.1. The study reported that although impacts in both planes supported the previously mentioned relationship between neck biomechanics and head dynamic response, there was evidence that impacts resulting in coronal plane lateral flexion produced more injurious head response than impacts resulting in sagittal plane flexion and extension [23]. In athletes specifically, muscle fatigue from prolonged participation in games and practices is a common cause of reduced neck strength and is shown to decrease neck force output and increase peak head kinematics, increasing an athlete's risk of concussion [20]. Because of the critical role that the neck plays in head impact dynamics, it is necessary to consider the neck when investigating the mechanisms of concussion and head injury.

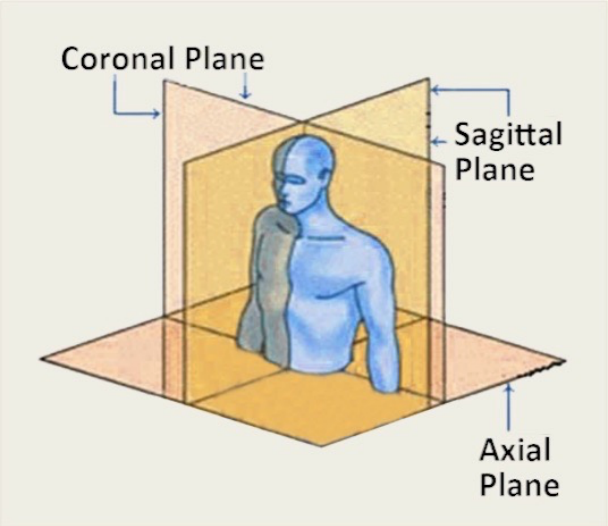

Figure 2.1: Coronal, sagittal, and axial anatomical planes [25].

2.3 Surrogate ATD Models

To demonstrate the effects of impact mechanics on a human head and test the impact performance of helmets, ATD head and neck models, also referred to as crash test dummies, are often used in research. These models can withstand greater impact forces without injury or damage to their structures compared to human volunteers [26]. A significant challenge with this approach, however, is developing ATD neck models that reliably and accurately represent human impact biomechanical responses. This challenge presents an ongoing demand for the development and refinement of human head and neck models to assist researchers in improving injury assessment effectiveness.

2.3.1 Surrogate Neck Design Requirements

Performance requirements have been developed for ATD neck models to ensure consistent and accurate responses to impact scenarios. Requirements for repeatability, reproducibility, durability, biofidelity, and sensitivity are evaluated using resultant head kinematics. Repeatability (within-neck) refers to a single ATD's ability to produce consistent results from the same impact conditions for repeated tests, assessed from peak impact metrics [27]. To be considered repeatable, an ATD must have a coefficient of variation of repeatability (CV_W) of 10% or less, measured by dividing the standard deviation (SD) by the mean response [27,28]. Reproducibility (between-neck) is the ability of an ATD to produce consistent mechanical results with copies of the same neck design from identical impact conditions. Reproducibility is determined by the coefficient of variation of reproducibility (CV_B), although the acceptable value of CV_B slightly differs. Most often, the same requirement for repeatability is used which is a CV_B of up to 10%, although some researchers deem an ATD reproducible with a CV_B value of up to 15% [29]. For an ATD to be durable, it must remain structurally intact and avoid damage after multiple impacts and results must be repeatable and biofidelic. Currently there are no standardized requirements for durability; thus, qualitative assessment is used to determine durability. A biofidelic ATD is one that simulates the biomechanical human response to an impact. Response requirements and loading corridors have been developed to determine if an ATD meets the biofidelity standards [30–32]. Finally, sensitivity is a measure of an ATD's ability to produce consistent results despite changes in extraneous conditions such as humidity or temperature and is qualitatively assessed [27,28].

2.3.2 Hybrid III Neck

In 1974, the Hybrid III neck model (Figure 2.2) was developed by General Motors under contract with the National Highway Traffic Safety Administration and became the most commonly used model in the automotive industry.

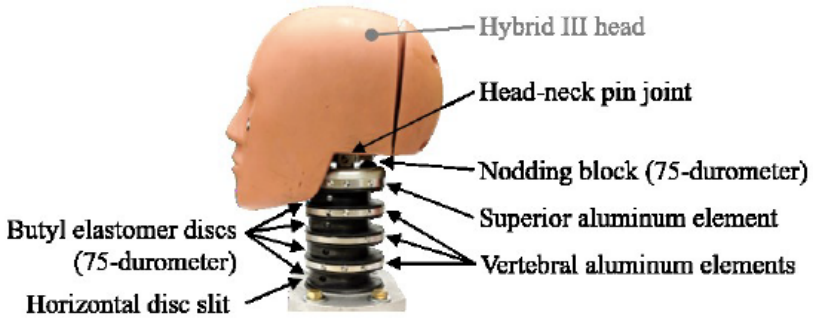

Figure 2.2: The Hybrid III head and neck with neck components emphasized. This image is included with permission from MacGillivray 2020 [33].

The Hybrid III neck was designed as an improvement from the Hybrid I, Hybrid II, and ATD 502 models, and aimed to account for general deficiencies seen in these designs, including a lack of biomechanical response [34]. Dynamic flexion and extension performance requirements for mechanical neck models were developed in 1973, and while the Hybrid III model did fall within the defined dynamic loading corridors for frontal impacts, peak flexion and extension moments were lower than the prescribed minimums [30,34]. A major limitation of the Hybrid III neck is that it was designed for indirect, frontal motion and ultimately resists motion in the lateral and front boss planes. When tested in axial compression and compared to human cadaver responses, the Hybrid III neck proved to be stiffer [35]. Despite these limitations, the Hybrid III has continued to serve as a standard for human surrogate impact testing, and although it was designed for automotive collision testing, the Hybrid III neck is increasingly used in sport injury analysis and helmet certification testing [36–47].

2.3.3 Other ATD Necks

There are several ATD models other than the Hybrid III that are used in impact research. Most commonly used are the Test device for Human Occupant Restraint (THOR), designed for frontal vehicle impacts, and models that have been developed specifically for side impact testing like the European Side Impact Dummy 2 (ES-2re), the Biofidelic Side Impact Dummy (BIOSID), and the Worldwide Harmonized Side Impact Dummy (WorldSID), all of which are representative of the 50^{th} percentile human male. These ATD models are typically used in automotive testing, as they were designed for such, so a lack of research exists on these models being used in sports and injury biomechanics research.

2.4 Development of a New Surrogate Neck

While multiple ATD neck models have demonstrated acceptable performance requirements and are currently used in impact testing, they have not been designed for use in omni-directional direct head impacts in sports. Therefore, the development of a surrogate neck for sports impact research was necessary.

2.4.1 Phase I Neck-Initial Prototype

A novel surrogate neck, referred to as the Phase I neck, was developed by Ogle in 2018 (Biomedical Instrumentation laboratory, University of Alberta) to represent the anthropometry of a 50th percentile male neck [48] (Figure 2.3).

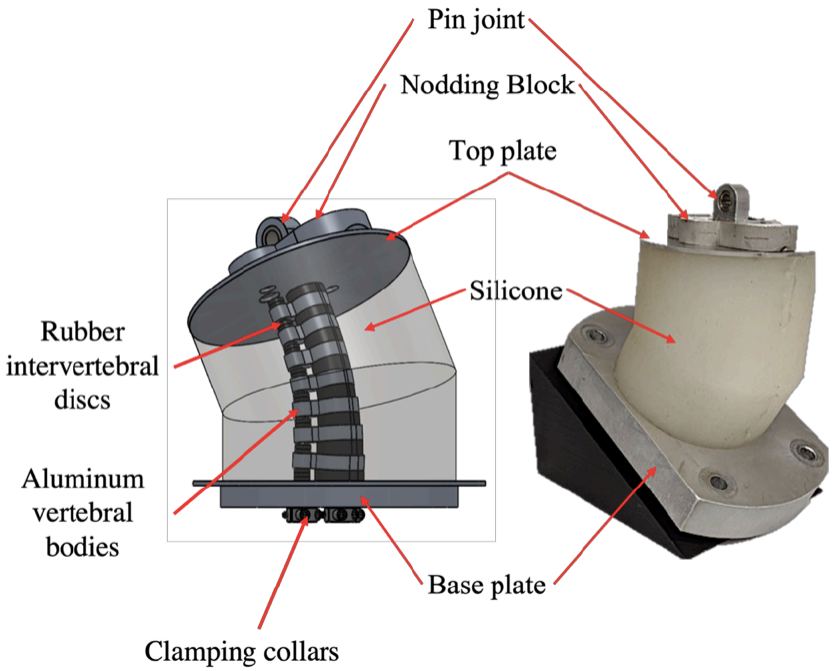

Figure 2.3: A CAD model (left) and a fully assembled prototype (right) of the Phase I surrogate neck model by Ogle, 2018 [48]. Images included with permission from Wynn, 2022 [29].

The Phase I neck consisted of three tensioned steel cables that passed through seven vertebral bodies waterjet cut from aluminum (6061-T6) and eight intervertebral discs composed of 3D printed rubber (TangoBlack – FullCure®970, 3D Printers Canada, Vaughan, ON), all encased in silicone rubber (Ecoflex® 00-30, Smooth-On Inc., Macungie, PA). The vertebral bodies and intervertebral discs were constructed from simplified dimensions of transverse process angles, vertebral body widths, vertebral body depths, and inclinations of intervertebral discs as defined by Panjabi et al [49]. The intervertebral rubber discs were designed with additional height on the

anterior side to produce lordotic curvature of the neck spinal column. The tension of the three steel cables was dictated by clamping collars at the base of the neck. A nodding joint with a similar design to the Hybrid III neck nodding joint was incorporated to attach the neck to the Hybrid III headform. The Phase I neck was tested in quasi-static bending and dynamic direct head impact and its mechanical response was compared to human cadaver data [48].

The Phase I neck is more mechanically compliant than the Hybrid III, causing hyperextension and separation of the silicone from the base plate, and resulting in significant differences in head COG kinematics and upper neck kinetics. Compliance of the Phase I neck was so extreme, however, that it could not support an ATD headform upright. Further, during impact tests, the clamping collars on the base of the neck would slip, contributing to large variance in impact measures and poor repeatability [48].

2.4.2 Phase II Neck

Modifications were made to the Phase I neck model by MacGillivray in 2020 to address its limitations [33] (Figure 2.4).

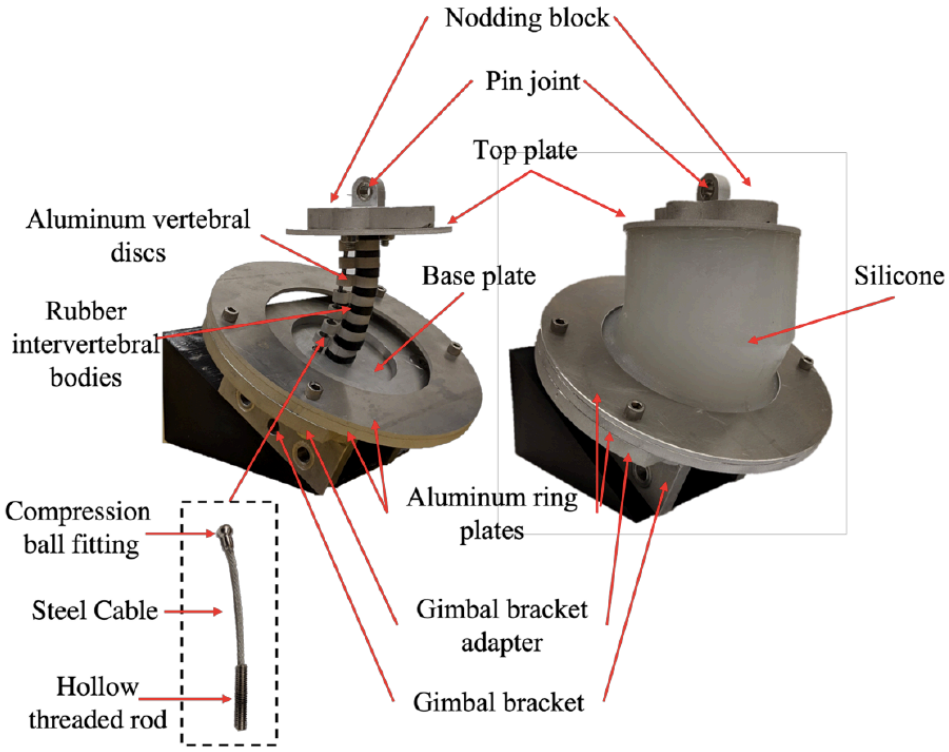

Figure 2.4: The internal structures (left) and the fully assembled prototype (right) of the Phase II surrogate neck by MacGillivray 2020 [33]. Images included with permission from Wynn, 2022 [29].

The overall dimensions of the Phase I neck were replicated in Phase II, and the design of the internal structural components remained the same aside from slight adjustments to accommodate cable design changes. To eliminate the clamping collars of the Phase I neck, the cervical cable assembly was modified to include a welded construction of steel cable (1/8 in diameter, 3450T28 Galvanized Steel Wire Rope, McMaster-Carr, Cleveland, OH), compression ball fitting (3869T63 Ball-with-Shank-End Roller Swage End Fitting, McMaster-Carr, Cleveland, OH), and hollow threaded rods (94624A121 Hollow Threaded Stud, McMaster-Carr, Cleveland, OH). In substitute of the clamping collars, locknuts were threaded onto the assembly below the baseplate to retain cable tension. Three compression springs were also added to the base of the cervical cable with aims to produce a method to tune impact mechanics. A silicone with higher shore hardness (Dragon

Skin ™ 20, Smooth-On Inc., Macungie, PA) replaced the Ecoflex ® 00-30 silicone to improve the mechanical compliance of the Phase II neck. Finally, to eliminate neck hyperextension, a silicone flange extended around the base of the neck and was clamped between two aluminum plates [33].

The Phase II neck was tested in direct head impacts attached to a helmeted Hybrid III headform and the neck's repeatability, tunability, durability, and biofidelity were assessed. The Phase II neck proved more repeatable than the Phase I neck and satisfied requirements for standardized ATD necks as described in Section 2.2.1 [33]. The Phase II neck introduced the ability to tune head mechanics for certain impact conditions. Durability of the Phase II neck exceeded the Phase I neck as seen in its consistent head mechanics and lack of structural damage after all experiments. The biofidelity of the Phase II neck was tested and compared against human volunteer head kinematic data, and preliminary data supports the biofidelity of the Phase II neck in low-speed lateral impacts by CORAplus ratings, a rating system that compares two curves for surrogate assessment in injury biomechanics research [33,50].

The Phase II neck presented minor limitations. During high-speed impacts, the silicone on the posterior side of the neck often slipped out of the aluminum clamping plates and would need to be reassembled. Additionally, separation of the silicone from the top plate occurred during impact, resulting in head mechanics that were independent of the silicone.

2.4.3 Phase II Neck-Modified

To account for the limitations of the Phase II neck, minor design changes were implemented by Wynn in 2022 [29] (Figure 2.5).

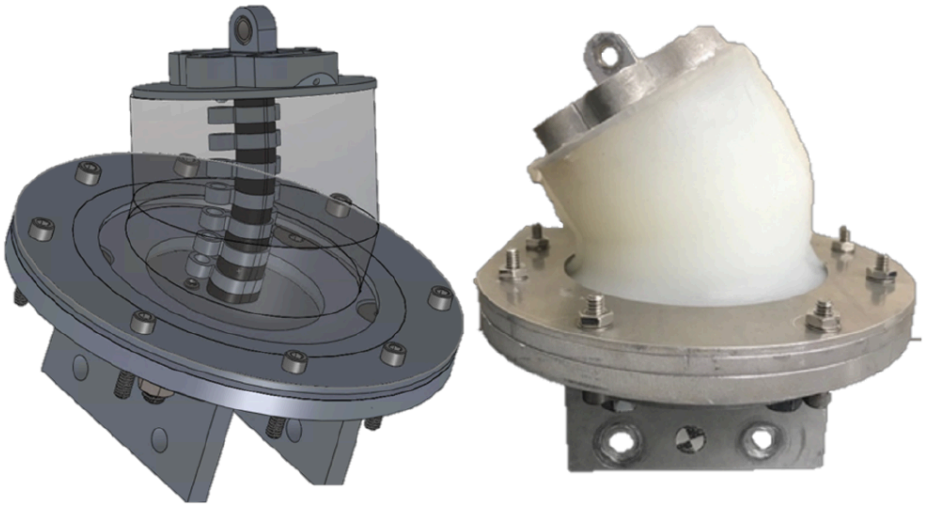

Figure 2.5: A CAD model (left) and a fully assembled prototype (right) of the modified Phase II neck by Wynn, 2022 [29]. Images included with permission from Wynn, 2022 [29].

To prevent the silicone from slipping out of the aluminum clamping plates, the anterior and posterior section of the gimbal bracket was extended into a complete circle. This allowed for additional bolts to be inserted through the base plates and increase clamping force. The top plate diameter was also decreased to eliminate interactions between the top plate and the chin of the Hybrid III head. The repeatability and reproducibility of the refined Phase II neck was assessed in direct helmeted and unhelmeted impacts. The repeatability of the Phase II neck satisfied standard requirements for physical surrogates for all impact conditions [29]. The peak head kinematics between three copies of the neck were significantly different; however, the absolute normalized differences between the three necks kinematics' fell within the range of acceptable values for head and neck certifications for all impact conditions [29]. The refined Phase II neck was also compared to the Hybrid III neck. For unhelmeted impacts, resultant head kinematics were significantly

different between the Phase II and Hybrid III necks and the normalized absolute differences for the Hybrid III neck were greater than those calculated for the Phase II necks. In helmeted impacts, resultant head kinematics were less significantly different between the Hybrid III and Phase II necks and the normalized absolute differences were relatively similar [29]. Therefore, a definitive conclusion could not be made as to if the kinematics differ between the Phase II and Hybrid III necks.

The only limitation reported for the refined Phase II neck is that upon inspection after all impacts, the nuts that compress the springs had loosened. The head kinematics did not seem to be affected by the loosened nuts over time, however, repeatability may have been negatively affected.

2.5 Helmet Testing and Laboratory Reconstruction Methods

To investigate sports-related head injury and evaluate the performance standards of football helmets, laboratory reconstructions and testing methods are implemented.

2.5.1 Head Injury Tolerances

Head injury tolerances have been defined by various methods and criteria have defined a concussion solely based on linear acceleration and impulse duration. For example, the Wayne State Tolerance Curve (WSTC) was developed to predict skull fracture in frontal impact in automotive crashes by relating linear acceleration and impulse duration to injury tolerance [51]. Additional

injury metric functions were developed from the WSTC, including the Severity Index (SI) (Eqn. 1), which defines a threshold for linear acceleration.

$$SI = \int_0^T a(t)^{2.5}\, dt \tag{1}$$

The SI equation was developed to consider the relative importance of impact duration and impact intensity, where, a(t) refers to the resultant head COG linear acceleration and T is the duration of acceleration [52]. Current helmet testing standards typically use SI in combination with peak resultant accelerations to define a passing helmet; however, the use of linear acceleration based tolerance criteria remains a point of contention among the biomedical community, as other metrics, such as rotational kinematics, may play a role in injury as described in Section 1.2.

2.5.2 NOCSAE Helmet Certification

Strict helmet certification standards have been established by the NOCSAE for impact attenuation and structural integrity of helmets with the goal of reducing the severity and frequency of head injuries in organized sports [53,54]. The NOCSAE standards are continuously being updated and modified, so the test procedures and requirements presented in this thesis are the most recent modifications as of 2020 and 2021. NOCSAE DOC ND 001-17m20, "Standard Test Method and Equipment Used in Evaluating the Performance Characteristics of Headgear/Equipment", and NOCSAE DOC ND 081-18am21 "Standard Pneumatic Ram Test Method and Equipment Used in Evaluating the Performance Characteristics of Protective Headgear and Face Guards", outline the test methods used for evaluating the performance characteristics of protective headgear [55,56].

NOCSAE DOC ND 001-17m20 describes the test procedure for the drop test method, which is used for testing helmets without face guards or face guard specific hardware [55]. This setup is shown in Figure 2.6. The drop test method provides reliable and repeatable measurements to assess protective equipment based on pass/fail criteria of resultant head kinematics.

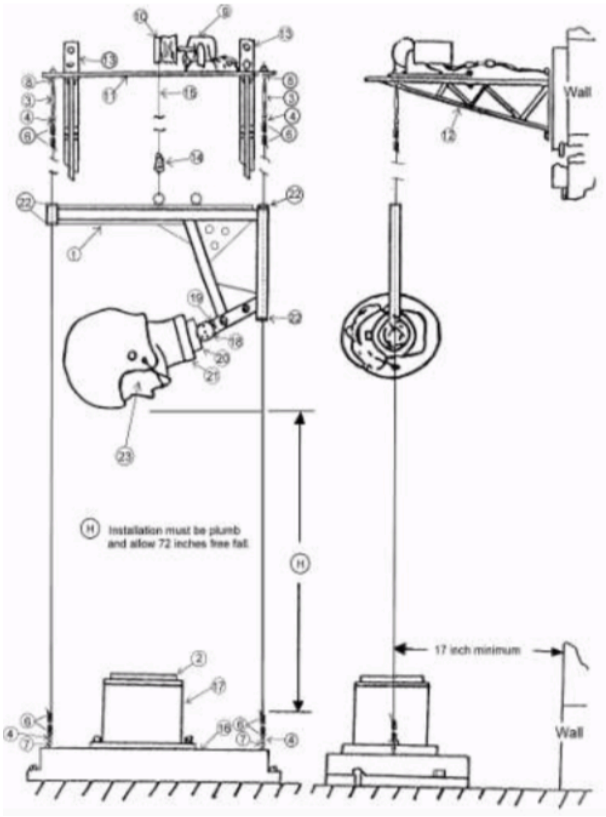

Figure 2.6: NOCSAE recommended guide and carriage assembly for the drop test method. Image from NOCSAE DOC ND 001-17m20 [55].

NOCSAE DOC (ND) 081-18am21 describes the test procedure for the pneumatic ram test method, which is used for testing helmets with face guards and face guard specific hardware [56]. The setup for this test method is shown in Figure 2.7.

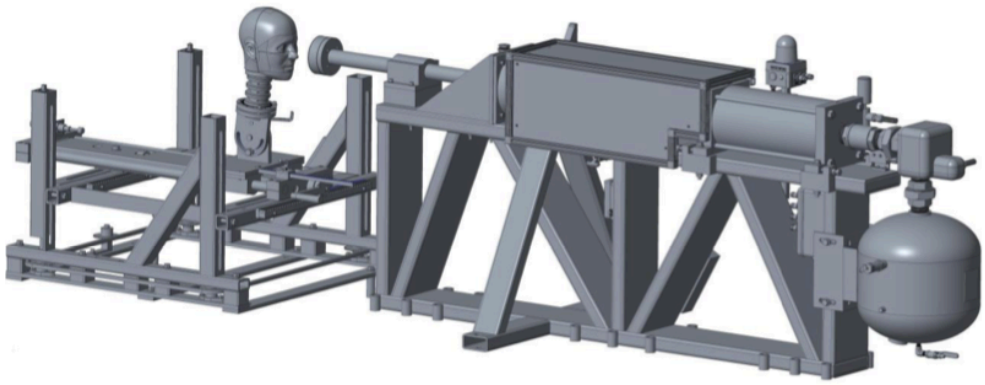

Figure 2.7: Recommended pneumatic ram and linear bearing table assembly. Image from NOCSAE DOC (ND) 081-18am21 [56].

For a single test report, at least four helmets of each model and size must be tested; two for the drop test without a face guard and two for the pneumatic ram test with a face guard. To be considered a passing helmet, rotational acceleration (rad/s^2) and severity index (SI) requirements must be met as stated in document NOCASE DOC (ND)002-17m21 [57]. These performance requirements for the pneumatic ram test for a passing helmet are 1) the head must not exceed 1200 SI, and 2) peak rotational acceleration on the medium (7 ¼ in) headform must not exceed 6,000 rad/s^2 [57]. Helmets must pass these performance requirements for both test methods to be considered a passing helmet.

2.5.3 Pneumatic Ram Test Method

The pneumatic ram test method for protective headgear with face guards works by impacting a helmeted, instrumented NOCSAE headform on a Hybrid III neck that is fixed to a linear bearing table which allows freedom of movement after impact. The required pneumatic ram impact

velocity for testing is 19.7 ft/s (6.0 m/s). Impact locations for the pneumatic ram test include front, side, front boss, rear boss, rear, top, and random. A visual of the front, side, and front boss impact locations is shown in Figure 2.8 as these are the impact locations presented in this thesis.

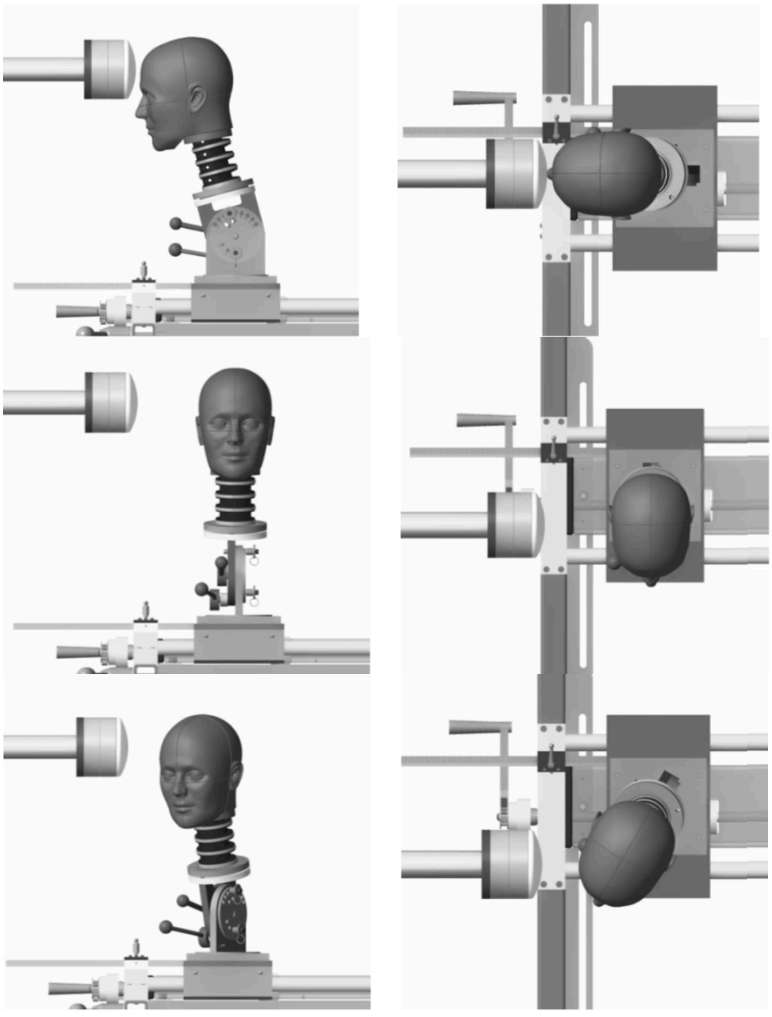

Figure 2.8: Front, side, and front boss impact locations, depicted without a helmet, for the NOCSAE pneumatic ram test [56] .

Since the establishment of the equipment performance and testing standards, there has been an increase research focus on football collision reconstructions to investigate concussion mechanics

and injury thresholds, and to improve the performance of helmets, specifically, the linear and rotational impact performance requirements.

2.5.4 Effect of Torso Mass

Laboratory reconstructions are conducted with multiple testing methods including linear drop tests, pendulum impactors, and linear impactors. In laboratory experiments investigating head and neck injury and helmet certification testing, it is common to use simplified head-neck assemblies without the attachment of an ATD torso [38,58–64] (Figure 2.9).

Figure 2.9: Examples of isolated head-neck assemblies in laboratory experiments [65–68].

In these simplified systems, the torso mass of a complete dummy is approximated or not considered, which ignores many biomechanical phenomena that would occur if the torso was included. Unrealistic constraining forces at the boundary conditions introduced by the absence of a torso mass can result in altered freedom of movement in the head, larger forces transmitted to the head through the neck, and unrealistic inertial effects of the head [69,70]. In addition to

differences in biomechanical parameters, some literature has commented on differences specifically in helmet impacts because of torso mass, such as frictional and deformation energy, that affect resultant head dynamics [71]. A recent study investigated the influence of body mass on the resultant head dynamics during dropped headform experiments and dropped dummy experiments when the head was equipped with a motorcycle helmet [69]. This study reported that head linear and angular accelerations are influenced by the dynamic effects of the body and the mechanical properties of the neck. Further, if rotational head acceleration is an indicator in head injury risk analysis, neck coupling needs to be considered. A separate study concluded that to accurately investigate concussion and brain tolerance on the basis of linear and angular accelerations in reconstructions of football collisions, the experimental impacts require a head-neck-torso system [69,72]. In these studies, the dummies are only dropped from a raised location above the ground and the position of the dummy body is parallel to the ground or at an angle with the head positioned to impact the ground first; which presents a gap in the literature for impacts with an upright dummy torso [44,69,70]. One investigation into the effect of torso mass on head dynamic response concluded that torso mass should be considered for injury reconstruction methodologies; however, the experimental setup for this investigation did not include a full dummy torso [43]. Rather, masses were added to the base of the neck and the whole head-neck-mass system was suspended without basal tethering as to not introduce a restrictive or resistive boundary condition. This setup introduces doubt of the effect of torso mass distribution as the "torso mass" in this scenario was localized at the base of the neck. Additionally, with the system suspended, the effect of ground reaction forces is ignored.

2.5.5 Computational Models

Researchers have developed computational models that represent the human body complex to investigate head injury [42,71–77]. These models have been used to investigate the influence of torso mass on a head-neck system, with differing results. MADYMO simulations were used in a study to investigate the head-neck-body coupling on the kinematics and dynamics of a helmeted head in reconstructed football impacts. The simulations in this investigation found that in lateral impacts, there is limited effect of neck coupling on linear head acceleration, but the rotational head response is greatly affected [72]. Another study used THUMS, a 50^{th} percentile male full-body model, to investigate body interactions with the head during helmeted oblique impacts in motorcycle accidents, compared to isolated head impacts. The study showed that the full-body impacts resulted in differences in peak head rotational acceleration of up to 40%, and there was a significant effect on peak linear acceleration [74]. As seen in the physical reconstructions, however, these simulations also tend to focus on head-first falling impact scenarios.

These is an absence of research investigating the direct comparison between upright direct head impacts with a complete ATD dummy and a translating linear rail, two common laboratory methods. Because of this, the current thesis presents quantitative results of the head dynamic response in direct helmeted head impacts with an upright (vertical) head and neck system compared to the head dynamic response with an upright head, neck, and torso system.

3 METHODS

This chapter summarizes the design and material properties of the surrogate neck and details the experimental methods and protocol performed in this thesis. Additionally, an explanation of the data analyses used to compare head COG impact metrics is presented.

3.1 Phase III Neck

The Hybrid III dummy torso is equipped with a metal "collar" in the center of which the Hybrid III mounts to the torso (Figure 3.1). However, the interference of the flange of the Phase II surrogate neck with that collar prevented the neck from attaching to the torso. Thus, removal of the flange was required for impact testing with the surrogate neck fixed to the head-neck-torso system.

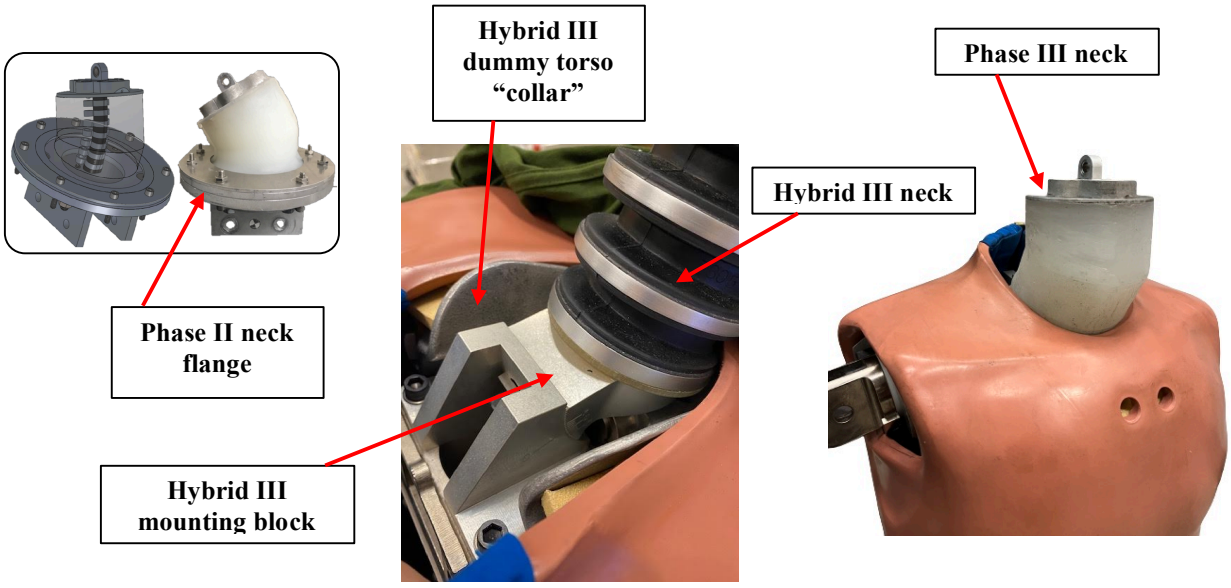

Figure 3.1: CAD model and fully assembled Phase II surrogate neck with flange (left). Posterior view of the Hybrid III neck fixed to the mounting block in the center of the metal "collar" of the Hybrid III dummy torso (center). Anterior view of the Phase III neck fixed to the mounting block on the Hybrid III torso after removal of the flange (right).

The internal structures of the Phase III surrogate neck that create the cervical spine remained unchanged from the Phase II neck, including the steel cables, intervertebral discs, and aluminum vertebrae. The Dragon Skin™ silicone also remained the same. The most substantial Phase III surrogate neck modifications include: removal of the silicone flange and subsequent aluminum clamping plates (top base ring and middle base ring), addition of an aluminum plate encased in the silicone at the base of the neck to serve as an internal mounting surface, addition of an aluminum outer clamping plate to provide a surface for the compression springs, and an increase of the neck length by 3.0 mm to account for the new internal aluminum mounting plate (Figure 3.2).

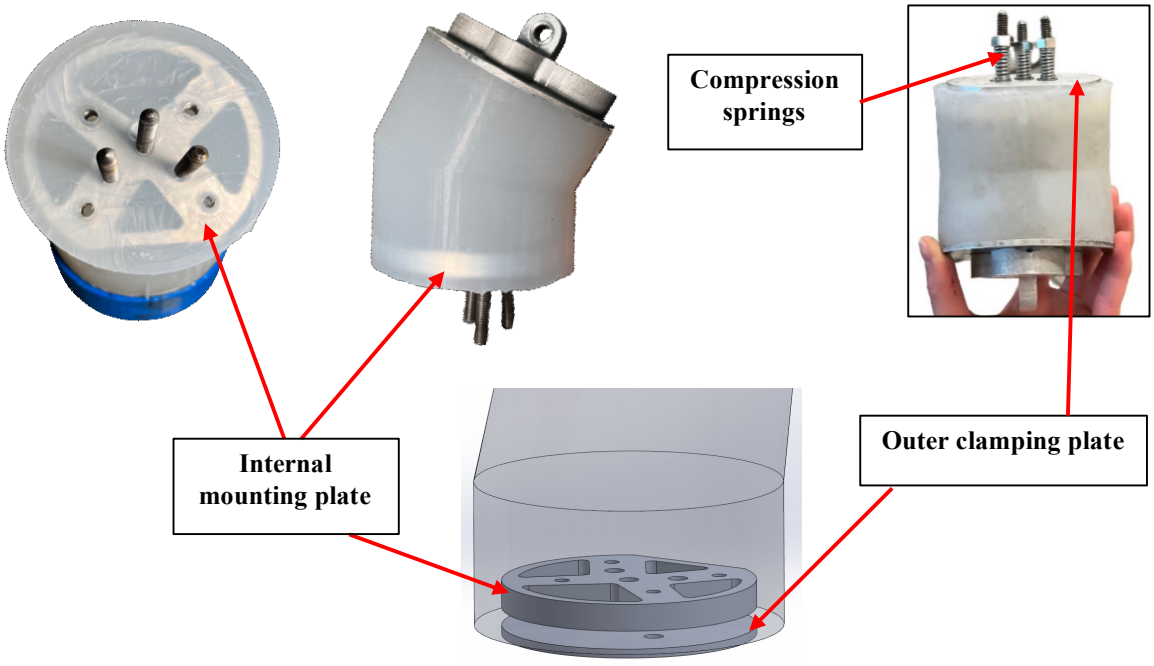

Figure 3.2: The Phase III surrogate neck, with illustration of the internal aluminum mounting plate (top left and center) and the compression springs and outer clamping plate (top right). A CAD image of the internal mounting plate and outer clamping plate (bottom).

All other modifications and additional components were implemented in direct response to the flange removal to allow for its attachment to the linear rail fixture and the Hybrid III dummy torso.

For example, the aluminum plate encased in the silicone at the base of the neck was a necessary addition to provide a surface to anchor screws for the neck to attach to the gimbal bracket adaptor for impacts on the linear rail. For the Phase III neck to attach to the Hybrid III dummy torso, two further modifications were also made. The first was a major modification to the mounting block of the Hybrid III dummy (Figure 3.3).

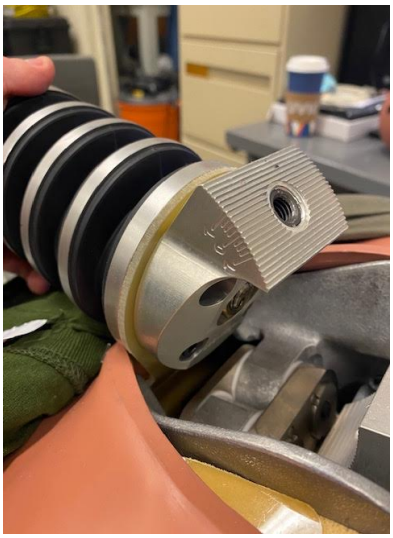

Figure 3.3: Posterior view of the Hybrid III neck fixed to the mounting block that is disassembled from the Hybrid III torso. The serrated edges allow for neck angle adjustment.

The mounting block serves as an adjustable surface for the Hybrid III neck to attach to the Hybrid III torso and has been manufactured specifically for the Hybrid III neck. Because of its complex design and time and resource constraints, the mounting block had to be modified to accommodate the Phase III neck while remaining compliant with the Hybrid III neck, rather than manufacturing a separate mounting block for the Phase III neck. The five existing holes of the mounting block had to be widened for the bolts, nuts, and the three center cables of the Phase III neck so that the outer clamping plate at the base of the Phase III neck could sit flush with the surface of the mounting block (Figure 3.4).

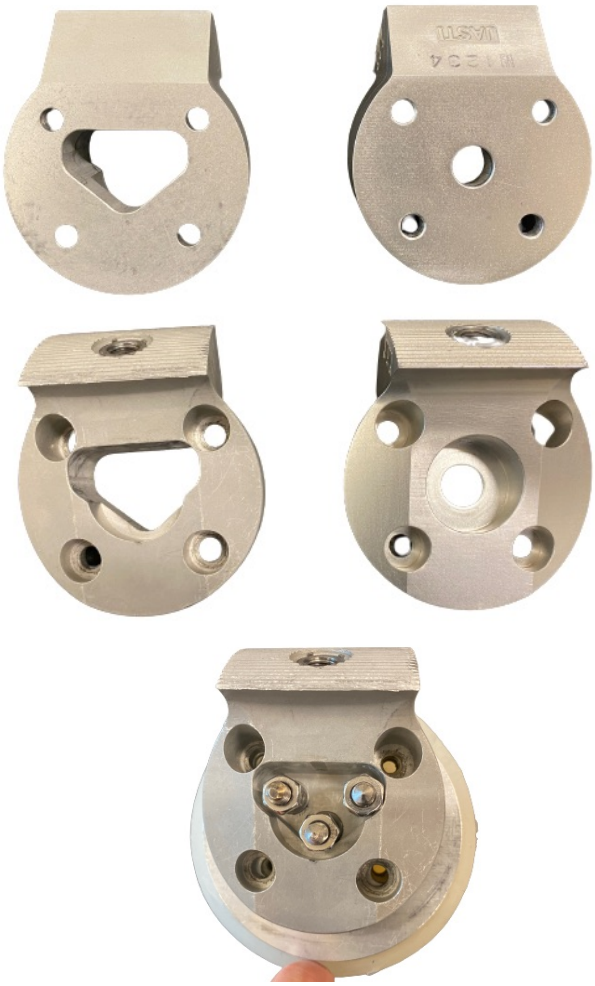

Figure 3.4: Modifications made to the mounting block for attachment of the Phase III surrogate neck to the Hybrid III torso (superior view: top left; inferior view: middle left), and the original mounting block design (superior view: top right; inferior view: middle right). The bottom center image shows the inferior view of the mounting block fixed to the Phase III neck.

3.2 Experimental Equipment

A custom pendulum impactor (Figure 3.5) constructed in the Biomedical Instrumentation Laboratory at the University of Alberta swings frictionless to directly impact a helmeted 50th percentile male Hybrid III headform fixed to one of the surrogate necks and the Hybrid III neck.

The pendulum's impacting arm was constructed of steel with a Modular Elastomer Programmers (MEP) pad as the impacting surface, compliant with helmet testing standards [54–57].

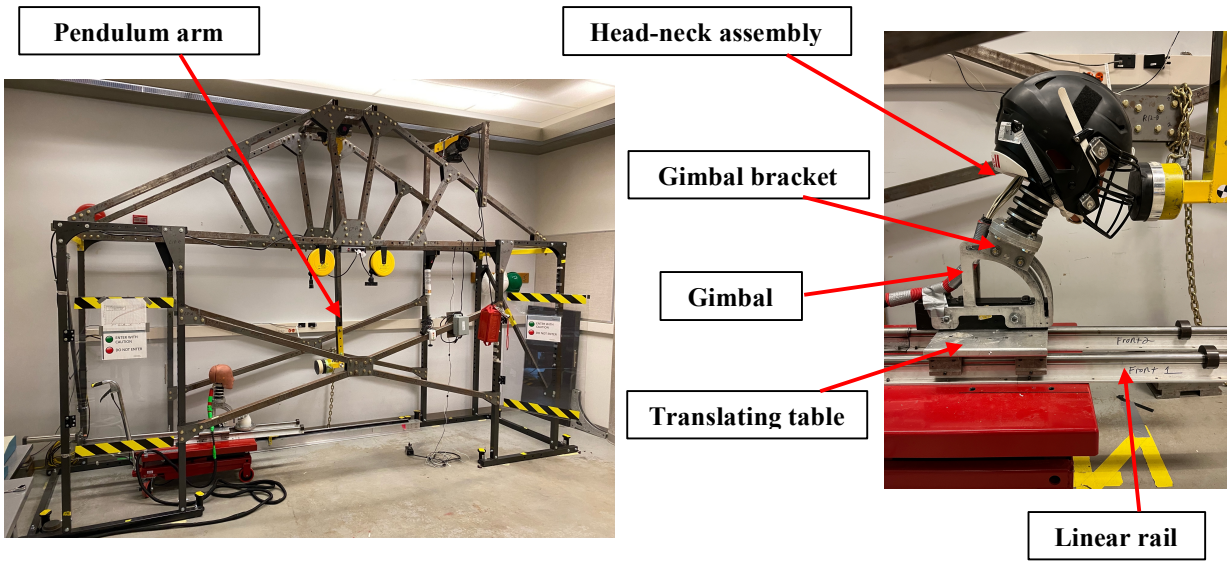

Figure 3.5: Custom pendulum impactor system (left). A helmeted Hybrid III head and neck fixed to the head-neck-rail system with major components illustrated (right).

In the first set of experiments, the head-neck assembly was mounted using a gimbal to a translating linear rail, shown in Figure 3.6. The head-neck assembly was free to translate across the rail after impact to reflect realistic impact movement and to prevent damage to the Hybrid III headform. The gimbal attachment was designed such that it could be positioned to achieve fontal, lateral, and front boss impact locations on the helmet. The mass of the translating platform, gimbal, and associated parts had a mass of 8.15kg, excluding the mass of the Hybrid III headform and a surrogate neck. In the second set of experiments, the head-neck assembly was mounted to a Hybrid III dummy torso and pelvis assembly. The Hybrid III pelvis was involved in the assembly so that the dummy could sit upright without assistance for impacts, and because of laboratory equipment and personnel restrictions that prohibited the pelvis from being removed. The mass of the Hybrid

III torso was 17.19kg and the mass of the pelvis was 23.04kg, a combined mass of 40.23kg [78]. The Hybrid III dummy torso was manually positioned after each impact with guidance from two laser levels to confirm impact location. The Hybrid III headform was fit with an NOCSAE certified Riddell helmet and the chin straps tightened to secure position. The pendulum arm was electromechanically raised and released from a predetermined height, confirmed using a laser level, and released to achieve desired impact speeds.

Figure 3.6: Location of frontal impacts to a surrogate neck fixed to head-neck-rail system (left), and location of frontal impacts to a surrogate neck fixed to head-neck-torso system (right).

Attached to the inner surface of the 50th percentile male Hybrid III headform (mass ≈ 4.54 kg) was a nine uniaxial accelerometer array (Measurement Specialties Inc. Hampton VA, model 64C-2000-360) positioned in a 3-2-2-2 configuration. Located at the head center of gravity (COG) were three accelerometers, while two accelerometers were mounted to the crown, front, and left side of the head. To measure upper neck forces and moments, a six-axis load cell (mg sensor GmbH, Iffexheim Germany, model N6ALB11A) was positioned at the base of the Hybrid III headform (Figure 3.7).

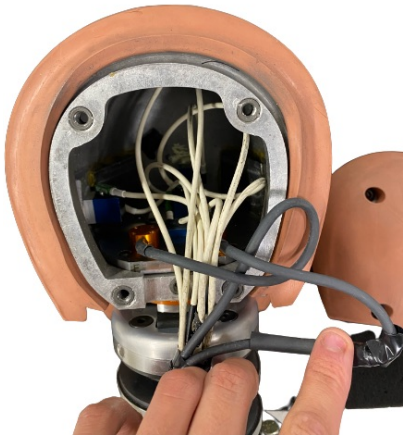

Figure 3.7: Posterior view of the inside of the Hybrid III head equipped with accelerometers and load cell.

Data from the sensors was collected at a sampling frequency of 100 kHz using a data acquisition system hardware (PX1 6251, National Instruments, Austin TX) and LabVIEW software (LabVIEW v8.5, National Instruments, Austin TX). Signals were filtered with an analog anti-aliasing hardware filter with a cutoff frequency of 4 kHz in compliance with SAE standard J211-1 [79]. Further, a 4^{th} order low-pass Butterworth filter was applied during post-processing in MATLAB R2019a (MathWorks Inc., MA United States) with a cutoff frequency of 1650 Hz for head COG linear and angular accelerations and neck forces as per Channel Frequency Class (CFC) 1000, and a cutoff frequency of 1000 Hz for neck moments as per CFC 600. Head COG linear accelerations were directly measured from the accelerometers, angular accelerations were calculated using equations by Padgaonkar, and angular velocity values were found through integration of angular accelerations [80]. The positive coordinate systems specified by SAE Standard, J211-1 for head COG accelerations and upper neck kinetics are shown in Figure 3.8.

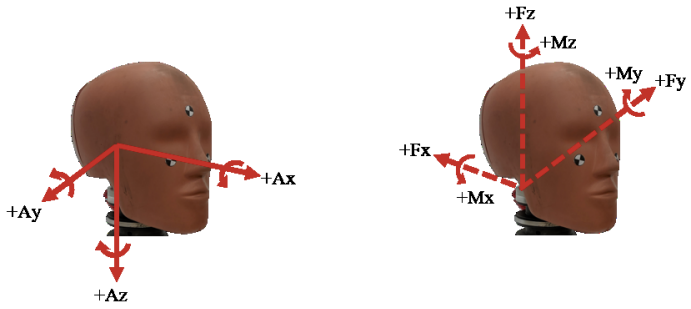

(a) (b)

Figure 3.8: Positive Hybrid III headform coordinate systems for (a) head COG accelerations and (b) upper neck kinetics. This image is included with permission from MacGillivray 2020 [33].

A high-speed camera (Phantom v611, Vision Research Inc., Wayne NJ) equipped with a Carl Zeiss (Jena, Germany) 50 mm f/1.4 macro lens was placed level with the Hybrid III head-neck assembly to capture video of the impact scenario for post-hoc confirmation of impact speed and general observation. Sufficient exposure of the impact event was provided by lights positioned behind the camera as it recorded at a sample rate of 3000 frames per second, with a 1280x800 resolution and 330 µs exposure time. The high-speed camera was calibrated by placing a ruler on the pendulum in the frame of the impact event and measuring a known distance. The camera was never moved during a set of impacts. Phantom CineViewer Software (v3.4, Vision Research, Wayne NJ) was used to confirm pendulum impact speed by manually selecting the center point on a high-contrast marker on the pendulum arm 10 frames before impact with the helmet and then selecting the same point in the frame during which the impact occurs. The speed between those two selected points is calculated in CineViewer by dividing the distance between the two points by the difference in time between the two points.

3.3 Experimental Protocol

The 50th percentile male Hybrid III headform was attached to three Phase III surrogate necks and one Hybrid III neck in repeat impact trials in two phases of experimental impacts:

Phase (1): Hybrid III headform attached to the three Phase III surrogate necks and Hybrid III neck; head-neck system fixed to gimbal translating on linear rail;

Phase (2): Hybrid III headform attached to the three Phase III surrogate necks and Hybrid III neck; head-neck system fixed to Hybrid III dummy torso and pelvis.

3.3.1 Experimental Setup

In both phases, the pendulum arm was raised to a predetermined height to achieve an impact speed of 4.0 m/s at three impact locations: (1) frontal impacts to the center forehead above facemask (n=20/neck), (2) lateral impacts above the ear (n=20/neck), and (3) front boss impacts near the temple (n=20/neck) (Figure 3.9). The frontal, lateral, and front boss impact locations were chosen because they have been determined to be the most common impact locations in real football collisions [39,81,82]. The impact speed of 4 m/s and pendulum effective mass of 15.42 kg were chosen because they reflect common impact energies commonly seen in football collisions and used in football reconstruction experiments [81,83]. Ranges of impact metrics found in the literature are reported in Table 3.1. The ranges of impact metrics from the experiments in this thesis are 26.4-60.1g for linear acceleration, 2149.9-4829.1 rad/s^2 for angular acceleration, 13.7-26.9 rad/s for angular velocity, 206.6-2354.2 N for force, and 2.1-59.4 Nm for moment. Therefore, the data presented in this thesis falls in the acceptable range of kinematics and kinetics for real-life head impacts in football.

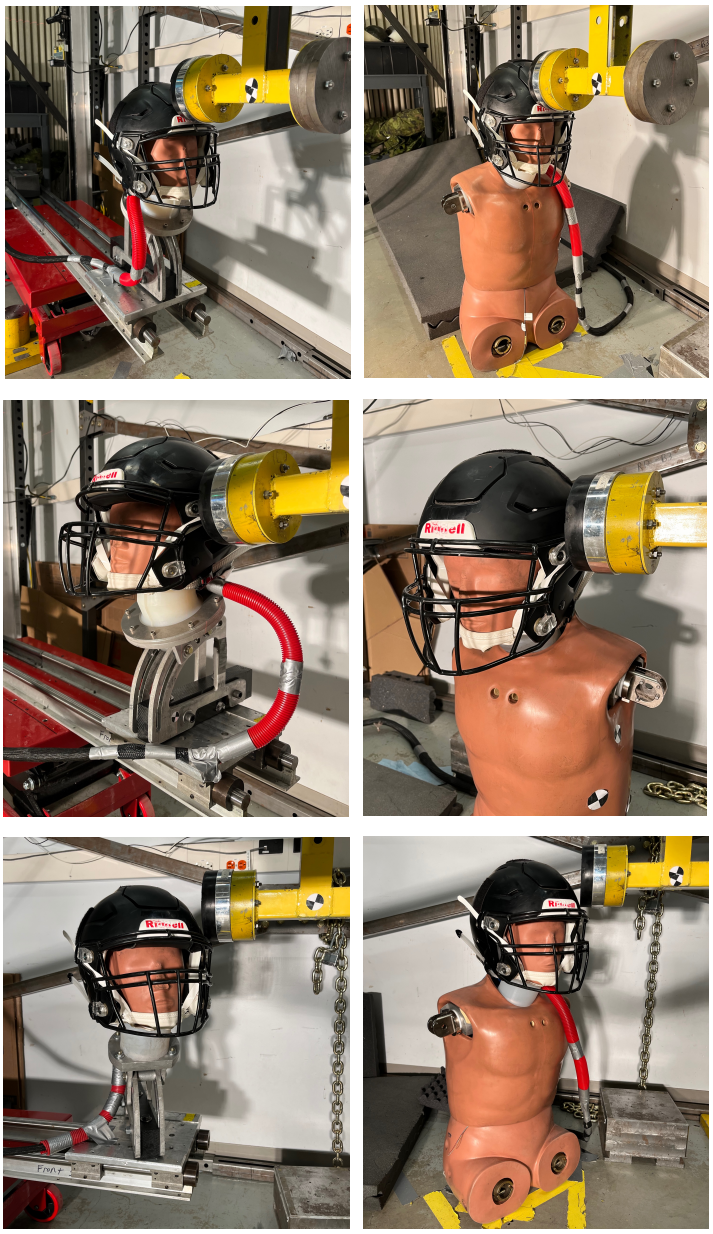

Figure 3.9: Frontal, lateral, and front boss impact locations with the head-neck-rail system (left) and the head-neck-torso system (right).

Table 3.1: Various research studies that have reported kinematic and kinetic impact metric values from real-life football impacts [81,83–93].

Study	Methods	Impact Metric	Percentile	Range	Impact Type
McIntosh et al. (2014)	Unhelmeted players	Linear Acceleration	50	65.1g	
			75	88.5g	
		Angular Acceleration	50	3958 rad/s^2	
			75	6633 rad/s^2	
			50	1747 rad/s^2	Coronal plane
			75	2296 rad/s^2	Coronal plane
		Angular Velocity	50	22.2 rad/s	
			75	27.5 rad/s	
			50	10.8 rad/s	Coronal plane
			75	15.9 rad/s	Coronal plane
		Linear Acceleration	Average	32g	Sub-concussive
Duma et al. (2005)	In-helmet 6-accelerometer system	Angular Acceleration	Average	905 rad/s^2	Sub-concussive, Coronal plane
				2020 rad/s^2	Sub-concussive, Sagittal plane
				5600 rad/s^2	Concussive, Coronal plane
				5590 rad/ s^2	Concussive, Sagittal plane
Brooks et al. (2021)	Helmet GForce Tracker	Linear Acceleration	50	13.9g	
			Average	18.5 – 26.8g	
		Angular Acceleration	50	740.2 rad/s^2	
			Average	1320 – 2340 rad/s^2	
		Angular Velocity	50	12.5 rad/s	
			Average	12.1 – 21.7 rad/s	

Fukuda et al. (2017)	Vector Mouthguard	Linear Acceleration	50	16.77g	In game
			95	43.18g	In game
			50	15.87g	In practice
			95	37.68g	In practice
		Angular Acceleration	50	1369 rad/s^2	In game
			95	1070 rad/s^2	In practice
Rowson et al. (2009)	In helmet accelerometers	Linear Acceleration	Average	22.3g	
			50	17.5g	
		Angular Acceleration	Average	1355 rad/s^2	
			50	1017 rad/s^2	
Rowson et al. (2012)	Head Impact Telemetry	Angular Acceleration	50	872 rad/s^2	Sub-concussive
			75	1447 rad/s^2	Sub-concussive
			Average	1158 rad/s^2	Sub-concussive
			50	4948 rad/s^2	Concussive
			75	6209 rad/s^2	Concussive
			Average	5022 rad/s^2	Concussive
Crisco et al. (2011)	Head Impact Telemetry	Linear Acceleration	50	20.5g	
			95	62.7g	
		Angular Acceleration	50	1400 rad/s^2	
			95	4378 rad/s^2	
Beckwith et al. (2013)	Head Impact Telemetry	Linear Acceleration	50	20.7g	Sub-concussive
			50	22.5g	Concussive
			95	63.5g	Sub-concussive
			95	82.0g	Concussive
		Angular Acceleration	50	848 rad/s^2	Sub-concussive
			50	874 rad/s^2	Concussive
			95	2761 rad/s^2	Sub-concussive
			95	3376 rad/s^2	Concussive
Broglio et al. (2012)	Head Impact Telemetry	Linear Acceleration	Average	24.8g	In game
				23.3g	In practice

		Angular Acceleration	Average	1670 rad/s^2 1469 rad/s^2	In game In practice
Broglio et al. (2009)	Head Impact Telemetry	Impact Force	Average	1282 N 1358 N 1286 N 1094 N	In practice In game Frontal Lateral
		Linear Acceleration	Average	24.8g 23.3g	In practice In game
Broglio et al. (2010)	Head Impact Telemetry	Linear Acceleration	Average	24.2g 26.1g	In practice In game
		Angular Acceleration	Average	1554 rad/s^2 1711 rad/s^2	In practice In game
Brolinson et al. (2006)	Head Impact Telemetry	Linear Acceleration	50 Average	15.3g 20.9	

The impact metrics chosen for analysis of neck performance were the resultant head COG linear acceleration (a), angular acceleration (α), angular velocity (ω), upper neck impact force, upper neck impact moment, upper neck peak force, and upper neck peak moment. The upper neck forces and moments are measured from a load cell in the Hybrid III headform as shown in Figure 3.10, where the headform is fixed to the Hybrid III neck.

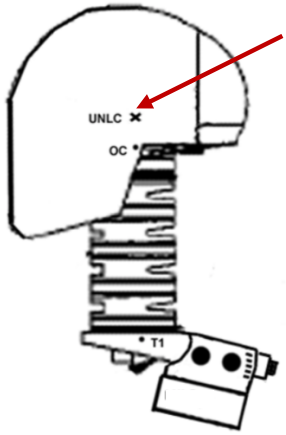

Figure 3.10: Location of the upper neck load cell (UNLC) in the Hybrid III headform. Positioned centrally along the sagittal plane, superior to the occipitocervical (OC) joint [94].

Peak values of resultant kinematics and kinetics were found as the maximum value within a 60 ms time frame, as most kinematic peaks occurred within 60 ms. The exception to this time frame is seen in some peak moment values in the lateral and front boss directions with the three surrogate necks. In these situations, the peak moment occurs between 70-90 ms. In some cases, typically with angular velocity and moment, the maximum peak values did not occur at the first peak in the time series data (Figure 3.11). In these scenarios, the maximum peak was reported as the peak value. For angular velocity time series data in frontal, lateral, and front boss impacts with the Hybrid III neck only, the signal increases after the initial impact until the end of the recorded time

window (Figure 3.11). High speed video of the impacts confirm that this increasing signal was not representative of the impact event, and the peak value was recorded as the peak within the first 60 ms of the impact.

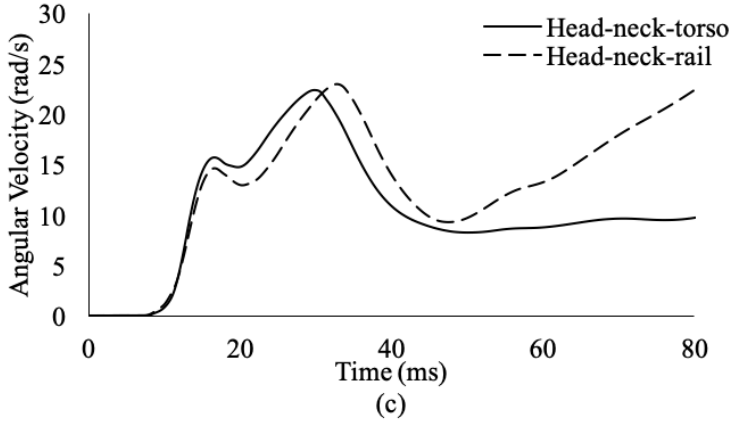

Figure 3.11: Ensemble angular velocity time series curve. The maximum peak was reported as the peak value, not the first peak.

Peak kinematics were found for each impact and averaged to determine the mean peak kinematics. The peak values for linear acceleration, angular acceleration, and angular velocity generally occurred between 12-40 ms. Because the peak kinetics of all impacts occurred slightly after the peak kinematics, discrete impact kinetic values were determined as the upper neck impact force value at the time of peak head COG linear acceleration, and upper neck impact moment value at the time of peak COG angular acceleration; while upper neck peak force and peak moment values are the true peaks.

3.3.2 Sample Size Estimation

Preliminary impacts were conducted with identical experimental setup and procedures outlined in Section 3.3. Previous work by Wynn, 2022 determined a sample size of n=10 for front impacts and n=20 for front boss impacts was sufficient for determining differences between surrogate neck models on the translating linear rail [29]. Thus, a sample size of n=20 for frontal, lateral, and front boss impacts were used to run a power analysis with a power of 0.8 and significance level of 0.05 (G*Power 3.1) for the head-neck-rail system. Additionally, a sample size of n=20 for frontal, lateral, and front boss was used to run a power analysis for impacts with the Hybrid III torso. The analysis showed a wide range in the sample sizes required for the seven desired metrics in all impact locations. Fifteen of the eighty-four impact metrics required n>20; however, a sample size of n=20 was used for all impact locations because conducting more than twenty impacts per impact location would require an exceptional amount of time and the number of impacts required from the analysis was unrealistic. A sensitivity analysis was also conducted and the following minimum effect sizes that the ANOVAs could reliably detect were identified:

- All impact locations – just prototype surrogate necks: Cohen's f>0.41 (n=60, 3 groups)
- All impact locations – surrogate necks and Hybrid III: Cohen's f>0.38 (n=80, 4 groups)

Effect sizes presented in this thesis were all acceptable, thus all experiments were adequately powered to determine statistical differences.

3.4 Data Analysis

All statistical analyses were conducted using IBM SPSS Statistics V27 (Armonk, New York, USA) with a significance of $p<0.05$. Means and standard deviations (SD) of all peak kinematics (linear acceleration, angular acceleration, and angular velocity) and kinetics (impact and peak force and

moment) for all impacts were analyzed using multiple data analysis methods. For all repeat impacts, impact velocity ranged from 3.85 m/s – 4.20 m/s and was determined not to be a covariate in the impact metrics.

3.4.1 Phase III Neck Repeatability

A repeatability analysis of the Phase III surrogate neck was conducted in two parts following the methods detailed in Section 3.4.1 and 3.4.2 of Wynn, 2022 [29]. To summarize, the first part of the repeatability analysis, within-neck repeatability, utilized the coefficient of variation of repeatability (CV_W) for analysis within each of the three surrogate necks. The equation for CV_W is shown in Equation 2 where, σ is the standard deviation of the mean kinematics, $\bar{x}$, where x refers to any one of the impact metrics. The average overall CV_W of the surrogate neck was also found using equations described in Section 3.4.1 of Wynn, 2022 [29]. This calculation estimates the general CV_W of the surrogate neck. CV_W values ≤10% are deemed acceptable [29].

$$CV_W = \frac{\sigma}{\bar{x}} \times 100\% \tag{2}$$

The second part, between-neck repeatability, utilized the coefficient of variation of reproducibility (CV_B), ANOVAs and post-hoc tests, and normalized absolute differences (NAD) for analysis between the three surrogate neck models. The equation for CV_B is shown in Equation 3 where, S_B is the total standard deviation, and $\bar{X}$ is the means kinematics of all models, where X refers to any one of the impact metrics. CV_B values ≤15% are deemed acceptable [29].

$$CV_B = \frac{S_B}{\bar{X}} \times 100\% \quad (3)$$

For investigation between the three Phase III surrogate necks and between the Phase III surrogate necks and the Hybrid III neck, an ANOVA was performed on each full dataset from which, outliers were identified from boxplots of each impact metric dataset. The outliers were then removed and a second ANOVA was conducted to determine if the outliers effected the ANOVA results. The only post-hoc tests that showed statistical difference when the outliers were removed was the angular acceleration between surrogate neck #2 and #3 for frontal impacts on the linear rail, and the moment between surrogate neck #1 and #3 for frontal impacts with the dummy torso. Therefore, outliers were left in the datasets for the analysis. Normality of each impact metric dataset was assessed with the Shapiro-Wilk Test ($p<0.05$). Some datasets were not normally distributed, and while some datasets were made normal with the removal of outliers, it was determined that the removal of the outliers did not sufficiently change the results of the ANOVA and were left in the datasets. The resultant peak kinematics and kinetics were analyzed using a one-way ANOVA and Tukey post-hoc test for datasets that were normally distributed and passed Levene's test for homogeneity of variances based on means ($p<0.05$). Datasets that violated these requirements were assessed using a one-way Welch ANOVA and Games-Howell post-hoc test. Cohen's d effect sizes of 0.20 are small, 0.50 are medium, and 0.80 are large, while Cohen's f effect size values are 0.10 for small, 0.25 for medium, and 0.40 for large.

The normalized absolute difference was also calculated to assess between-neck repeatability. For analysis between the three Phase III surrogate necks, Equation 4 was utilized where i, j, k refers to

the number of each surrogate neck. A normalized absolute difference of ≤20% is acceptable for current neck certification standards [29].

$$\frac{|x_j - x_k|}{\frac{1}{3}\sum_{i=1}^{3} x_i} \times 100\% \begin{cases} j,k = 1,2,3 \\ j \neq k \end{cases} \quad (4)$$

To calculate the normalized absolute difference for comparison between the Hybrid III neck and the surrogate necks, Equation 5 was used, where x_j refers to the mean kinematics of the surrogate necks and x_{Hy3} refers to the mean kinematics of the Hybrid III neck.

$$\frac{|x_j - x_{Hy3}|}{\frac{1}{3}\sum_{i=1}^{3} x_i} \times 100\% \{ j = 1,2,3 \quad (5)$$

3.4.2 Comparison of Head-Neck-Torso and Head-Neck-Rail Systems

Independent samples, two-tailed t-test for equal means ($p<0.05$) was used to determine statistical significance between impact metrics that met all statistical requirements for the head-neck-torso system and the head-neck-rail system. Levene's test for Equality of Variances was performed and for impact metrics that failed this test, results of the Welch t-test are reported. For variables that violated the normal distribution requirement and failed Levene's test, a Mann-Whitney U Test to compare means was performed. The statistical test used is indicated in the results. Time series ensemble averages are also presented for the kinematic and kinetic impact metrics for the head-neck-rail and head-neck-torso for visual comparison.

4 RESULTS

This chapter provides a summary of the repeatability results of the Phase III surrogate neck and a brief comparison to the Hybrid III neck. Additionally, surrogate head and neck biomechanics are compared between the head-neck-torso system and the head-neck-rail system.

4.1 Phase III Neck Repeatability

The Phase III surrogate neck showed acceptable within-neck and between-neck repeatability based on CV_W, CV_B, and normalized absolute difference values. However, NAD values of >20% between the surrogate necks and the Hybrid III neck and significantly different ANOVA results indicate the Phase III neck and the Hybrid III neck produce differing head kinematics during impact.

Within-neck and between-neck repeatability was tested with three copies of the Phase III modified surrogate neck in direct head impacts in frontal, lateral, and front boss locations. Included in the following repeatability analysis is linear acceleration, angular acceleration, and angular velocity. Impact and peak kinetics are not included because these impact metrics are of less relevance in evaluation of ATDs and so a poor CV value may not be a sufficient cause for concern [95]. Within-neck repeatability CV_W values were all under 10% except for angular velocity in frontal impacts with surrogate neck #2. The average CV_W of the Phase III necks for linear acceleration in frontal, lateral, and front boss impacts is 4.5%, 3.7%, and 4.6%, respectively; for angular acceleration, it's 9.6%, 3.7%, and 4.0%; and for angular velocity, it's 2.8%, 2.6%, and 2.7%. These values suggest acceptable repeatability of the Phase III surrogate neck (Table 4.1) [29].

Table 4.1: Coefficient of variance for repeatability (CV_W) for the Phase III necks and Hybrid III neck from impacts on the linear rail. Cells with CV_W values greater than 10% are shaded in gray.

		Δa (%)	$\Delta\alpha$ (%)	$\Delta\omega$ (%)
Neck 1	Frontal	2.7	1.4	5.7
	Lateral	4.1	2.3	2.1
	Front Boss	1.8	1.7	2.6
Neck 2	Frontal	7.3	3.2	17.1
	Lateral	2.1	2.8	3.2
	Front Boss	5.3	4.1	4.5
Neck 3	Frontal	3.5	3.7	6.0
	Lateral	5.0	2.6	5.8
	Front Boss	6.7	2.5	4.9
Hybrid III	Frontal	1.7	2.0	1.3
	Lateral	3.8	5.3	0.8
	Front Boss	2.2	2.4	6.5

a = linear acceleration, α = angular acceleration, ω = angular velocity

In the three impact locations, all CV_B values were under 10% except for linear acceleration in frontal (11.4%) and front boss (12.6%) impacts, although ≤15% is acceptable (Table 4.2). Most NAD values presented in Table 4.3 are less than 20%, further indicating that the between-neck repeatability of the Phase III surrogate neck is acceptable. On average, the impact metrics differed by less than 15% between necks except for linear acceleration in front boss impacts (16.8%).

Table 4.2: Coefficient of variance of reproducibility (CV_B) values between Phase III surrogate necks for frontal, lateral, and front boss impacts.

	Δa (%)	$\Delta\alpha$ (%)	$\Delta\omega$ (%)
Frontal	11.4	9.0	7.4
Lateral	5.2	5.9	7.6
Front Boss	12.6	8.7	6.4

a = linear acceleration, α = angular acceleration, ω = angular velocity

Table 4.3: Normalized absolute differences between Phase III surrogate necks for frontal, lateral, and front boss impacts on the linear rail. Cells with values greater than 20% are shaded in gray.

		Δa (%)	$\Delta\alpha$ (%)	$\Delta\omega$ (%)
Frontal	Neck 1-Neck 2	22.1	4.3	18.0
	Neck 2-Neck 3	15.9	14.4	9.6
	Neck 1-Neck 3	6.1	10.1	8.4
	Average	14.7	9.6	12.0
Lateral	Neck 1-Neck 2	1.8	1.9	3.4
	Neck 2-Neck 3	9.7	14.1	11.5
	Neck 1-Neck 3	7.9	12.1	8.1
	Average	6.5	9.4	7.7
Front Boss	Neck 1-Neck 2	12.4	12.5	9.1
	Neck 2-Neck 3	12.9	8.2	8.3
	Neck 1-Neck 3	25.2	4.3	17.4
	Average	16.8	8.3	11.6

a = linear acceleration, α = angular acceleration, ω = angular velocity

To investigate the difference of impact metrics between the Hybrid III neck and the three Phase III surrogate necks, the NAD between each Phase III neck and the Hybrid III neck was calculated. These results are presented in Table 4.4. Overall, the normalized absolute difference between the kinematics of the Phase III necks and the Hybrid III neck were greater than the difference between the three Phase III necks.

To further investigate differences between the surrogate necks and the Hybrid III neck, an ANOVA was performed on the full dataset for each impact metric after determining that outliers did not affect the ANOVA results. The results of the ANOVA and time series plots of all impact metrics are provided in Appendix A: for visual comparison. Overall, the ANOVA results showed significant differences between the Hybrid III neck and the Phase III surrogate necks for frontal, lateral, and front boss impacts.

Table 4.4: Normalized absolute difference between surrogate necks and Hybrid III neck for frontal, lateral, and front boss impacts with the linear rail. Values greater than 20% are shaded in gray.

		Δa (%)	$\Delta\alpha$ (%)	$\Delta\omega$ (%)
Frontal	Neck 1-Hy3	4.4	44.8	75.4
	Neck 2-Hy3	26.5	62.8	71.1
	Neck 3-Hy3	10.5	53.2	85.6
	Average	13.8	53.6	77.4
Lateral	Neck 1-Hy3	2.7	5.5	3.9
	Neck 2-Hy3	18.6	22.3	20.2
	Neck 3-Hy3	83.7	85.1	77.4
	Average	35.0	37.7	33.8
Front Boss	Neck 1-Hy3	21.6	20.6	0.3
	Neck 2-Hy3	34.0	8.1	8.9
	Neck 3-Hy3	46.8	16.3	17.1
	Average	34.1	15.0	8.8

a = linear acceleration, α = angular acceleration, ω = angular velocity

4.2 Comparison of Head-Neck-Torso and Head-Neck Rail Systems

This investigation showed significant differences in almost all impact metrics between the head-neck-torso system and the head-neck-rail system.

One Hybrid III neck and three Phase III surrogate necks were tested in repeat experiments in three impact locations with the necks fixed to a translating linear rail (head-neck-rail system) and fixed to a Hybrid III torso and pelvis (head-neck-torso system). Out of a combination of 84 impact metric comparisons (7 impact metrics x 3 impact locations x 4 surrogate necks), only 14 were not statistically different. The impact location in which the most significant differences were found between the head-neck-torso and head-neck-rail systems was frontal impacts. The lateral and front boss impact locations had the same number of significantly different results.

Overall, 65% (55 of 84) of the resultant impact metrics were higher for the head-neck-torso system than the head-neck-rail system. In frontal impacts, 75% (21 of 28) (7 impact metrics x 4 surrogate necks) of the kinematic and kinetic impact metrics were higher from the head-neck-torso system than the head-neck rail system. A similar result is seen in lateral impacts with 71% (20 of 28) of the impact metrics being higher in the head-neck-torso system. In front boss impacts, both kinematic and kinetic impact metrics were evenly split, with 50% of metrics being higher in the head-neck-torso system. These results are visually summarized in Table 4.5. Resultant impact metrics are presented in the following sections organized by impact location and surrogate neck model.

Table 4.5: Comparing impact metrics from the head-neck-torso system and the head-neck-rail system. Cells highlighted in green are metrics that had higher values from the head-neck-torso system. Cells highlighted in red are metrics that had lower values from the head-neck-torso system. Cells with an X indicate the result was NOT statistically different.

	Frontal				Lateral				Front Boss			
	Hy. III	SN #1	SN #2	SN #3	Hy. III	SN #1	SN #2	SN #3	Hy. III	SN #1	SN #2	SN #3
Peak a (g)			X									
Peak α (rad/s^2)								X				
Peak ω (rad/s)					X					X		
Impact F (N)								X				X
Impact M (Nm)					X					X		X
Peak F (N)					X	X				X		
Peak M (Nm)				X					X			

a = linear acceleration, α = angular acceleration, ω = angular velocity, F = force, M = moment, SN = surrogate neck

4.2.1 Frontal

Out of a combination of 28 impact metric comparisons, 75% (21 of 28) were higher for the head-neck-torso system compared to the head-neck-rail system. In frontal impacts, more impact metrics were higher for the torso system when compared to lateral (70%) or front boss (50%) impact locations, and there were more statistical differences. Linear acceleration was the only impact metric that was higher for the head-neck-torso system for all four surrogate necks in frontal impacts. Angular acceleration, impact force, impact moment, peak force, and peak moment were all higher in the torso system for three of the four necks. Lastly, angular velocity was higher for the torso system for two of the four necks.

4.2.1.1 Hybrid III

Mean ± standard deviation, 95% confidence interval, mean difference, and percent change values of the kinematic impact metrics are presented in Table 4.6 and the kinetic impact metrics are presented in Table 4.7 for impacts with the Hybrid III neck fixed to the head-neck-torso system and the head-neck-rail system. Independent samples two-tailed t-test or Welch t-test results are shown in Table 4.8 for angular acceleration, angular velocity, impact force, peak force, and peak moment. Mean ranks, U statistics, z-scores, and p-values from a Mann-Whitney U Test are presented in Table 4.9 for linear acceleration and impact moment. A visual representation of the average peak kinematic and kinetic data is presented in Figure 4.1. Time series data of ensemble averages for all impact metrics with the head-neck-torso system and the head-neck-rail system are shown in Figure 4.2. The mean resultant impact metrics from the head-neck-torso assembly were

higher than the values from the head-neck-rail assembly for peak linear acceleration, impact force, impact moment, and peak force, and lower for peak angular acceleration, peak angular velocity, and peak moment.

Table 4.6: Mean±SD, 95% CI, mean difference (M.D.), and percent change (P.C.) values of kinematic impact metrics from frontal impacts with Hybrid III neck fixed to the head-neck-torso system and head-neck-rail system.

		Peak *a* (g)	Peak α (rad/s^2)	Peak ω (rad/s)
Torso	Mean±SD	60.1±2.7	2431.0±152.8	13.7±0.3
	95% CI	(58.8, 61.4)	(2359.5, 2502.6)	(13.5, 13.8)
Rail	Mean±SD	26.4±0.4	4153.9±82.8	24.0±0.3
	95% CI	(26.2, 26.6)	(4115.2, 4192.7)	(23.8, 24.1)
	M.D.	33.7	-1722.9	-10.3
	P.C.	+127.7%	-41.5%	-42.9%

a = linear acceleration, α = angular acceleration, ω = angular velocity

Table 4.7: Mean±SD, 95% CI, mean difference (M.D.), and percent change (P.C.) values of kinetic impact metrics from frontal impacts with Hybrid III neck fixed to the head-neck-torso system and head-neck-rail system.

		Impact F (N)	Impact M (Nm)	Peak F (N)	Peak M (Nm)
Torso	Mean±SD	1824.4±180.4	13.8±5.3	2354.2±205.9	51.9±1.9
	95% CI	(1740.0, 1908.8)	(11.3, 16.2)	(2257.9, 2450.6)	(51.0, 52.8)
Rail	Mean±SD	1520.7±80.0	13.2±0.4	2047.1±30.7	59.4±1.0
	95% CI	(1483.3, 1558.1)	(13.0, 13.4)	(2032.7, 2061.5)	(58.9, 59.9)
	M.D.	303.7	0.6	307.1	-7.5
	P.C.	+20.0%	+4.6%	+15.0%	-12.6%

F = force, M = moment

All average peak impact metrics were statistically different between the head-neck-torso system and the head-neck-rail system for frontal impacts with the Hybrid III neck. The largest difference, with a percent change of 127.7%, was linear acceleration between the torso assembly (mean rank = 30.50) and the rail assembly (mean rank = 10.50), U = 0.00, z = -5.410, p = 0.000. The smallest percent difference in means, 4.6%, was seen in the impact moment values between the head-neck-

torso assembly (mean rank = 16.80) and the head-neck-rail assembly (mean rank = 24.20), although a significant difference was still calculated, U = 274, z = 2.002, p = 0.046.

Table 4.8: Independent samples two-tailed t-test or Welch t-test results for appropriate impact metrics from frontal impacts with the Hybrid III neck. Significant p-values are shaded in grey.

	t-statistic	df	95% CI of the Difference	p-value
Peak α (rad/s^2)*	-44.330	29.270	-1802.3, -1643.4	p<0.001
Peak ω (rad/s)	-101.8	38	-10.5, -10.1	p<0.001
Impact F (N)*	6.885	26.176	213.1, 394.4	p<0.001
Peak F (N)*	6.597	19.846	210.0, 404.3	p<0.001
Peak M (Nm)	-15.535	38	-8.4, -6.5	p<0.001

a = linear acceleration, ω = angular velocity, F = force, M = moment
*Welch t-test

Table 4.9: Mean ranks, U statistics, z-scores, and p-values from a Mann-Whitney U Test for frontal impacts with the Hybrid III neck for peak acceleration and impact moment. Significant p-values are shaded in grey.

	Mean Rank				
	Head-neck-torso	Head-neck-rail	*U* Statistic	z-score	p-value
Peak *a* (g)	30.50	10.50	0.000	-5.410	p = 0.000
Impact M (Nm)	16.80	24.20	274.000	2.002	p = 0.046

a = linear acceleration, M = moment

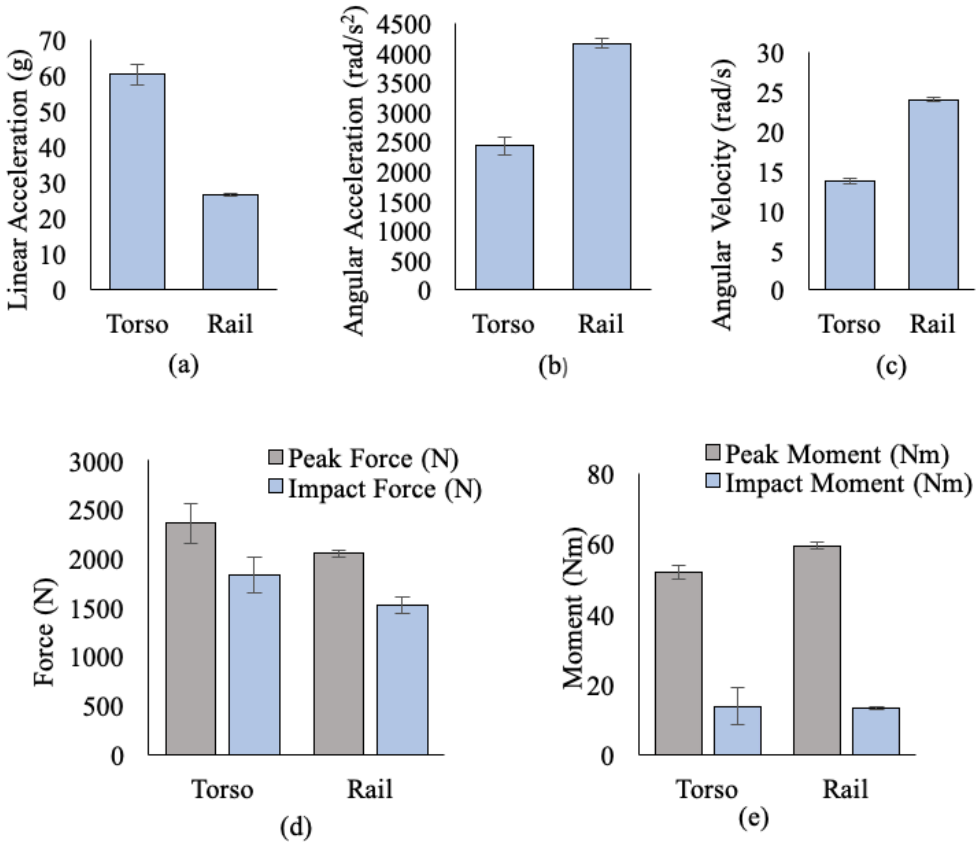

Figure 4.1: Bar charts of means and standard deviations for the head-neck-torso system and the head-neck-rail system for (a) linear acceleration, (b) angular acceleration, (c) angular velocity, (d) peak and impact force, and (e) peak and impact moment from frontal impacts with the Hybrid III neck.

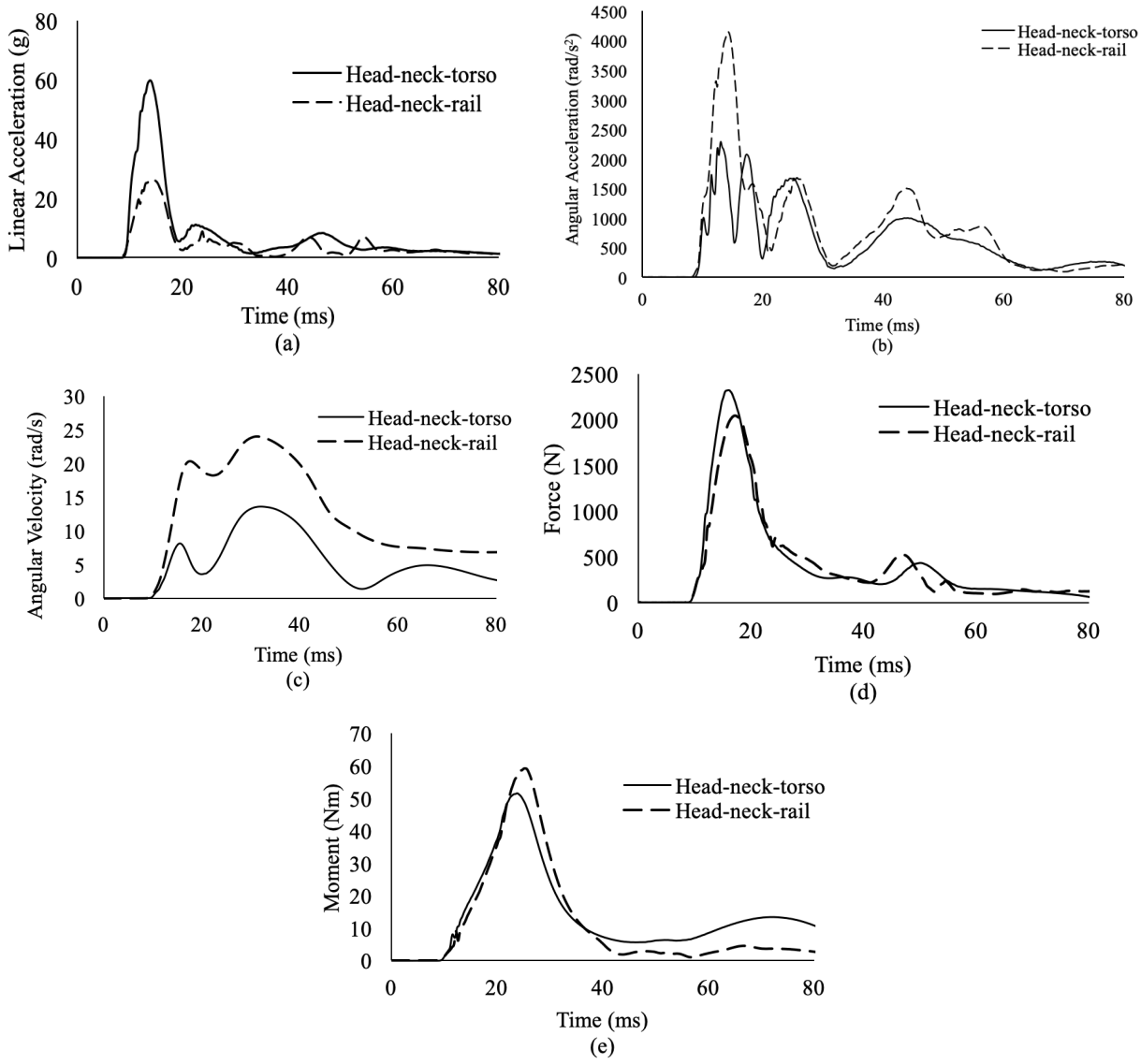

Figure 4.2: Comparison of ensemble averages from frontal impacts with the Hybrid III fixed to the head-neck-torso system and head-neck-rail system for (a) linear acceleration, (b) angular acceleration, (c) angular velocity, (d) force, and (e) moment.

4.2.1.2 Surrogate Neck #1

Mean±standard deviation, 95% confidence interval, mean difference, and percent change values of the kinematic impact metrics are presented in Table 4.10 and the kinetic impact metrics are presented in Table 4.11 for impacts with surrogate neck #1 fixed to the head-neck-torso system

and the head-neck-rail system. Welch t-test results are shown in Table 4.12 for linear acceleration and peak moment. Mean ranks, U statistics, z-scores, and p-values from a Mann-Whitney U Test are presented in Table 4.13 for angular acceleration, angular velocity, impact force, impact moment, and peak force. A visual representation of the average peak kinematic and kinetic data is presented in Figure 4.3. Time series data of ensemble averages for all impact metrics with the head-neck torso system and the head-neck-rail system are shown in Figure 4.4. All impact metrics from the head-neck-torso system were higher except for peak angular velocity.

Table 4.10: Mean±SD, 95% CI, mean difference (M.D.), and percent change (P.C.) values of kinematic impact metrics from frontal impacts with surrogate neck #1 fixed to the head-neck-torso system and head-neck-rail system.

		Peak a (g)	Peak α (rad/s^2)	Peak ω (rad/s)
Torso	Mean±SD	38.6±2.1	2991.1±331.9	16.3±0.7
	95% CI	(37.7, 39.6)	(2835.8, 3146.4)	(15.9, 16.6)
Rail	Mean±SD	27.7±0.7	2387.4±135.8	17.0±0.2
	95% CI	(27.4, 28.1)	(2323.8, 2451.0)	(16.9, 17.1)
	M.D.	10.9	603.7	-0.7
	P.C.	+39.3%	+25.3%	-4.3%

a = linear acceleration, α = angular acceleration, ω = angular velocity

Table 4.11: Mean±SD, 95% CI, mean difference (M.D.), and percent change (P.C.) values of kinetic impact metrics from frontal impacts with surrogate neck #1 fixed to the head-neck-torso system and head-neck-rail system.

		Impact F (N)	Impact M (Nm)	Peak F (N)	Peak M (Nm)
Torso	Mean±SD	782.9±138.1	9.1±1.0	1163.1±108.3	19.5±0.9
	95% CI	(718.3, 847.5)	(8.6, 9.5)	(1112.4, 1213.8)	(19.1, 19.9)
Rail	Mean±SD	438.8±13.1	4.1±0.4	589.7±16.4	16.5±0.6
	95% CI	(432.6, 444.9)	(3.9, 4.3)	(582.0, 597.4)	(16.2, 16.8)
	M.D.	344.1	5.0	573.4	3.00
	P.C.	+78.4%	+123.2%	+97.2%	+18.0%

F = force, M = moment

All average peak impact metrics were statistically different between the head-neck-torso system and the head-neck-rail system for frontal impacts with surrogate neck #1. The average resultant angular velocity was the only impact metric that was higher for the head-neck-rail system (mean rank = 13.50) than the head-neck-torso system (27.50), U = 340.000, z = 3.787, p = 0.000, and had the smallest percent change in means (4.3%). The largest percent change was seen in impact moment, where a statistical difference occurred between the head-neck-torso assembly (mean rank = 30.50) and the head-neck-rail assembly (mean rank = 10.50), U = 0.000, z = -5.410, p = 0.000.

Table 4.12: Welch t-test results for appropriate impact metrics from frontal impacts with the surrogate neck #1. Significant p-values are shaded in grey.

	t-statistic	df	95% CI of the difference	p-value
Peak a (g)	22.164	23.906	9.87, 11.90	p<0.001
Peak M (Nm)	12.775	34.026	2.50, 3.44	p<0.001

a = linear acceleration, M = moment

Table 4.13: Mean ranks, U statistics, z-scores, and p-values from a Mann-Whitney U Test for frontal impacts with surrogate neck #1 for all impact metrics. Significant p-values are shaded in grey.

	Mean Rank				
	Head-neck-torso	Head-neck-rail	*U* Statistic	z-score	p-value
Peak α (rad/s^2)	30.50	10.50	0.000	-5.410	p = 0.000
Peak ω (rad/s)	13.50	27.50	340.000	3.787	p = 0.000
Impact F (N)	30.50	10.50	0.000	-5.410	p = 0.000
Impact M (Nm)	30.50	10.50	0.000	-5.410	p = 0.000
Peak F (N)	30.50	10.50	0.000	-5.410	p = 0.000

α = angular acceleration, ω = angular velocity, F = force, M = moment

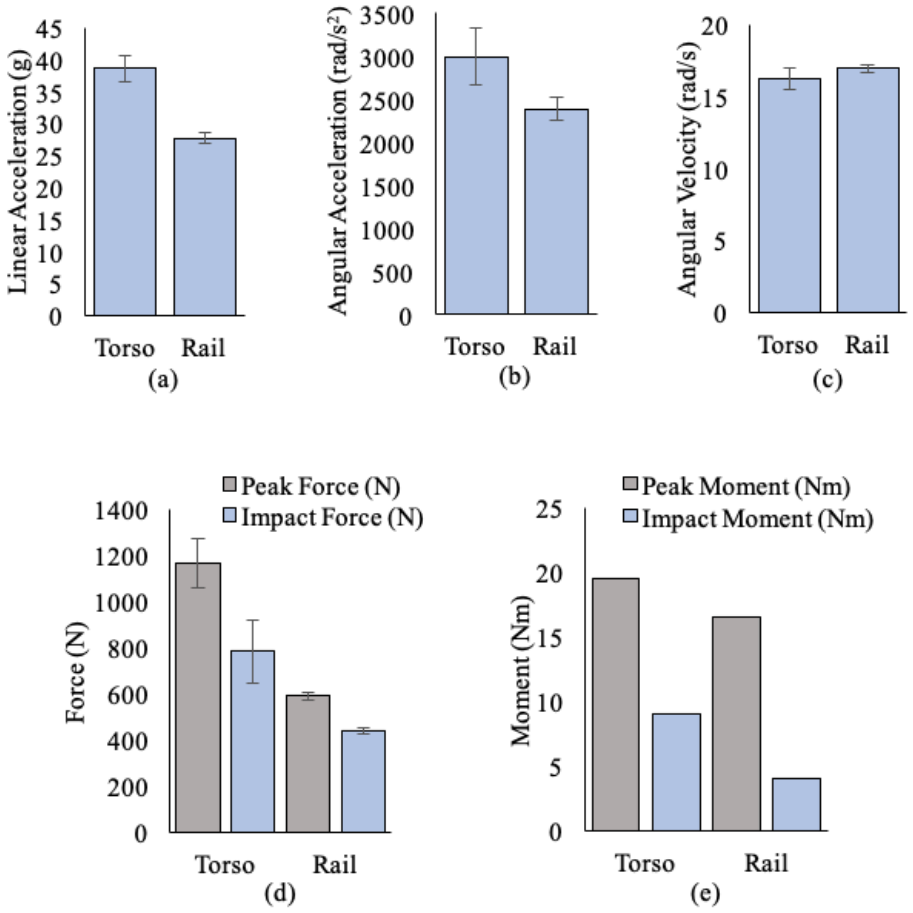

Figure 4.3: Bar charts of means and standard deviations for the head-neck-torso system and the head-neck-rail system for (a) linear acceleration, (b) angular acceleration, (c) angular velocity, (d) peak and impact force, and (e) peak and impact moment from frontal impacts with surrogate neck #1.

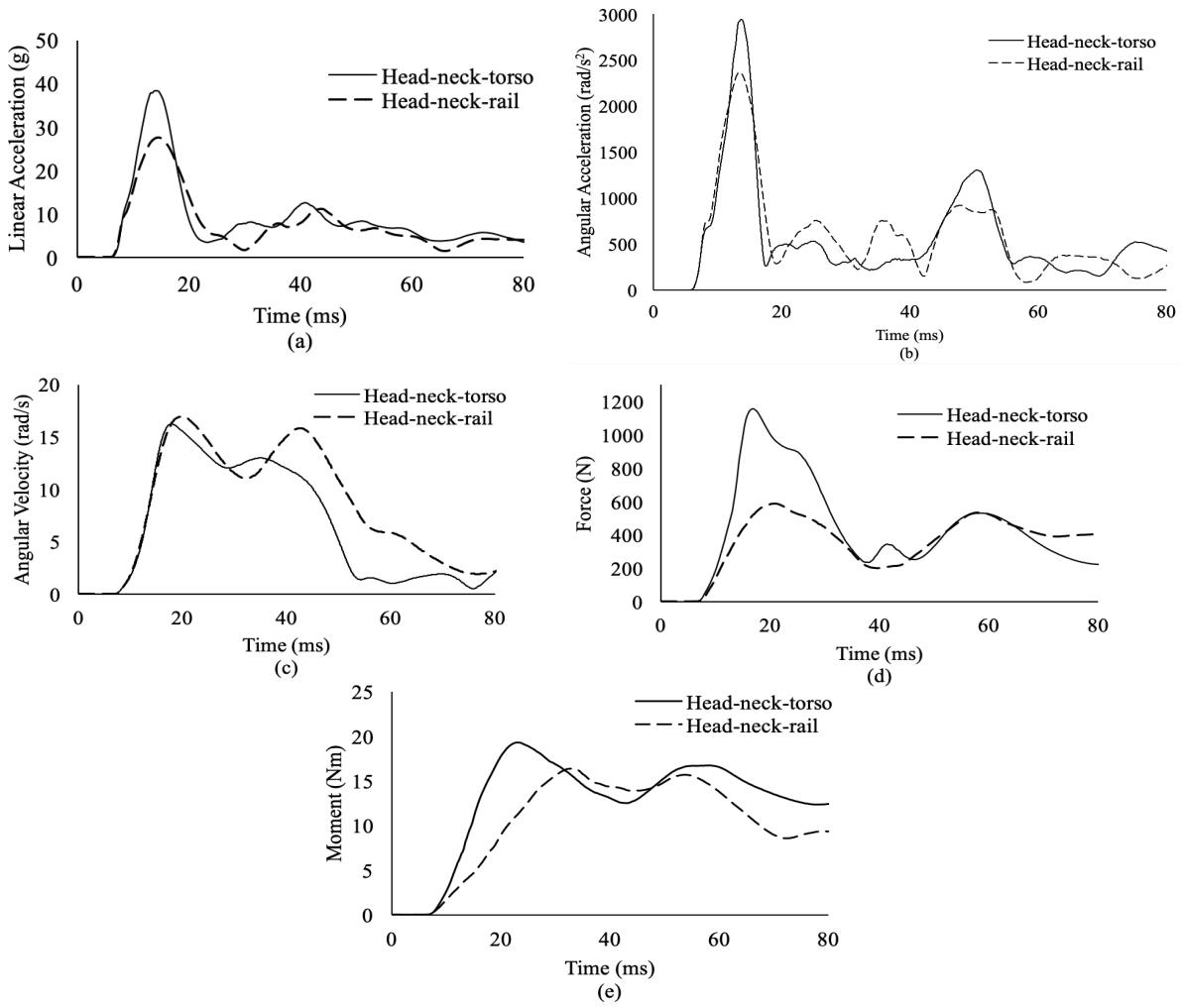

Figure 4.4: Comparison of ensemble averages from frontal impacts with the surrogate neck #1 fixed to the head-neck-torso system and head-neck-rail system for (a) linear acceleration, (b) angular acceleration, (c) angular velocity, (d) force, and (e) moment.

4.2.1.3 Surrogate Neck #2

Mean±standard deviation, 95% confidence interval, mean difference, and percent change values of the kinematic impact metrics are presented in Table 4.14 and the kinetic impact metrics are presented in Table 4.15 for impacts with surrogate neck #2 fixed to the head-neck-torso system and the head-neck-rail system. Independent samples two-tailed t-test and Welch t-test results are shown in Table 4.16 for angular velocity and peak moment. Mean ranks, U statistics, z-scores, and

p-values from a Mann-Whitney U Test are presented in Table 4.17 for linear acceleration, angular acceleration, impact force, impact moment, and peak force. A visual representation of the average peak kinematic and kinetic data is presented in Figure 4.5. Time series data of ensemble averages for all impact metrics with the head-neck torso system and the head-neck-rail system are shown in Figure 4.6.

Table 4.14: Mean±SD, 95% CI, mean difference (M.D.), and percent change (P.C) values of kinematic impact metrics from frontal impacts with surrogate neck #2 fixed to head-neck-torso system and head-neck-rail system.

		Peak a (g)	Peak α (rad/s^2)	Peak ω (rad/s)
Torso	Mean±SD	34.5±3.4	3095.5±723.0	18.7±1.2
	95% CI	(32.9, 36.2)	(2757.2, 3433.9)	(18.1, 19.3)
Rail	Mean±SD	34.5±2.5	2488.1±424.9	14.2±0.5
	95% CI	(33.3, 35.7)	(2289.2, 2687.0)	(14.0, 14.4)
	M.D.	0.06	607.4	4.5
	P.C.	+0.2%	+24.4%	+31.9%

a = linear acceleration, α = angular acceleration, ω = angular velocity

Table 4.15: Mean±SD, 95% CI, mean difference (M.D.), and percent change (P.C.) values of kinetic impact metrics from frontal impacts with surrogate neck #2 fixed to head-neck-torso system and head-neck-rail system.

		Impact F (N)	Impact M (Nm)	Peak F (N)	Peak M (Nm)
Torso	Mean±SD	733.3±65.9	8.2±1.5	895.3±61.0	18.6±0.6
	95% CI	(702.4, 764.1)	(7.5, 8.9)	(866.8, 923.9)	(18.3, 18.9)
Rail	Mean±SD	848.6±56.9	9.1±1.1	1042.6±76.3	16.8±0.6
	95% CI	(822.0, 875.2)	(8.6, 9.6)	(1006.9, 1078.4)	(16.6, 17.0)
	M.D.	-115.3	-0.9	-147.3	1.8
	P.C.	-13.6%	-10.5%	-14.1%	+10.7%

F = force, M = moment

All average peak impact metrics were statistically different between the head-neck-torso system and the head-neck-rail system for frontal impacts with surrogate neck #2 except linear acceleration. The smallest difference in means was seen between the linear acceleration values for the head-neck-torso system (mean rank = 19.80) and the head-neck-rail assembly (mean rank = 21.20). A statistical difference was not found, $U = 214.000$, $z = 0.379$, $p = 0.718$. The resultant mean angular velocity for the head-neck-torso system (18.7 ± 1.2 rad/s) was 31.9% higher than the mean angular velocity of the head-neck-rail system (14.2 ± 0.5 rad/s) (95% CI: 3.9, 5.1 rad/s), $t(24.028)=15.349$, $p<0.001$, which was the greatest difference in means.

Table 4.16: Independent samples two-tailed t-test or Welch t-test results for appropriate impact metrics from frontal impacts with the surrogate neck #2. Significant p-values are shaded in grey.

	t-statistic	df	95% CI of the Difference	p-value
Peak ω (rad/s)*	15.349	24.028	3.91, 5.13	p<0.001
Peak M (Nm)	10.451	38	1.45, 2.15	p<0.001

ω = angular velocity, M = moment
*Welch t-test

Table 4.17: Mean ranks, U statistics, z-scores, and p-values from a Mann-Whitney U Test for frontal impacts with surrogate neck #2 for all impact metrics. Significant p-values are shaded in grey.

	Mean Rank				
	Head-neck-torso	Head-neck-rail	*U* Statistic	z-score	p-value
Peak *a* (g)	19.80	21.20	214.000	0.379	p = 0.718
Peak α (rad/s^2)	25.90	15.10	92.000	-2.921	p = 0.003
Impact F (N)	12.05	28.95	369.000	4.571	p = 0.000
Impact M (Nm)	15.90	25.10	292.000	2.489	p = 0.012
Peak F (N)	12.00	29.00	370.000	4.599	p = 0.000

a = linear acceleration, α = angular acceleration, F = force, M = moment

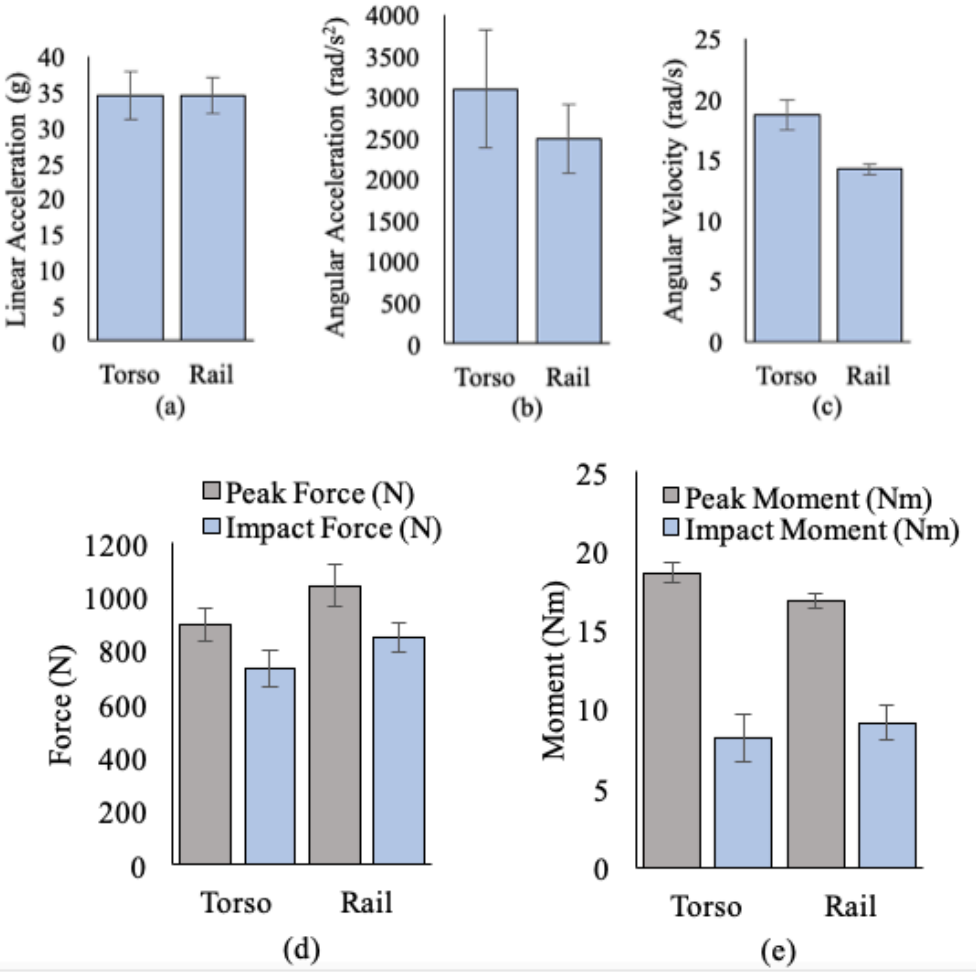

Figure 4.5: Bar charts of means and standard deviations for the head-neck-torso system and the head-neck-rail system for (a) linear acceleration, (b) angular acceleration, (c) angular velocity, (d) peak and impact force, and (e) peak and impact moment from frontal impacts with surrogate neck #2.

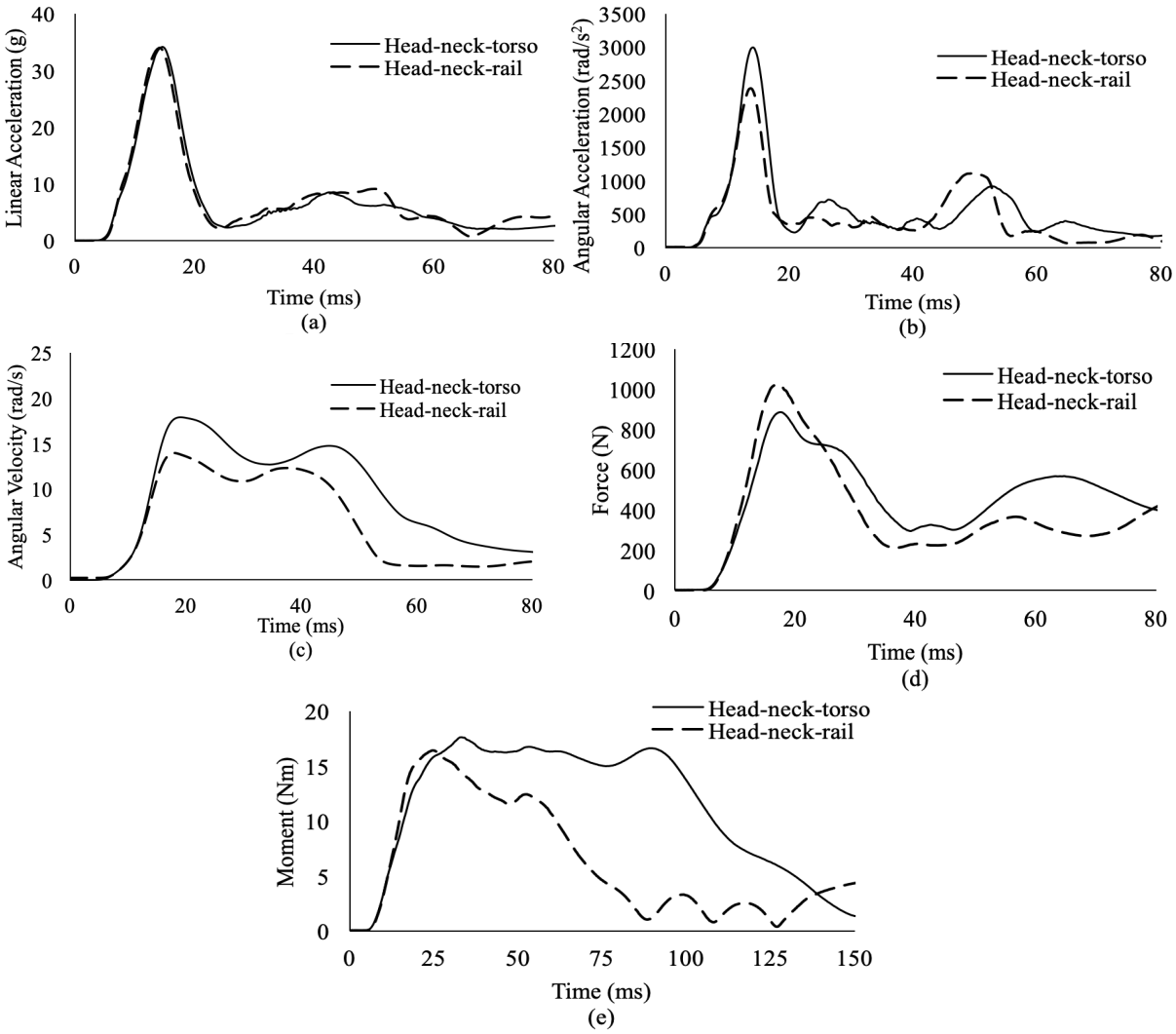

Figure 4.6: Comparison of ensemble averages from frontal impacts with the surrogate neck #2 fixed to the head-neck-torso system and head-neck-rail system for (a) linear acceleration, (b) angular acceleration, (c) angular velocity, (d) force, and (e) moment.

4.2.1.4 Surrogate Neck #3

Mean±standard deviation, 95% confidence interval, mean difference, and percent change values of the kinematic impact metrics are presented in Table 4.18 and the kinetic impact metrics are presented in Table 4.19 for impacts with surrogate neck #3 fixed to the head-neck-torso system

and the head-neck-rail system. Welch t-test results are shown in Table 4.20 for angular acceleration. Mean ranks, U statistics, z-scores, and p-values from a Mann-Whitney U Test are presented in Table 4.21 for linear acceleration, angular velocity, impact force, impact moment, peak force, and peak moment. A visual representation of the average peak kinematic and kinetic data is presented in Figure 4.7. Time series data of ensemble averages for all impact metrics with the head-neck torso system and the head-neck-rail system are shown in Figure 4.8. In frontal impacts with surrogate neck #3, all kinematic and kinetic impact metrics were higher for the head-neck-torso system compared to the head-neck-rail system.

Table 4.18: Mean±SD, 95% CI, mean difference (M.D.), and percent change (P.C.) values of kinematic impact metrics from frontal impacts with surrogate neck #3 fixed to head-neck-torso system and head-neck-rail system.

		Peak a (g)	Peak α (rad/s^2)	Peak ω (rad/s)
Torso	Mean±SD	34.6±2.4	3080.7±645.6	17.9±1.9
	95% CI	(33.4, 35.7)	(2778.5, 3382.8)	(17.0, 18.8)
Rail	Mean±SD	29.6±1.3	2149.9±128.4	15.7±0.6
	95% CI	(29.1, 30.1)	(2089.8, 2209.9)	(15.4, 16.0)
	M.D.	5.0	930.8	2.2
	P.C.	+16.7%	+43.3%	+14.2%

a = linear acceleration, α = angular acceleration, ω = angular velocity

Table 4.19: Mean±SD, 95% CI, mean difference (M.D.), and percent change (P.C.) values of kinetic impact metrics from frontal impacts with surrogate neck #3 fixed to head-neck-torso system and head-neck-rail system.

		Impact F (N)	Impact M (Nm)	Peak F (N)	Peak M (Nm)
Torso	Mean±SD	762.5±51.5	9.4±1.5	1128.4±50.9	19.0±1.3
	95% CI	(738.3, 786.6)	(8.7, 10.2)	(1104.6, 1152.3)	(18.4, 19.6)
Rail	Mean±SD	569.9±71.4	6.2±1.4	790.0±54.4	18.5±0.9
	95% CI	(536.5, 603.3)	(5.5, 6.8)	(764.5, 815.4)	(18.1, 18.9)
	M.D.	192.6	3.2	338.4	0.5
	P.C.	+33.8%	+52.6%	+42.8%	+2.6%

F = force, M = moment

A statistical difference was found between all variables for frontal impacts with surrogate neck #3. The largest difference was seen in peak force values for the head-neck-torso system (mean rank = 30.50) and the head-neck-rail system (mean rank = 10.50), and a statistical difference was found, U = 0.000, z = -5.410, p = 0.000. The smallest difference was seen between peak moment measurements from the head-neck-torso system (mean rank = 21.70) and the head-neck-rail system (mean rank = 19.30). A statistical difference was not found, U = 176.000, z = -0.649, p = 0.529.

Table 4.20: Welch t-test results for angular acceleration from frontal impacts with the surrogate neck #3. Significant p-values are shaded in grey.

	t-statistic	df	95% CI of the Difference	p-value
Peak α (rad/s^2)	6.324	20.500	624.3, 1237.4	p<0.001

α = angular acceleration

Table 4.21: Mean ranks, U statistics, z-scores, and p-values from a Mann-Whitney U Test for frontal impacts with surrogate neck #3 for all impact metrics. Significant p-values are shaded in grey.

	Mean Rank				
	Head-neck-torso	Head-neck-rail	*U* Statistic	z-score	p-value
Peak *a* (g)	30.10	10.90	8.000	-5.194	p = 0.000
Peak ω (rad/s)	28.55	12.45	39.000	-4.355	p = 0.000
Impact F (N)	30.05	10.95	9.000	-5.167	p = 0.000
Impact M (Nm)	29.45	11.55	21.000	-4.842	p = 0.000
Peak F (N)	30.50	10.50	0.000	-5.410	p = 0.000
Peak M (Nm)	21.70	19.30	176.000	-0.649	p = 0.529

a = linear acceleration, ω = angular velocity, F = force, M = moment

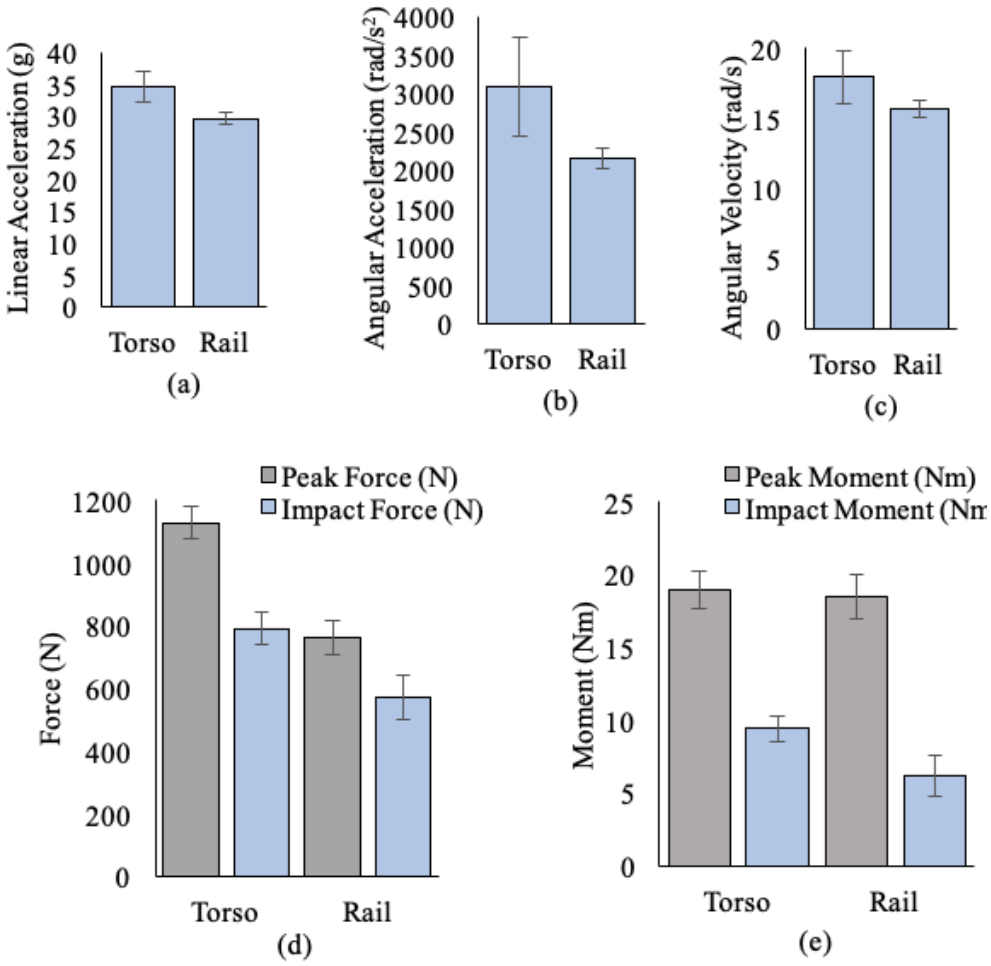

Figure 4.7: Bar charts of means and standard deviations for the head-neck-torso system and the head-neck-rail system for (a) linear acceleration, (b) angular acceleration, (c) angular velocity, (d) peak and impact force, and (e) peak and impact moment from frontal impacts with surrogate neck #3.

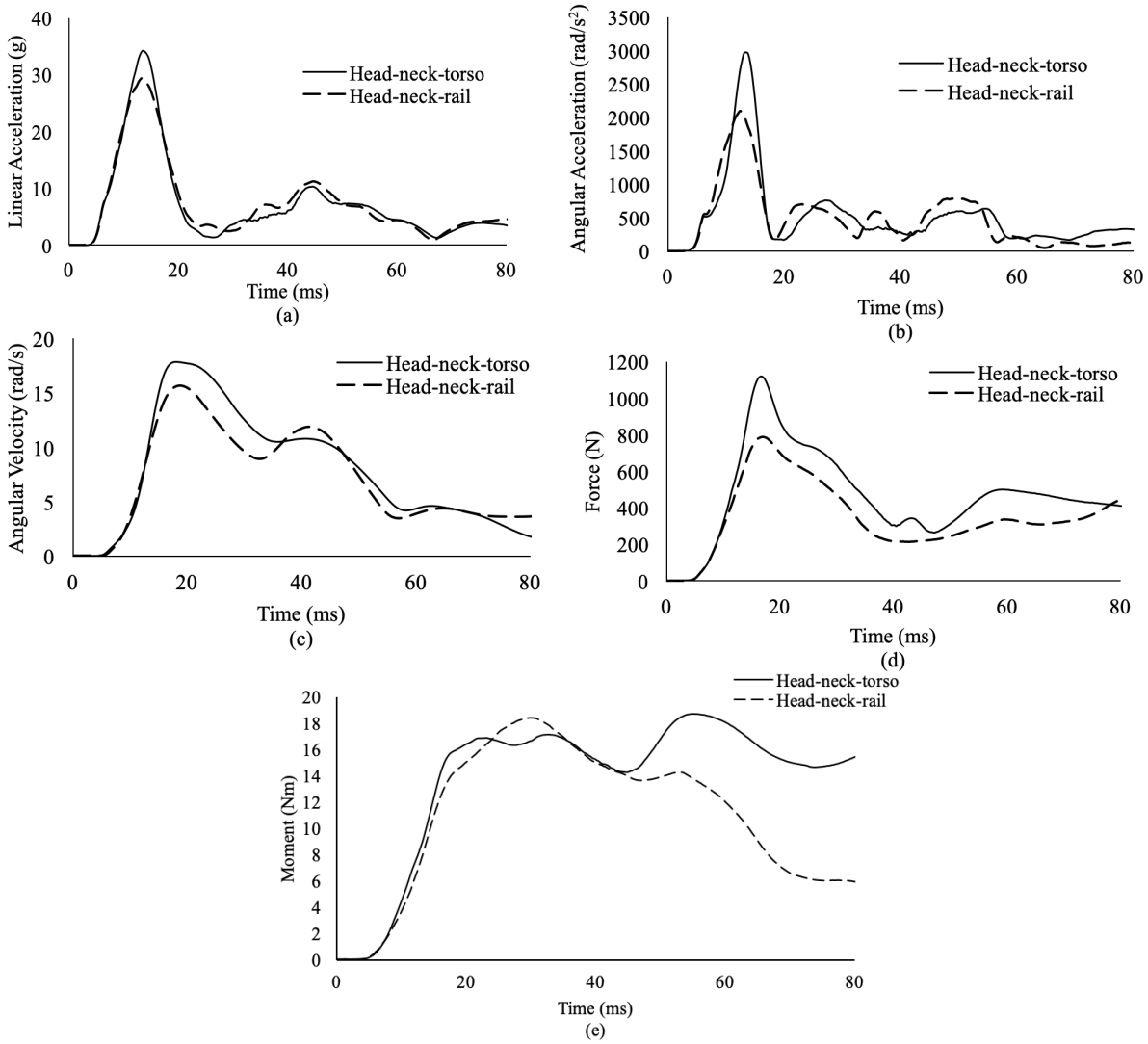

Figure 4.8:Comparison of ensemble averages from frontal impacts with the surrogate neck #3 fixed to the head-neck-torso system and head-neck-rail system for (a) linear acceleration, (b) angular acceleration, (c) angular velocity, (d) force, and (e) moment.

4.2.2 Lateral

Out of a combination of 28 impact metric comparisons, 71.4% (20 of 28) were higher for the head-neck-torso system compared to the head-neck-rail system. In addition to all linear acceleration values being higher for the torso system than the rail system, impact moment and peak force are

also higher for all surrogate necks from the torso system in the lateral direction. Conversely, all four necks showed lower peak moment values for the torso system than rail system.

4.2.2.1 Hybrid III

Mean±standard deviation, 95% confidence interval, mean difference, and percent change values of the kinematic impact metrics are presented in Table 4.22 and the kinetic impact metrics are presented in Table 4.23 for impacts with the Hybrid III fixed to the head-neck-torso system and the head-neck-rail system. Independent samples two-tailed t-test and Welch t-test results are shown in Table 4.24 for linear acceleration, angular acceleration, and angular velocity. Mean ranks, U statistics, z-scores, and p-values from a Mann-Whitney U Test are presented in Table 4.25 for impact force, impact moment, peak force, and peak moment. A visual representation of the average peak kinematic and kinetic data is presented in Figure 4.9. Time series data of ensemble averages for all impact metrics with the head-neck torso system and the head-neck-rail system are shown in Figure 4.10. The only kinematic and kinetic impact metric that resulted in higher peak values for the head-neck-rail system was peak angular velocity and peak moment.

Table 4.22: Mean±SD, 95% CI, mean difference (M.D.), and percent change (P.C.) values of kinematic impact metrics from lateral impacts with the Hybrid III neck fixed to head-neck-torso system and head-neck-rail system.

		Peak *a* (g)	Peak α (rad/s^2)	Peak ω (rad/s)
Torso	Mean±SD	48.6±2.1	4054.7±182.1	22.7±0.8
	95% CI	(47.6, 49.9)	(3969.5, 4140.0)	(22.3, 23.0)
Rail	Mean±SD	40.8±1.5	3532.7±185.6	22.9±0.2
	95% CI	(40.1, 41.5)	(3445.8, 3619.5)	(22.9, 23.1)
	M.D.	7.8	522.0	-0.3

P.C.	+19.2%	+14.8%	-1.3%

a = linear acceleration, α = angular acceleration, ω = angular velocity

Table 4.23: Mean±SD, 95% CI, mean difference (M.D.), and percent change (P.C.) values of kinetic impact metrics from lateral impacts with the Hybrid III neck fixed to head-neck-torso system and head-neck-rail system.

		Impact F (N)	Impact M (Nm)	Peak F (N)	Peak M (Nm)
Torso	Mean±SD	334.4±26.2	4.4±1.9	541.5±47.5	28.8±1.4
	95% CI	(322.1, 346.6)	(3.5, 5.3)	(519.2, 563.7)	(28.2, 29.5)
Rail	Mean±SD	285.0±16.4	3.5±1.4	524.7±25.0	35.0±0.6
	95% CI	(277.3, 292.7)	(2.9, 4.1)	(513.1, 536.4)	(34.7, 35.3)
	M.D.	49.4	0.9	16.8	-6.2
	P.C.	+17.3%	+24.9%	+3.2%	-17.6%

F = force, M = moment

All average peak impact metrics except angular velocity, impact moment, and peak force were statistically different between the head-neck-torso system and the head-neck-rail system for lateral impacts with the Hybrid III neck. The resultant mean angular velocity for the head-neck-torso system (22.7 ± 0.8 rad/s) was 1.3% lower than the mean angular velocity of the head-neck-rail system (22.9 ± 0.2 rad/s), and no statistical difference was found (95% CI: -0.8, 0.02 rad/s), t(20.952)=-1.965, p=0.063. Despite no statistical difference found for impact moment, the largest percent change in means, 24.9%, was seen, U = 136.000, z = -1.731, p = 0.086.

Table 4.24: Independent samples two-tailed t-test or Welch t-test results for appropriate impact metrics from lateral impacts with the Hybrid III neck. Significant p-values are shaded in grey.

	t-statistic	df	95% CI of the Difference	p-value
Peak a (g)	13.531	38	6.6, 9.0	p<0.001
Peak α (rad/s^2)	8.979	38	404.3, 639.7	p<0.001
Peak ω (rad/s)*	-1.965	20.952	-0.8, 0.02	p=0.063

a = linear acceleration, α = angular acceleration, ω = angular velocity
*Welch t-test

Table 4.25: Mean ranks, U statistics, z-scores, and p-values from a Mann-Whitney U Test for lateral impacts with the Hybrid III neck for all impact metrics. Significant p-values are shaded in grey.

	Mean Rank				
	Head-neck-torso	Head-neck-rail	*U* Statistic	z-score	p-value
Impact F (N)	29.90	11.10	12.000	-5.085	p = 0.000
Impact M (Nm)	23.70	17.30	136.000	-1.731	p = 0.086
Peak F (N)	22.45	18.55	161.000	0.291	p = 0.301
Peak M (Nm)	10.50	30.50	400.000	5.410	p = 0.000

F = force, M = moment

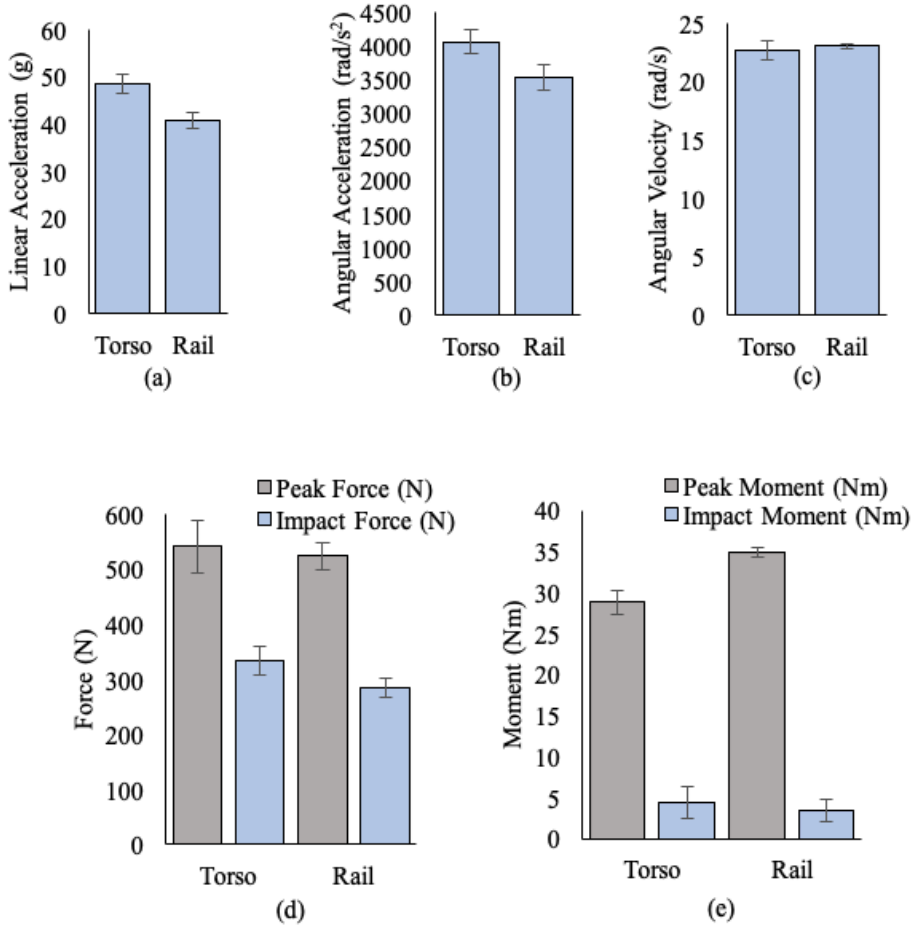

Figure 4.9: Bar charts of means and standard deviations for the head-neck-torso system and the head-neck-rail system for (a) linear acceleration, (b) angular acceleration, (c) angular velocity, (d) peak and impact force, and (e) peak and impact moment from lateral impacts with the Hybrid III neck.

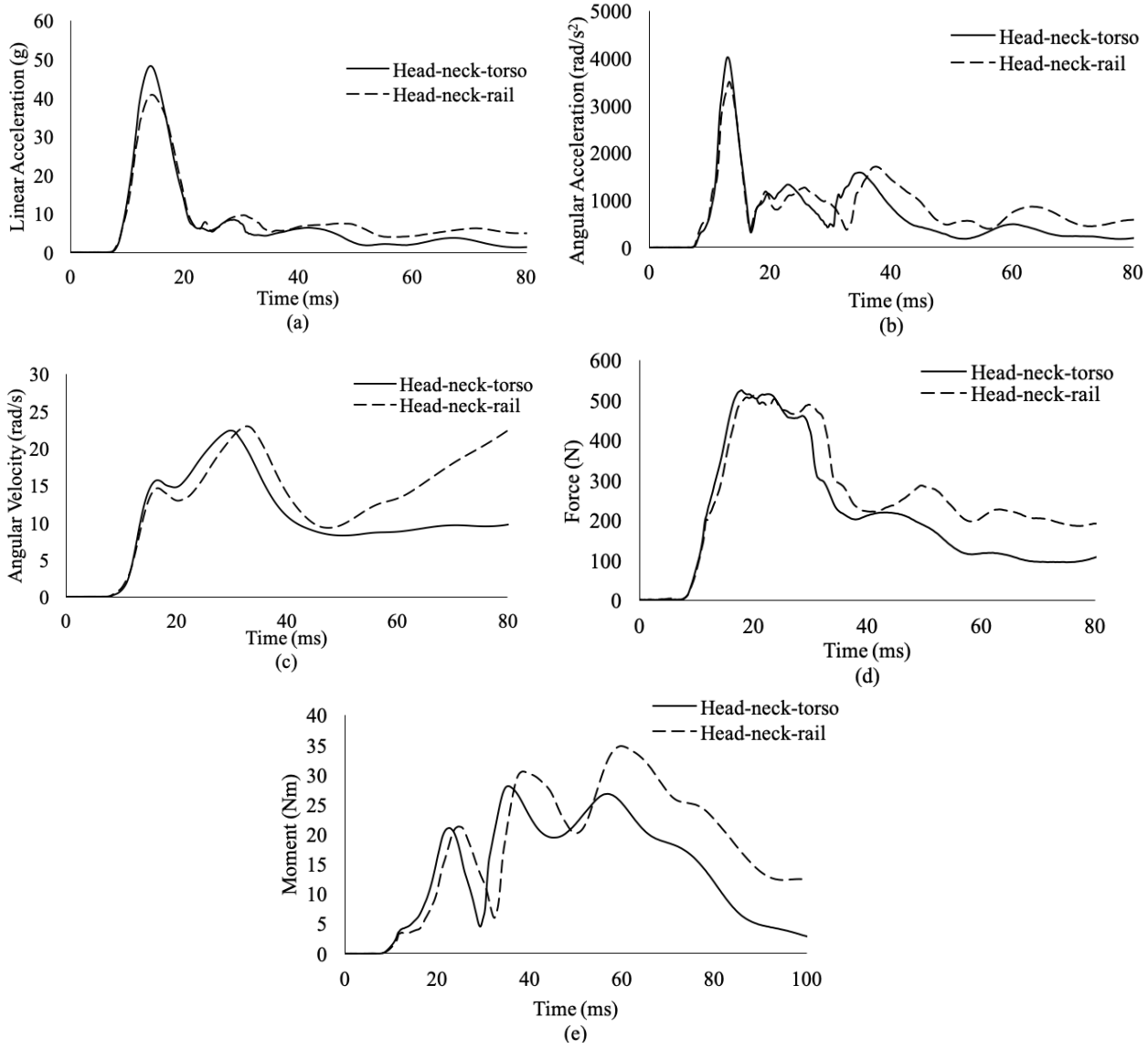

Figure 4.10: Comparison of ensemble averages from lateral impacts with the Hybrid III neck fixed to the head-neck-torso system and head-neck-rail system for (a) linear acceleration, (b) angular acceleration, (c) angular velocity, (d) force, and (e) moment.

4.2.2.2 Surrogate Neck #1

Mean±standard deviation, 95% confidence interval, mean difference, and percent change values of the kinematic impact metrics are presented in Table 4.26 and the kinetic impact metrics are

presented in Table 4.27 for impacts with surrogate neck #1 fixed to the head-neck-torso system and the head-neck-rail system. Independent samples two-tailed t-test and Welch t-test results are shown in Table 4.28 for linear acceleration, angular acceleration, impact force, impact moment, and peak moment. Mean ranks, U statistics, z-scores, and p-values from a Mann-Whitney U Test are presented in Table 4.29 for angular velocity and peak force. A visual representation of the average peak kinematic and kinetic data is presented in Figure 4.11. Time series data of ensemble averages for all impact metrics with the head-neck torso system and the head-neck-rail system are shown in Figure 4.12. All impact metrics were higher from the head-neck-torso system except for peak moment.

Table 4.26: Mean±SD, 95% CI, mean difference (M.D.), and percent change (P.C.) values of kinematic impact metrics from lateral impacts with surrogate neck #1 fixed to head-neck-torso system and head-neck-rail system.

		Peak a (g)	Peak α (rad/s^2)	Peak ω (rad/s)
Torso	Mean±SD	48.8±2.2	3617.4±253.0	25.4±0.7
	95% CI	(47.8, 49.8)	(3499.0, 3735.8)	(25.1, 25.8)
Rail	Mean±SD	43.1±1.8	3063.5±65.2	24.9±0.6
	95% CI	(42.3, 44.0)	(3033.0, 3094.0)	(24.6, 25.2)
	M.D.	5.7	553.9	0.5
	P.C.	+13.2%	+18.1%	+2.2%

a = linear acceleration, α = angular acceleration, ω = angular velocity

Table 4.27: Mean±SD, 95% CI, mean difference (M.D.), and percent change (P.C.) values of kinetic impact metrics from lateral impacts with surrogate neck #1 fixed to head-neck-torso system and head-neck-rail system.

		Impact F (N)	Impact M (Nm)	Peak F (N)	Peak M (Nm)
Torso	Mean±SD	251.1±13.2	4.7±0.7	705.5±121.9	20.1±0.6
	95% CI	(244.9, 257.2)	(4.4, 5.0)	(648.5, 762.6)	(19.9, 20.4)
Rail	Mean±SD	206.6±11.4	4.0±0.4	661.4±34.3	25.2±0.6
	95% CI	(201.3, 211.9)	(3.8, 4.2)	(645.4, 677.5)	(25.0, 25.5)
	M.D.	44.5	0.7	44.1	-5.1
	P.C.	+21.5%	+17.2%	+6.7%	-20.1%

F = force, M = moment

A statistically significant difference was seen in all impact metrics except peak force between the head-neck-torso system (mean rank = 21.75) and the head-neck-rail system (mean rank = 19.25) was not statistically different, U = 175.000, z = -0.676, p = 0.512. The greatest percent change, 21.5%, was seen in the impact force measurements between the head-neck-torso system (251.1 ± 13.2 N) than the head-neck-rail system (206.6 ± 11.4 N), (95% CI: 36.6, 52.4 N), t(38)=11.421, p<0.001. The smallest percent change was seen in peak angular velocity values for the head-neck-torso system (mean rank = 25.55) and the head-neck-rail system (mean rank = 15.45), although a statistical difference was still found, U = 99.000, z = -2.732, p = 0.006.

Table 4.28: Independent samples two-tailed t-test or Welch t-test results for appropriate impact metrics from lateral impacts with the surrogate neck #1. Significant p-values are shaded in grey.

	t-statistic	df	95% CI of the Difference	p-value
Peak a (g)	9.081	38	4.42, 6.94	p<0.001
Peak α (rad/s^2)*	9.482	21.513	432.6, 675. 2	p<0.001
Impact F (N)	11.421	38	36.6, 52.4	p<0.001
Impact M (Nm)	3.950	38	0.34, 1.05	p<0.001
Peak M (Nm)	53.724	38	9.39, 10.12	p<0.001

a = linear acceleration, α = angular acceleration, F = force, M = moment
*Welch t-test

Table 4.29: Mean ranks, U statistics, z-scores, and p-values from a Mann-Whitney U Test for lateral impacts with surrogate neck #1 for all impact metrics. Significant p-values are shaded in grey.

	Mean Rank				
	Head-neck-torso	Head-neck-rail	*U* Statistic	z-score	p-value
Peak ω (rad/s)	25.55	15.45	99.000	-2.732	p = 0.006
Peak F (N)	21.75	19.25	175.000	-0.676	p = 0.512

ω = angular velocity, F = force

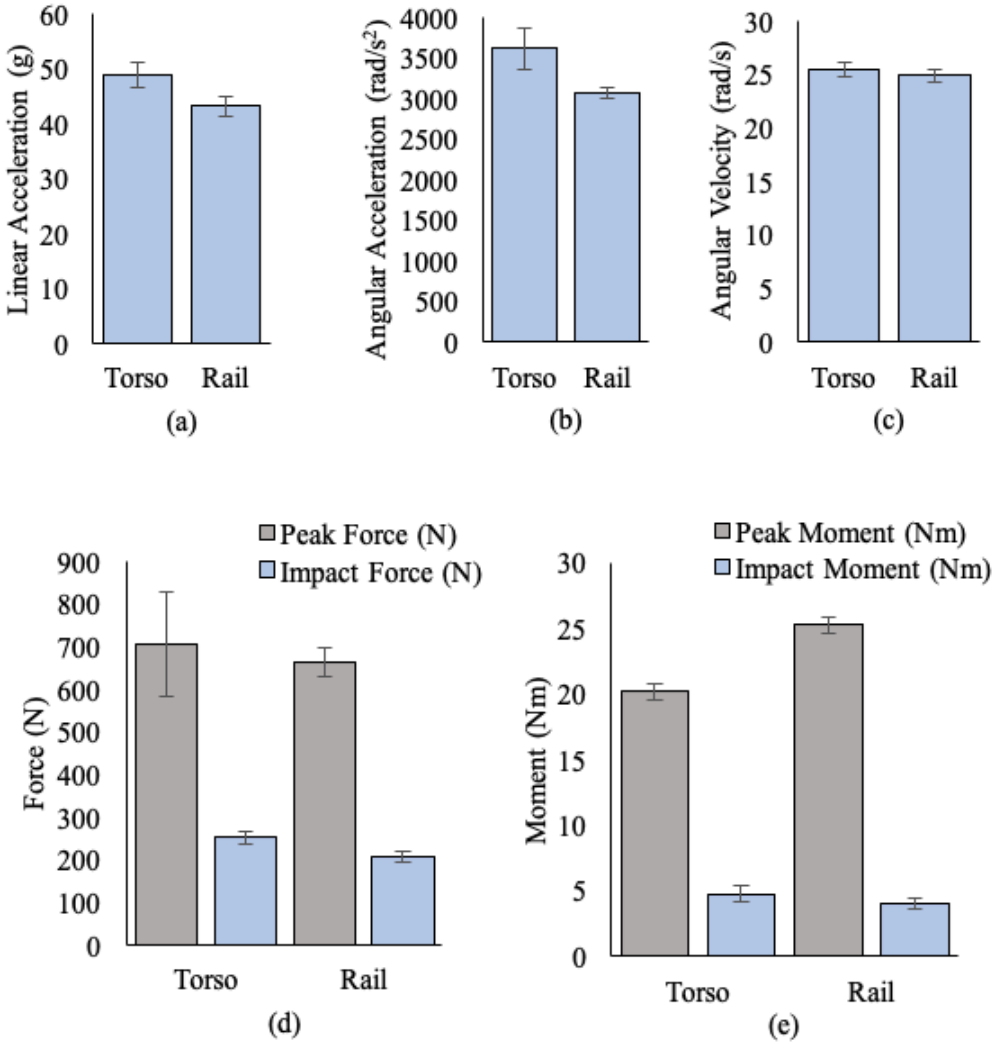

Figure 4.11: Bar charts of means and standard deviations for the head-neck-torso system and the head-neck-rail system for (a) linear acceleration, (b) angular acceleration, (c) angular velocity, (d) peak and impact force, and (e) peak and impact moment from lateral impacts with the surrogate neck #1.

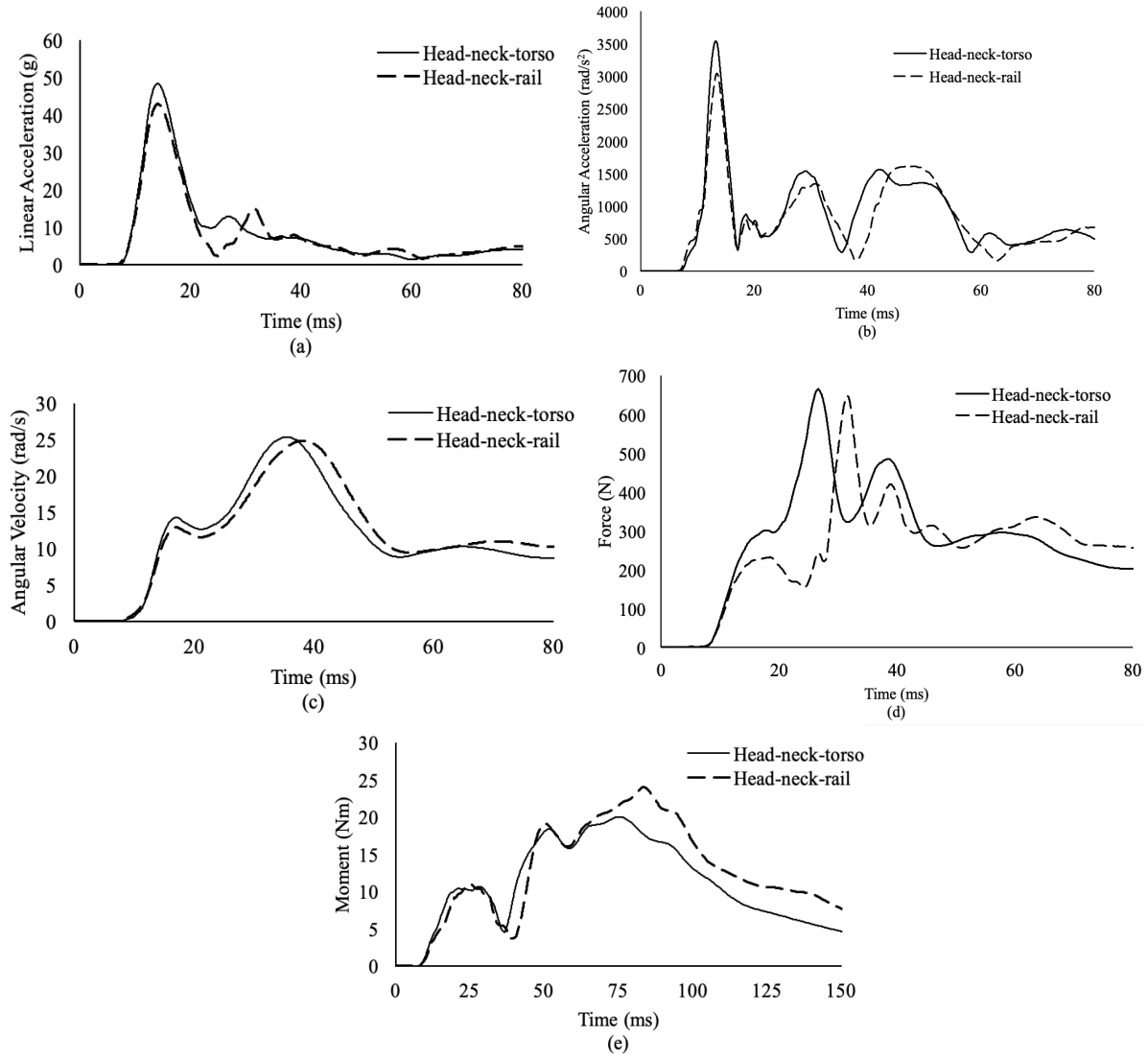

Figure 4.12: Comparison of ensemble averages from lateral impacts with the surrogate neck #1 fixed to the head-neck-torso system and head-neck-rail system for (a) linear acceleration, (b) angular acceleration, (c) angular velocity, (d) force, and (e) moment.

4.2.2.3 Surrogate Neck #2

Mean±standard deviation, 95% confidence interval, mean difference, and percent change values of the kinematic impact metrics are presented in Table 4.30 and the kinetic impact metrics are presented in Table 4.31 for impacts with surrogate neck #2 fixed to the head-neck-torso system

and the head-neck-rail system. Independent samples two-tailed t-test and Welch t-test results are shown in Table 4.32 for linear acceleration, angular acceleration, angular velocity, impact force, impact moment, and peak force. Mean rank, U statistic, z-score, and p-value from a Mann-Whitney U Test are presented in Table 4.33 for peak moment. A visual representation of the average peak kinematic and kinetic data is presented in Figure 4.13. Time series data of ensemble averages for all impact metrics with the head-neck torso system and the head-neck-rail system are shown in Figure 4.14. Similar to results from lateral impacts with surrogate neck #1, all impact metrics were higher from the head-neck-torso system except for peak moment.

Table 4.30: Mean±SD, 95% CI, mean difference (M.D.), and percent change (P.C.) values of kinematic impact metrics from lateral impacts with surrogate neck #2 fixed to head-neck-torso system and head-neck-rail system.

		Peak a (g)	Peak α (rad/s^2)	Peak ω (rad/s)
Torso	Mean±SD	49.2±1.8	3365.4±175.9	26.6±0.9
	95% CI	(48.3, 50.0)	(3283.0, 3447.7)	(26.2, 27.0)
Rail	Mean±SD	42.4±0.9	3001.9±95.3	24.0±0.7
	95% CI	(42.0, 42.8)	(2957.3, 3046.5)	(23.7, 24.3)
	M.D.	6.8	363.5	2.6
	P.C.	+16.1%	+12.1%	+10.7%

a = linear acceleration, α = angular acceleration, ω = angular velocity

Table 4.31: Mean±SD, 95% CI, mean difference (M.D.), and percent change (P.C.) values of kinetic impact metrics from lateral impacts with surrogate neck #2 fixed to head-neck-torso system and head-neck-rail system.

		Impact F (N)	Impact M (Nm)	Peak F (N)	Peak M (Nm)
Torso	Mean±SD	290.0±17.6	6.5±1.2	790.7±84.2	19.1±0.4
	95% CI	(281.7, 298.2)	(5.9, 7.0)	(751.2, 830.1)	(19.0, 19.3)
Rail	Mean±SD	209.7±7.3	3.2±0.3	466.9±31.1	22.1±0.7
	95% CI	(206.2, 213.1)	(3.0, 3.4)	(452.4, 481.5)	(21.8, 22.4)
	M.D.	80.3	3.3	323.7	-3.0
	P.C.	+38.3%	+102.1%	+69.3%	-13.4%

F = force, M = moment

All impact metrics were significantly different between the torso assembly and the rail assembly. The smallest percent change, 10.7%, was seen in angular velocity between the head-neck-torso system (26.6 ± 0.9 rad/s) than the head-neck-rail system (24.0 ± 0.7 rad/s), (95% CI: 2.1, 3.1 rad/s), t(38)=10.195, p<0.001. Conversely, the largest percent change, 102.1% was seen in impact moment between the head-neck-torso system (6.5 ± 1.2 Nm) and the head-neck-rail system (3.2 ± 0.3 Nm), (95% CI: 2.7, 3.9 Nm), t(11.538)=22.012, p<0.001.

Table 4.32: Independent samples two-tailed t-test or Welch t-test results for appropriate impact metrics from lateral impacts with the surrogate neck #2. Significant p-values are shaded in grey.

	t-statistic	df	95% CI of the Difference	p-value
Peak *a* (g)*	15.273	27.651	5.90, 7.73	p<0.001
Peak α (rad/s^2)*	8.125	29.267	272.02, 454.95	p<0.001
Peak ω (rad/s)	10.195	38	2.06, 3.08	p<0.001
Impact F (N)*	18.852	25.409	71.54, 89.07	p<0.001
Impact M (Nm)*	11.538	22.012	2.68, 3.86	p<0.001
Peak F (N)*	16.126	24.080	282.29, 365.13	p<0.001

a = linear acceleration, α = angular acceleration, ω = angular velocity, F = force, M = moment
*Welch t-test

Table 4.33: Mean ranks, U statistics, z-scores, and p-values from a Mann-Whitney U Test for lateral impacts with surrogate neck #2 for all impact metrics. Significant p-values are shaded in grey.

	Mean Rank				
	Head-neck-torso	Head-neck-rail	*U* Statistic	z-score	p-value
Peak M (Nm)	10.50	30.50	400.000	5.410	p = 0.000

M = moment

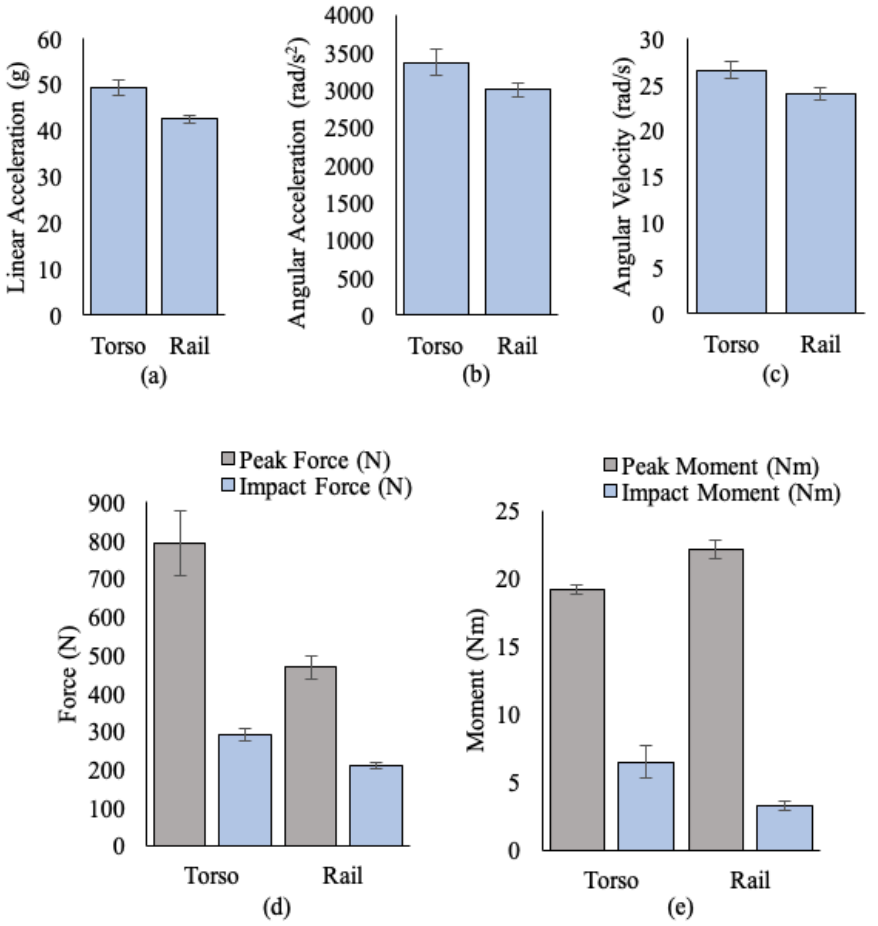

Figure 4.13: Bar charts of means and standard deviations for the head-neck-torso system and the head-neck-rail system for (a) linear acceleration, (b) angular acceleration, (c) angular velocity, (d) peak and impact force, and (e) peak and impact moment from lateral impacts with surrogate neck #2.

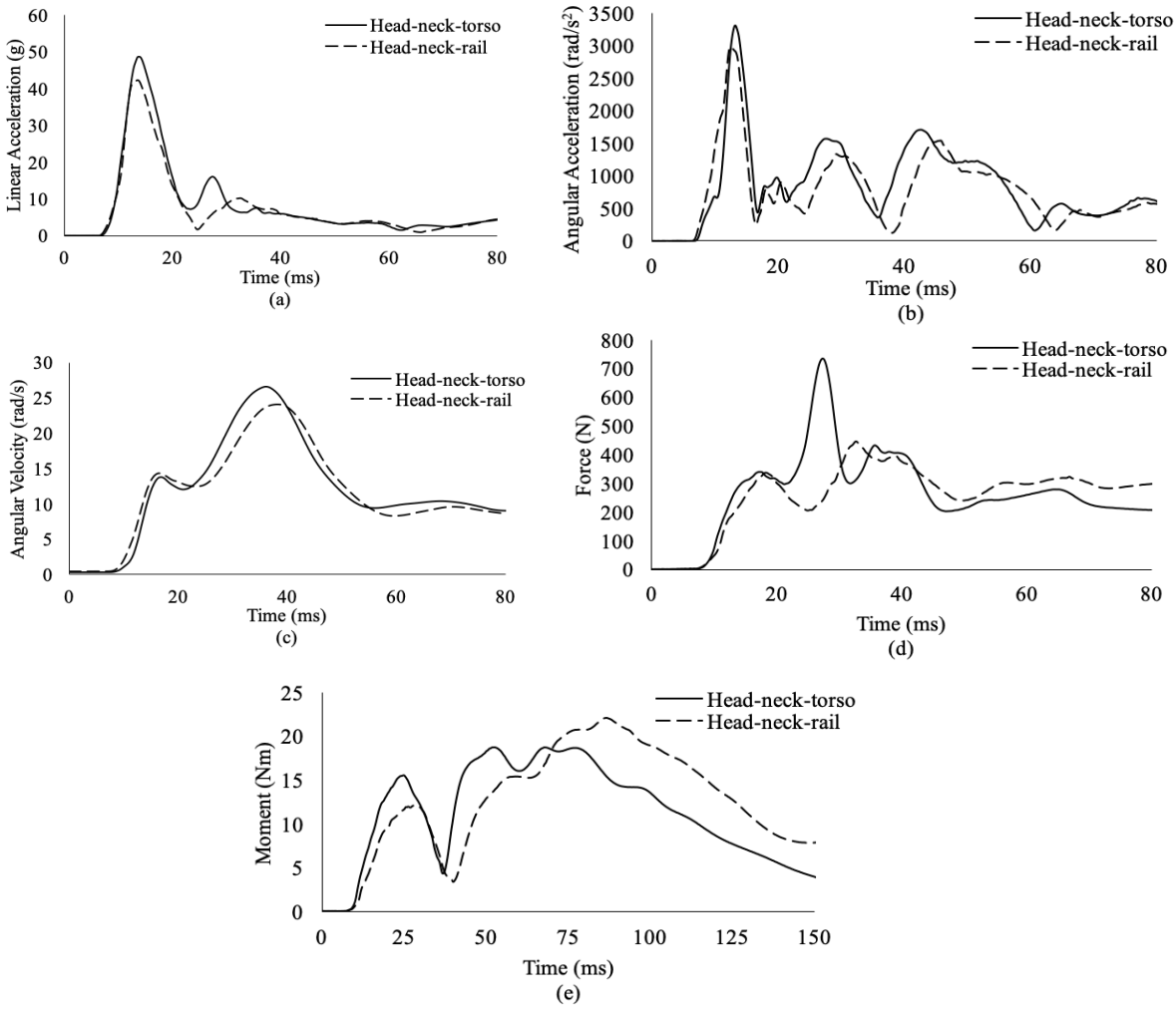

Figure 4.14: Comparison of ensemble averages from lateral impacts with the surrogate neck #2 fixed to the head-neck-torso system and head-neck-rail system for (a) linear acceleration, (b) angular acceleration, (c) angular velocity, (d) force, and (e) moment.

4.2.2.4 Surrogate Neck #3

Mean±standard deviation, 95% confidence interval, mean difference, and percent change values of the kinematic impact metrics are presented in Table 4.34 and the kinetic impact metrics are presented in Table 4.35 for impacts with surrogate neck #3 fixed to the head-neck-torso system and the head-neck-rail system. Independent samples two-tailed t-test results are shown in Table

4.36 for angular acceleration, impact force, impact moment, peak force, and peak moment. Mean rank, U statistic, z-score, and p-value from a Mann-Whitney U Test are presented in Table 4.37 for linear acceleration and angular velocity. A visual representation of the average peak kinematic and kinetic data is presented in Figure 4.15. Time series data of ensemble averages for all impact metrics with the head-neck torso system and the head-neck-rail system are shown in Figure 4.16.

Table 4.34: Mean±SD, 95% CI, mean difference (M.D.), and percent change (P.C.) values of kinematic impact metrics from lateral impacts with surrogate neck #3 fixed to head-neck-torso system and head-neck-rail system.

		Peak a (g)	Peak α (rad/s^2)	Peak ω (rad/s)
Torso	Mean±SD	48.9±3.5	3369.2±192.6	26.3±0.9
	95% CI	(47.3, 50.6)	(3279.1, 3459.4)	(25.9, 26.7)
Rail	Mean±SD	46.6±2.3	3447.7±198.7	26.9±0.7
	95% CI	(45.5, 47.7)	(3354.7, 3540.7)	(26.6, 27.3)
	M.D.	2.3	-78.5	-0.6
	P.C.	+4.9%	-2.3%	-2.4%

a = linear acceleration, α = angular acceleration, ω = angular velocity

Table 4.35: Mean±SD, 95% CI, mean difference (M.D.), and percent change (P.C.) values of kinetic impact metrics from lateral impacts with surrogate neck #3 fixed to head-neck-torso system and head-neck-rail system.

		Impact F (N)	Impact M (Nm)	Peak F (N)	Peak M (Nm)
Torso	Mean±SD	223.4±17.8	4.1±0.7	804.6±63.5	18.0±0.5
	95% CI	(215.1, 231.7)	(3.8, 4.4)	(774.9, 834.3)	(17.8, 18.3)
Rail	Mean±SD	234.7±18.8	2.2±0.7	538.9±40.4	25.0±0.5
	95% CI	(225.9, 243.5)	(1.9, 2.5)	(520.0, 557.8)	(24.8, 25.3)
	M.D.	-11.3	1.9	265.7	-7.0
	P.C.	-4.8%	+87.8%	+49.3%	-27.9%

F = force, M = moment

A statistical difference was seen between the head-neck-torso and head-neck-rail systems when comparing linear acceleration, angular velocity, impact moment, peak force, and peak moment.

Alternatively, no statistical difference was determined for angular acceleration and impact force between the head-neck-torso system (3369.2 ± 192.6 rad/s^2 and 804.6 ± 63.5 N) and the head-neck-rail system (3447.7 ± 198.7 rad/s^2 and 538.9 ± 40.4 N), (95% CI: -203.7, 46.8 rad/s^2), t(38)=-1.268, p=0.212, (95% CI: -23.0, 0.4 N), t(38)=-1.961, p=0.057, respectively. The largest percent change, 87.8%, was seen in impact moment values between the head-neck-torso system (4.1 ± 0.7 Nm) and the head-neck-rail system (2.2 ± 0.7 Nm), (95% CI: 1.5, 2.3 Nm), t(38)=9.149, p<0.001.

Table 4.36: Independent samples two-tailed t-test results for appropriate impact metrics from lateral impacts with the surrogate neck #3. Significant p-values are shaded in grey.

	t-statistic	df	95% CI of the Difference	p-value
Peak α (rad/s^2)	-1.268	38	-203.7, 46.8	p=0.212
Impact F (N)	-1.961	38	-23.04, 0.37	p=0.057
Impact M (Nm)	9.149	38	1.49, 2.33	p<0.001
Peak F (N)	15.776	38	231.6, 299.8	p<0.001
Peak M (Nm)	-45.086	38	-7.30, -6.67	p<0.001

a = linear acceleration, α = angular acceleration, ω = angular velocity, F = force, M = moment

Table 4.37: Mean ranks, U statistics, z-scores, and p-values from a Mann-Whitney U Test for lateral impacts with surrogate neck #3 for all impact metrics. Significant p-values are shaded in grey.

	Mean Rank				
	Head-neck-torso	Head-neck-rail	*U* Statistic	z-score	p-value
Peak *a* (g)	24.55	16.45	119.000	-2.191	p = 0.028
Peak ω (rad/s)	15.85	25.15	293.000	2.516	p = 0.011

a = linear acceleration, ω = angular velocity

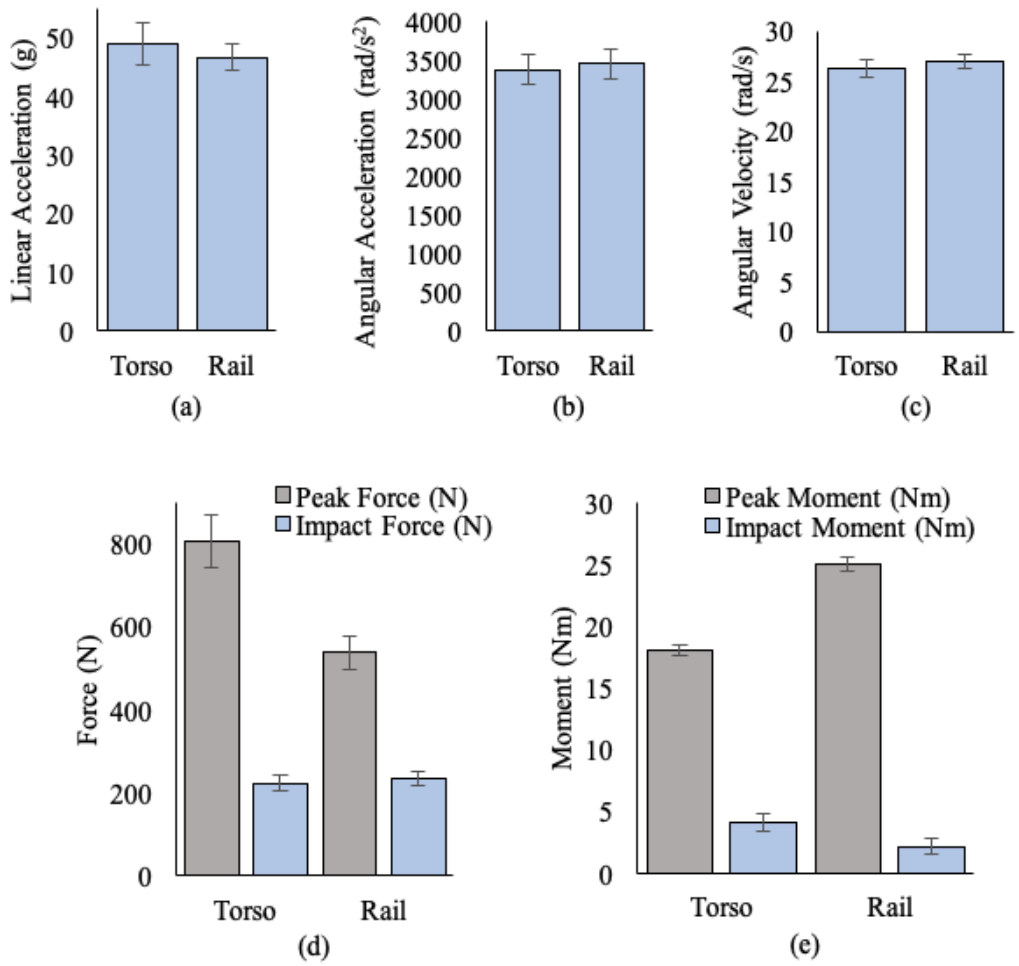

Figure 4.15: Bar charts of means and standard deviations for the head-neck-torso system and the head-neck-rail system for (a) linear acceleration, (b) angular acceleration, (c) angular velocity, (d) peak and impact force, and (e) peak and impact moment from lateral impacts with surrogate neck #3.

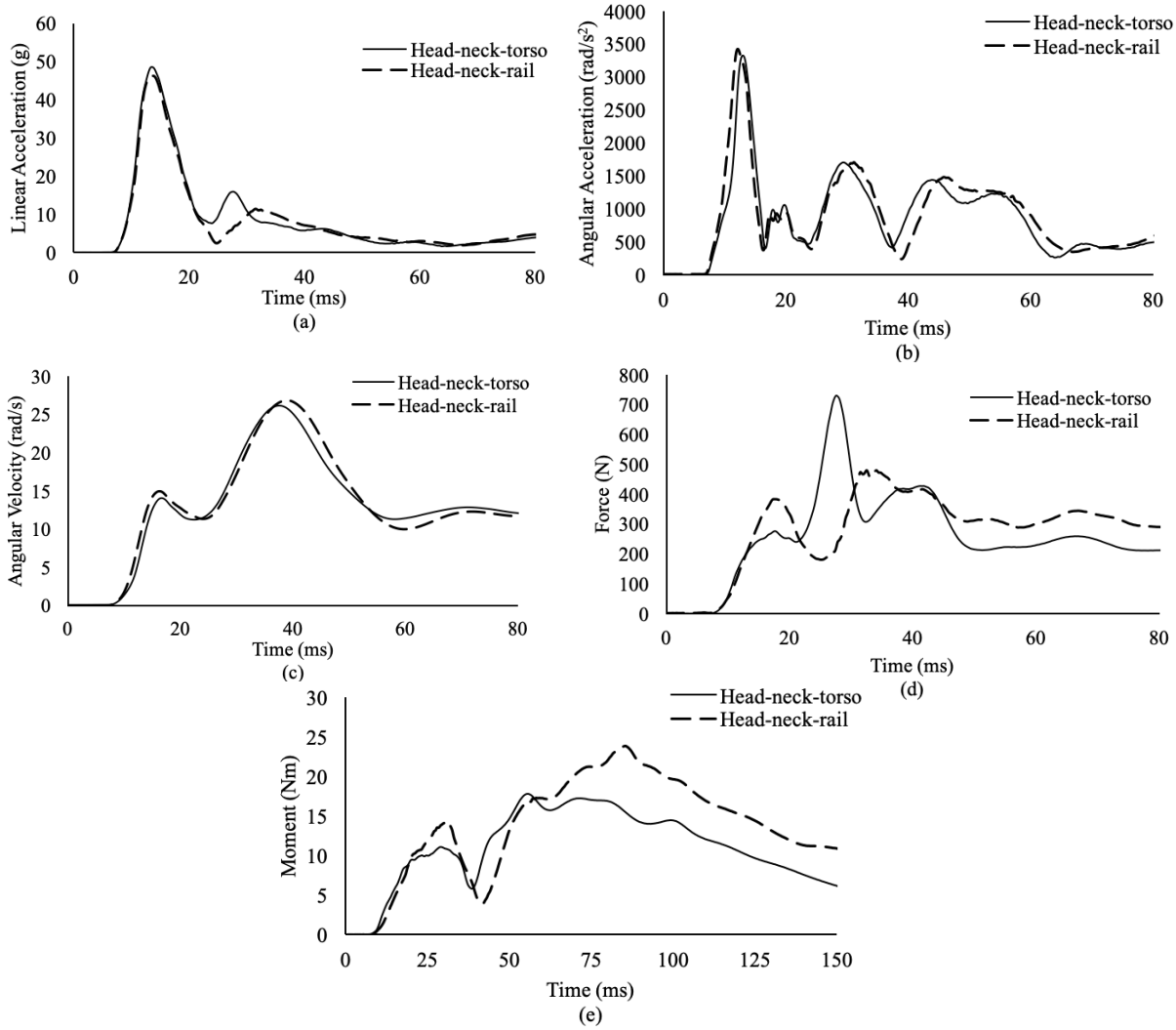

Figure 4.16: Comparison of ensemble averages from lateral impacts with the surrogate neck #3 fixed to the head-neck-torso system and head-neck-rail system for (a) linear acceleration, (b) angular acceleration, (c) angular velocity, (d) force, and (e) moment.

4.2.3 Front Boss

Out of a combination of 28 impact metric comparisons, there is an even split (14 of 28) between the number of impact metrics that are higher for the torso system than the rail system. Similar to frontal impacts, linear acceleration is the only impact metric that showed higher values in all four necks for the torso system than the rail system. Conversely, all four necks showed lower angular velocity values for the torso system than the rail system.

4.2.3.1 Hybrid III

Mean±standard deviation, 95% confidence interval, mean difference, and percent change values of the kinematic impact metrics are presented in Table 4.38 and the kinetic impact metrics are presented in Table 4.39 for impacts with Hybrid III neck fixed to the head-neck-torso system and the head-neck-rail system. Independent samples two-tailed t-test and Welch t-test results are shown in Table 4.40 for angular acceleration, impact force, impact moment, peak force, and peak moment. Mean rank, U statistic, z-score, and p-value from a Mann-Whitney U Test are presented in Table 4.41 for linear acceleration and angular velocity. A visual representation of the average peak kinematic and kinetic data is presented in Figure 4.17. Time series data of ensemble averages for all impact metrics with the head-neck torso system and the head-neck-rail system are shown in Figure 4.18. For front boss impact with the Hybrid III neck, all impact metrics were higher for the head-neck-torso system than the head-neck-rail system except for angular velocity.

Table 4.38: Mean±SD, 95% CI, mean difference (M.D.), and percent change (P.C.) values of kinematic impact metrics from front boss impacts with the Hybrid III neck fixed to head-neck-torso system and head-neck-rail system.

		Peak a (g)	Peak α (rad/s^2)	Peak ω (rad/s)
Torso	Mean±SD	44.0±2.2	4829.1±224.8	18.2±0.6
	95% CI	(43.0, 45.0)	(4723.8, 4934.3)	(18.0, 18.5)
Rail	Mean±SD	42.4±0.9	3872.0±93.3	19.6±1.3
	95% CI	(42.0, 42.8)	(3828.4, 3915.7)	(19.1, 20.3)
	M.D.	1.6	957.1	-1.4
	P.C.	+3.7%	+24.7%	-7.1%

a = linear acceleration, α = angular acceleration, ω = angular velocity

Table 4.39: Mean±SD, 95% CI, mean difference (M.D.), and percent change (P.C.) values of kinetic impact metrics from front boss impacts with the Hybrid III neck fixed to head-neck-torso system and head-neck-rail system.

		Impact F (N)	Impact M (Nm)	Peak F (N)	Peak M (Nm)
Torso	Mean±SD	1252.2±124.0	7.6±0.9	1919.0±97.0	32.2±1.8
	95% CI	(1194.1, 1310.2)	(7.2, 8.1)	(1873.6, 1964.4)	(31.4, 33.0)
Rail	Mean±SD	626.8±45.1	4.2±0.6	1004.0±28.4	31.7±1.6
	95% CI	(605.7, 647.9)	(3.9, 4.5)	(990.7, 1017.3)	(30.9, 32.4)
	M.D.	625.4	3.4	915.0	0.5
	P.C.	+99.8%	+82.5%	+91.1%	+1.8%

F = force, M = moment

A statistical difference was seen for all impact metrics except peak moment between the head-neck-torso system (32.2 ± 1.8 Nm) and the head-neck-rail system (31.7 ± 1.6 Nm), (95% CI: -0.5, 1.6 Nm), t(38)=1.057, p=0.297. The smallest percent change, 3.7%, was seen in linear acceleration values between the head-neck-torso system (mean rank = 25.30) than the head-neck-rail system (mean rank = 15.70), although a statistical difference was still found, U = 104.000, z = -2.597, p = 0.009. The largest percent change, 99.8%, was seen in impact force values (95% CI: 564.5, 686.3 N), t(23.943)=21.188, p<0.001.

Table 4.40: Independent samples two-tailed t-test or Welch t-test results for appropriate impact metrics from front boss impacts with the Hybrid III neck. Significant p-values are shaded in grey.

	t-statistic	df	95% CI of the Difference	p-value
Peak α (rad/s^2)*	17.581	25.358	845.0, 1069.0	p<0.001
Impact F (N)*	21.188	23.943	564.5, 686.3	p<0.001
Impact M (Nm)	13.920	38	2.9, 4.0	p<0.001
Peak F (N)*	40.476	22.236	868.2, 961.0	p<0.001
Peak M (Nm)	1.057	38	-0.5, 1.6	p=0.297

α = angular acceleration, F = force, M = moment
*Welch t-test

Table 4.41: Mean ranks, U statistics, z-scores, and p-values from a Mann-Whitney U Test for front boss impacts with the Hybrid III neck for all impact metrics. Significant p-values are shaded in grey.

	Mean Rank				
	Head-neck-torso	Head-neck-rail	*U* Statistic	z-score	p-value
Peak *a* (g)	25.30	15.70	104.000	-2.597	p = 0.009
Peak ω (rad/s)	14.40	26.60	322.000	3.300	p = 0.001

a = linear acceleration, ω = angular velocity

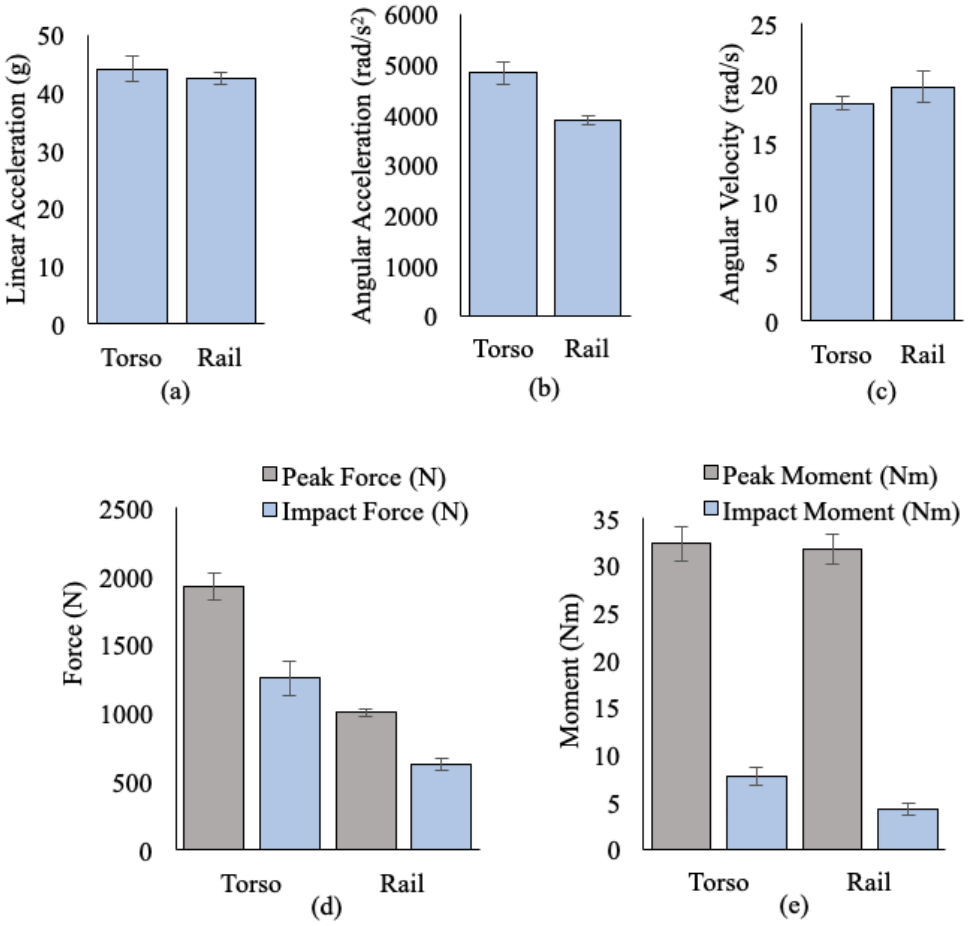

Figure 4.17: Bar charts of means and standard deviations for the head-neck-torso system and the head-neck-rail system for (a) linear acceleration, (b) angular acceleration, (c) angular velocity, (d) peak and impact force, and (e) peak and impact moment from front boss impacts with the Hybrid III neck.

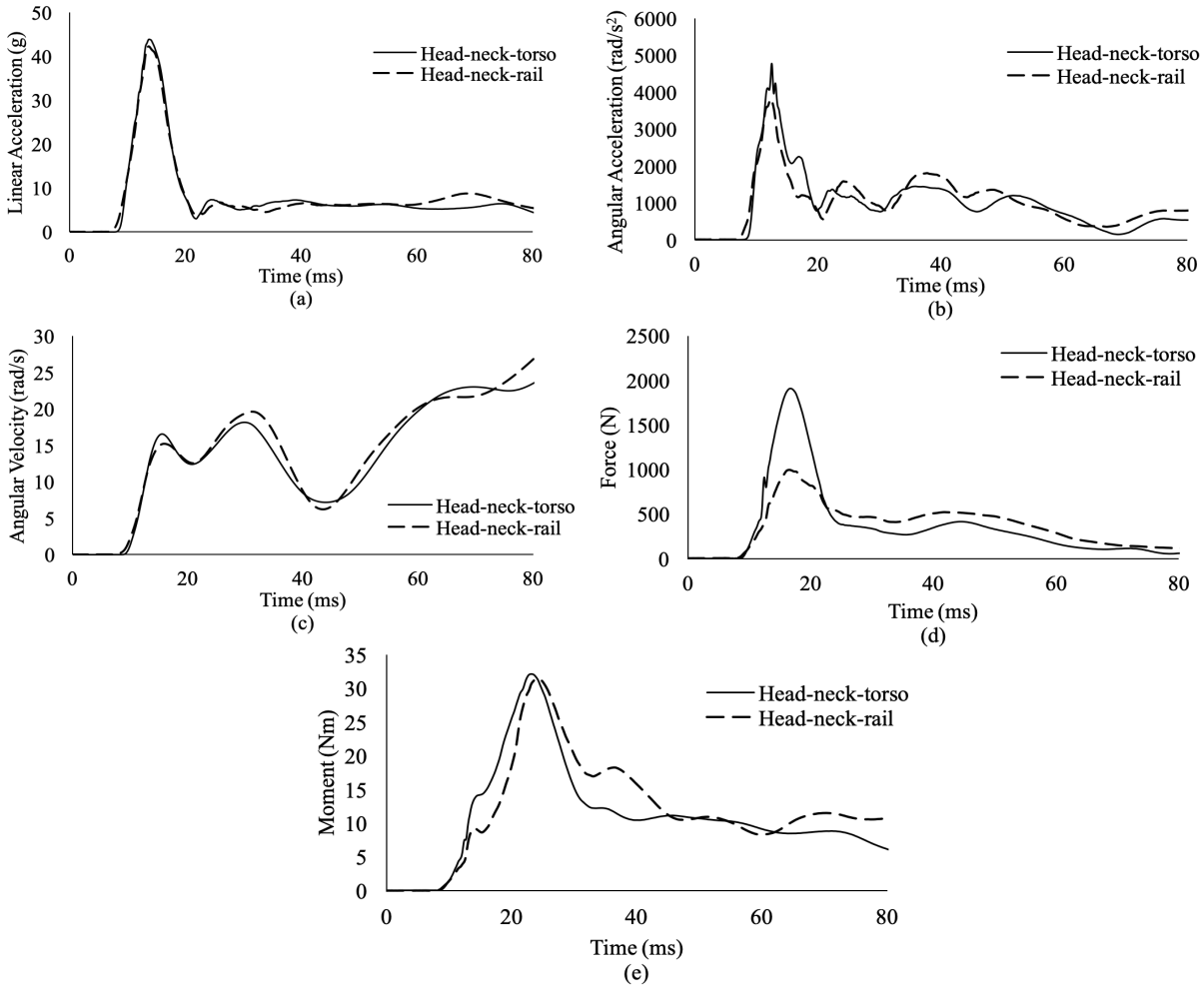

Figure 4.18: Comparison of ensemble averages from front boss impacts with the Hybrid III neck fixed to the head-neck-torso system and head-neck-rail system for (a) linear acceleration, (b) angular acceleration, (c) angular velocity, (d) force, and (e) moment.

4.2.3.2 Surrogate Neck #1

Mean±standard deviation, 95% confidence interval, mean difference, and percent change values of the kinematic impact metrics are presented in Table 4.42 and the kinetic impact metrics are presented in Table 4.43 for impacts with surrogate neck #1 fixed to the head-neck-torso system and the head-neck-rail system. Independent samples two-tailed t-test and Welch t-test results are

shown in Table 4.44 for linear acceleration, angular velocity, impact force, impact moment, and peak force. Mean rank, U statistic, z-score, and p-value from a Mann-Whitney U Test are presented in Table 4.45 for angular acceleration and peak moment. A visual representation of the average peak kinematic and kinetic data is presented in Figure 4.19. Time series data of ensemble averages for all impact metrics with the head-neck torso system and the head-neck-rail system are shown in Figure 20. Most impact metrics were higher for the head-neck-torso system for front boss impact with surrogate neck #1, except for angular velocity and peak moment.

Table 4.42: Mean±SD, 95% CI, mean difference (M.D.), and percent change (P.C.) values of kinematic impact metrics from front boss impacts with surrogate neck #1 fixed to head-neck-torso system and head-neck-rail system.

		Peak a (g)	Peak α (rad/s^2)	Peak ω (rad/s)
Torso	Mean±SD	38.0±1.3	3434.8±104.5	19.4±0.2
	95% CI	(37.4, 38.6)	(3385.9, 3483.7)	(19.3, 19.5)
Rail	Mean±SD	35.5±0.6	3175.5±84.5	19.7±0.3
	95% CI	(35.2, 35.8)	(3133.4, 3217.5)	(19.5, 19.8)
	M.D.	2.5	259.3	-0.3
	P.C.	+7.0%	+8.2%	-1.2%

a = linear acceleration, α = angular acceleration, ω = angular velocity

Table 4.43: Mean±SD, 95% CI, mean difference (M.D.), and percent change (P.C.) values of kinetic impact metrics from front boss impacts with surrogate neck #1 fixed to head-neck-torso system and head-neck-rail system.

		Impact F (N)	Impact M (Nm)	Peak F (N)	Peak M (Nm)
Torso	Mean±SD	395.8±57.3	2.9±0.3	684.5±72.9	13.1±2.0
	95% CI	(369.0, 422.6)	(2.8, 3.1)	(650.3, 719.0)	(12.2, 14.0)
Rail	Mean±SD	250.8±11.1	2.1±0.2	369.7±18.0	23.4±0.5
	95% CI	(245.3, 256.3)	(2.0, 2.2	(361.3, 378.1)	(23.1, 23.6)
	M.D.	145.0	0.8	314.8	-10.3
	P.C.	+57.8%	+40.5%	+85.1%	-44.0%

F = force, M = moment

All impact metrics showed statistically significant differences between the head-neck-torso and the head-neck-rail systems. The smallest percent change, 1.2%, was seen in angular velocity values from the head-neck-torso system (19.4 ± 0.2 rad/s) than the head-neck-rail system (19.7 ± 0.3 rad/s), (95% CI: -0.4, -0.04 rad/s), t(38)=-2.528, p=0.016. Peak force had the greatest percent change, 85.1%, between the average peaks of the head-neck-torso system (684.5 ± 72.9 N) and the head-neck-rail system (369.7 ± 18.0 N), (95% CI: 280.8, 348.8 N), t(21.288)=18.747, p<0.001.

Table 4.44: Independent samples two-tailed t-test or Welch t-test results for appropriate impact metrics from front boss impacts with the surrogate neck #1. Significant p-values are shaded in grey.

	t-statistic	df	95% CI of the Difference	p-value
Peak a (g)*	7.535	28.067	1.76, 3.05	p<0.001
Peak ω (rad/s)	-2.528	38	-0.41, -0.05	p=0.016
Impact F (N)*	11.039	20.408	117.6, 170.4	p<0.001
Impact M (Nm)	9.737	38	0.66, 1.00	p<0.001
Peak F (N)*	18.747	21.288	280.8, 348.8	p<0.001

a = linear acceleration, ω = angular velocity, F = force, M = moment
*Welch t-test

Table 4.45: Mean ranks, U statistics, z-scores, and p-values from a Mann-Whitney U Test for front boss impacts with surrogate neck #1 for all impact metrics. Significant p-values are shaded in grey.

	Mean Rank				
	Head-neck-torso	Head-neck-rail	*U* Statistic	z-score	p-value
Peak α (rad/s^2)	29.80	11.20	14.000	-5.031	p = 0.000
Peak M (Nm)	10.50	30.50	400.000	5.410	p = 0.000

α = angular acceleration, M = moment

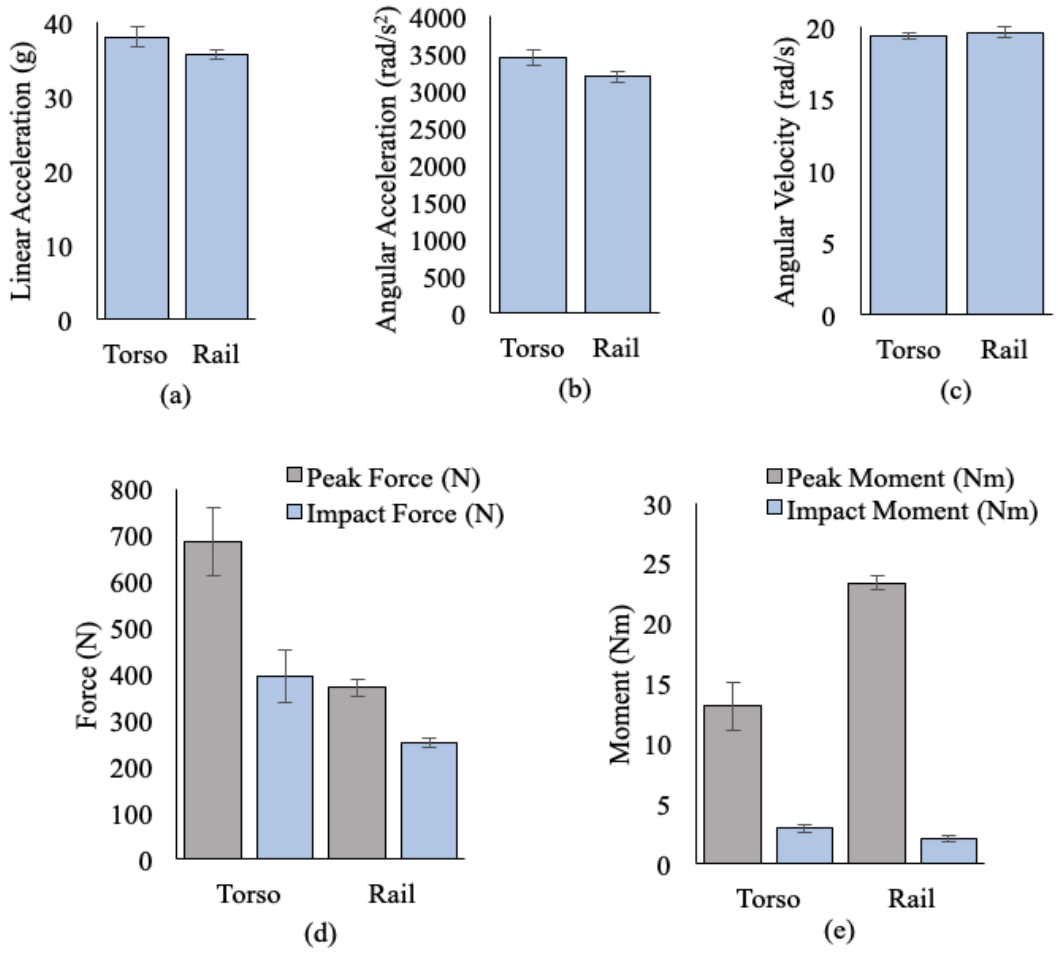

Figure 4.19: Bar charts of means and standard deviations for the head-neck-torso system and the head-neck-rail system for (a) linear acceleration, (b) angular acceleration, (c) angular velocity, (d) peak and impact force, and (e) peak and impact moment from front boss impacts with the surrogate neck #1.

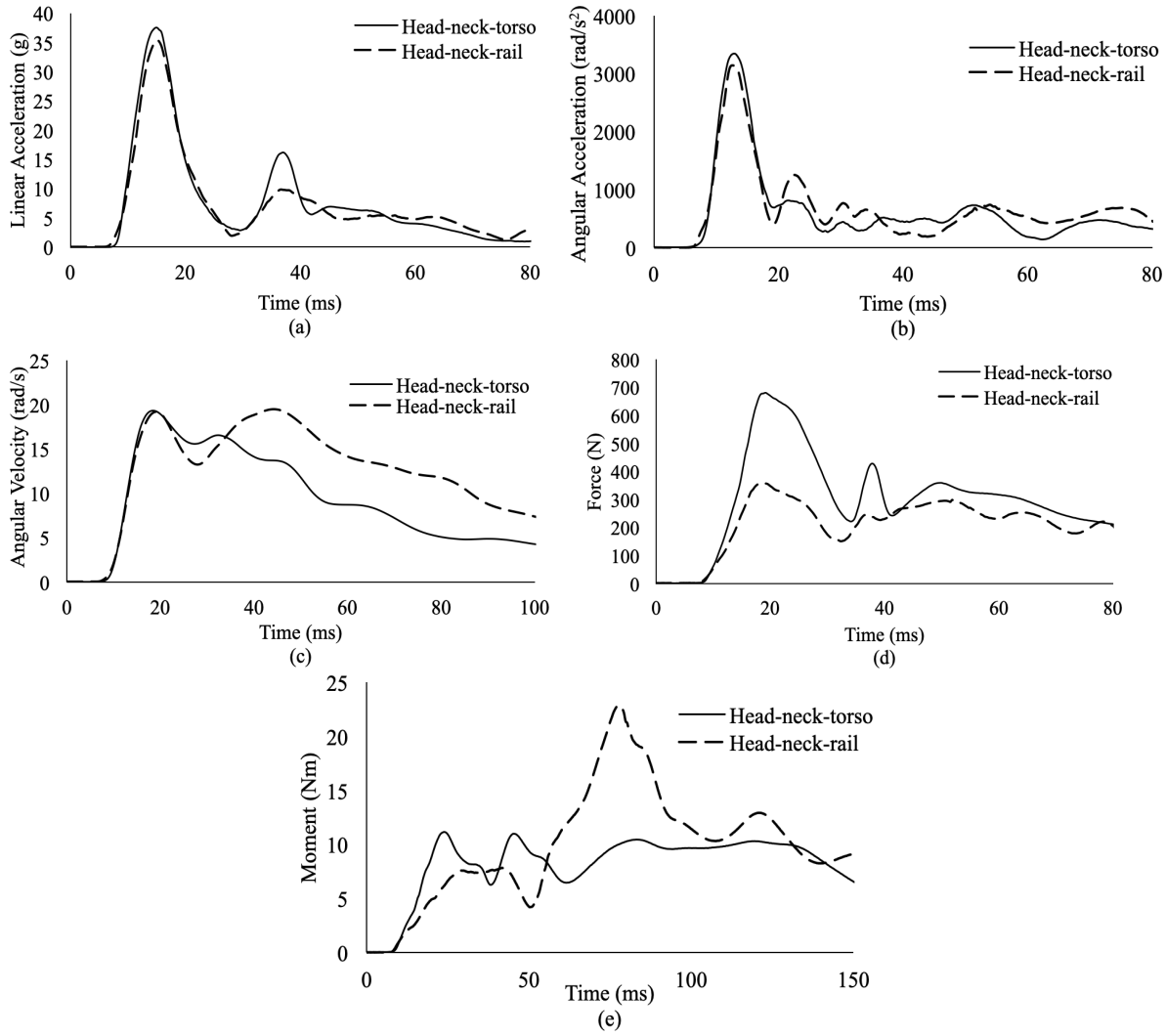

Figure 4.20: Comparison of ensemble averages from front boss impacts with the surrogate neck #1 fixed to the head-neck-torso system and head-neck-rail system for (a) linear acceleration, (b) angular acceleration, (c) angular velocity, (d) force, and (e) moment.

4.2.3.3 Surrogate Neck #2

Mean±standard deviation, 95% confidence interval, mean difference, and percent change values of the kinematic impact metrics are presented in Table 4.46 and the kinetic impact metrics are presented in Table 4.47 for impacts with surrogate neck #2 fixed to the head-neck-torso system and the head-neck-rail system. Independent samples two-tailed t-test and Welch t-test results are shown in Table 4.48 for linear acceleration, angular acceleration, impact moment, and peak

moment. Mean rank, U statistic, z-score, and p-value from a Mann-Whitney U Test are presented in Table 4.49 for impact force and peak force. A visual representation of the average peak kinematic and kinetic data is presented in Figure 4.21. Time series data of ensemble averages for all impact metrics with the head-neck torso system and the head-neck-rail system are shown in Figure 4.22. For front boss impacts with surrogate neck #2, all impact metrics were higher for the head-neck-rail system except for linear acceleration when compared to the head-neck-torso system.

Table 4.46: Mean±SD, 95% CI, mean difference (M.D.), and percent change (P.C.) values of kinematic impact metrics from front boss impacts with surrogate neck #2 fixed to head-neck-torso system and head-neck-rail system.

		Peak a (g)	Peak α (rad/s^2)	Peak ω (rad/s)
Torso	Mean±SD	35.8±1.1	3173.0±133.7	21.5±0.4
	95% CI	(35.3, 36.3)	(3110.4, 3235.5)	(21.3, 21.7)
Rail	Mean±SD	31.7±1.7	3600.7±160.4	21.6±0.9
	95% CI	(30.9, 32.5)	(3525.6, 3675.7)	(21.2, 22.0)
	M.D.	4.1	-427.7	-0.1
	P.C.	+12.9%	-11.9%	-0.6%

a = linear acceleration, α = angular acceleration, ω = angular velocity

Table 4.47: Mean±SD, 95% CI, mean difference (M.D.), and percent change (P.C.) values of kinetic impact metrics from front boss impacts with surrogate neck #2 fixed to head-neck-torso system and head-neck-rail system.

		Impact F (N)	Impact M (Nm)	Peak F (N)	Peak M (Nm)
Torso	Mean±SD	418.0±29.5	3.3±0.5	682.9±146.3	14.7±0.8
	95% CI	(404.2, 431.8)	(3.0, 3.5)	(614.4, 751.3)	(14.3, 15.1)
Rail	Mean±SD	560.3±34.0	3.5±0.3	725.3±28.4	17.8±1.1
	95% CI	(544.4, 576.2)	(3.3, 3.6)	(712.0, 738.6)	(17.3, 18.3)
	M.D.	-142.3	-0.2	-42.4	-3.1
	P.C.	-25.4%	-6.8%	-5.8%	-17.5%

F = force, M = moment

All impact metrics were significantly different between the torso assembly and the rail assembly except angular velocity, impact moment, and peak force. Average peak angular velocity values were almost identical for the head-neck-torso system (21.5 ± 0.4 rad/s) and the head-neck-rail system (21.6 ± 0.9 rad/s), (95% CI: -0.57, 0.32 rad/s), t(26.835)=-0.583, p = 0.565. The largest percent change, 25.4%, was seen in impact force values for the head-neck-torso system (mean rank = 10.60) and the head-neck-rail system (mean rank = 30.40), U = 398.000, z = 5.356, p = 0.000.

Table 4.48: Independent samples two-tailed t-test or Welch t-test results for appropriate impact metrics from front boss impacts with the surrogate neck #2. Significant p-values are shaded in grey.

	t-statistic	df	95% CI of the Difference	p-value
Peak a (g)	9.035	38	3.18, 5.01	p<0.001
Peak α (rad/s^2)	-9.161	38	-522.2, -333.2	p<0.001
Peak ω (rad/s)*	-0.583	26.835	-0.57, 0.32	p=0.565
Impact M (Nm)*	-1.851	33.755	-0.50, 0.02	p=0.073
Peak M (Nm)	-10.181	38	-3.74, -2.50	p<0.001

a = linear acceleration, α = angular acceleration, ω = angular velocity, F = force, M = moment
*Welch t-test

Table 4.49: Mean ranks, U statistics, z-scores, and p-values from a Mann-Whitney U Test for front boss impacts with surrogate neck #2 for all impact metrics. Significant p-values are shaded in grey.

	Mean Rank				
	Head-neck-torso	Head-neck-rail	*U* Statistic	z-score	p-value
Impact F (N)	10.60	30.40	398.000	5.356	p = 0.000
Peak F (N)	18.70	22.30	236.000	0.974	p = 0.341

F = force

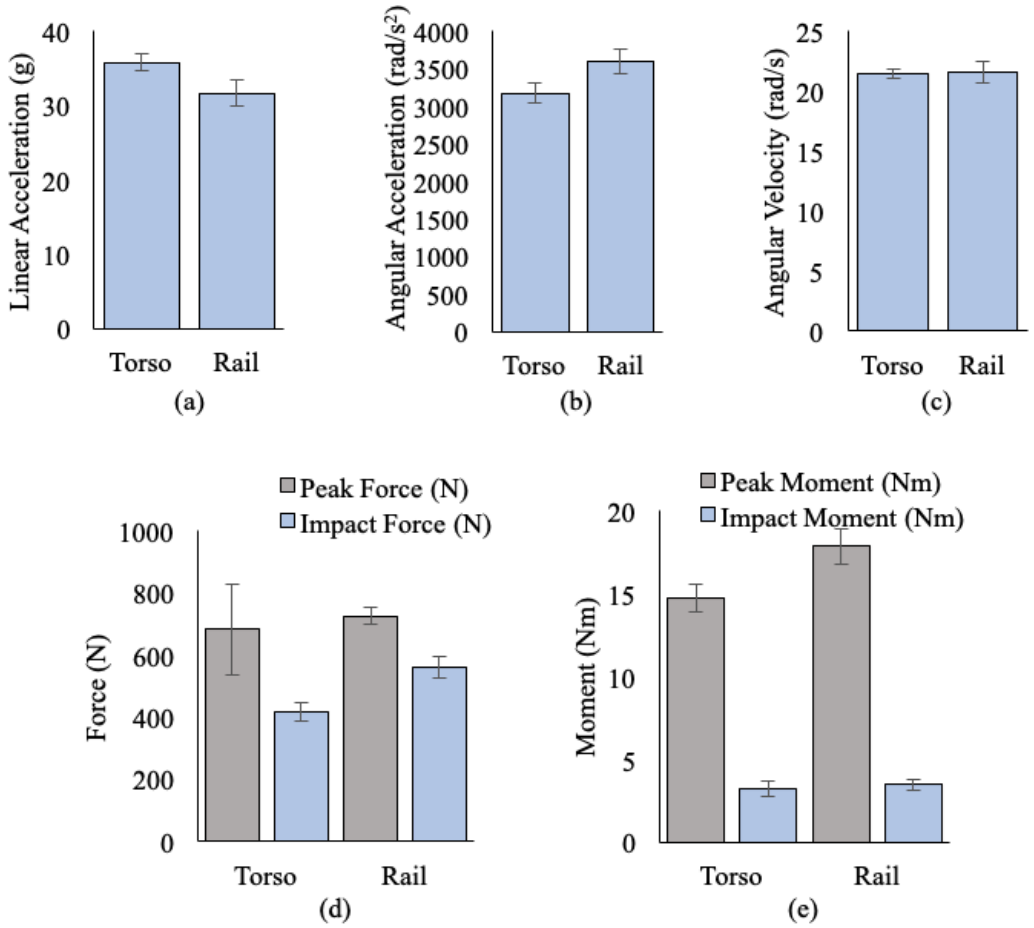

Figure 4.21: Bar charts of means and standard deviations for the head-neck-torso system and the head-neck-rail system for (a) linear acceleration, (b) angular acceleration, (c) angular velocity, (d) peak and impact force, and (e) peak and impact moment from front boss impacts with the surrogate neck #2.

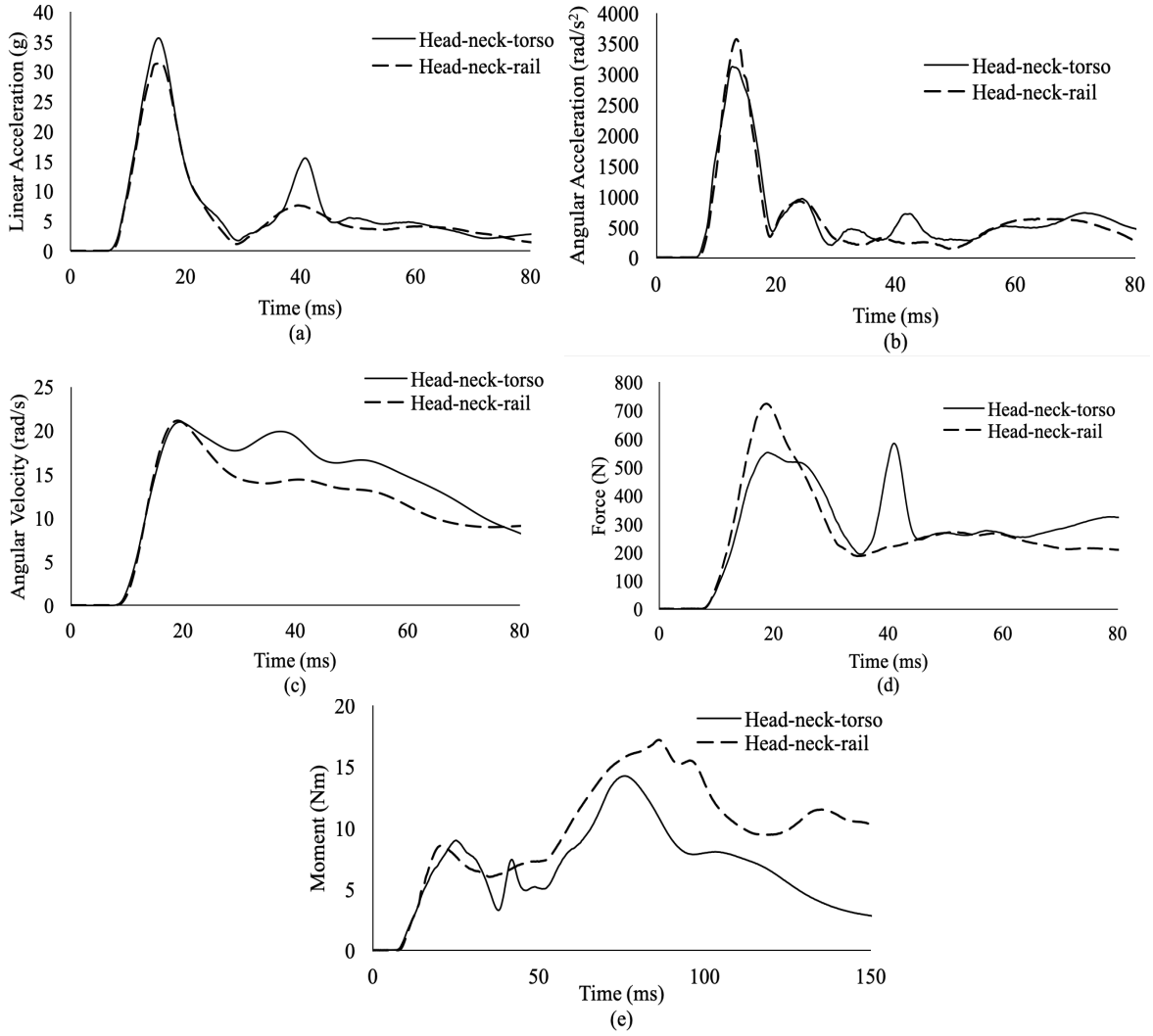

Figure 4.22: Comparison of ensemble averages from front boss impacts with the surrogate neck #2 fixed to the head-neck-torso system and head-neck-rail system for (a) linear acceleration, (b) angular acceleration, (c) angular velocity, (d) force, and (e) moment.

4.2.3.4 Surrogate Neck #3

Mean±standard deviation, 95% confidence interval, mean difference, and percent change values of the kinematic impact metrics are presented in Table 4.50 and the kinetic impact metrics are presented in Table 4.51 for impacts with surrogate neck #3 fixed to the head-neck-torso system

and the head-neck-rail system. Independent samples two-tailed t-test and Welch t-test results are shown in Table 4.52 for linear acceleration, angular acceleration, angular velocity, and peak force. Mean rank, U statistic, z-score, and p-value from a Mann-Whitney U Test are presented in Table 4.53 for impact force, impact moment, and peak moment. A visual representation of the average peak kinematic and kinetic data is presented in Figure 4.23. Time series data of ensemble averages for all impact metrics with the head-neck torso system and the head-neck-rail system are shown in Figure 4.24.

Table 4.50: Mean±SD, 95% CI, mean difference (M.D.), and percent change (P.C.) values of kinematic impact metrics from front boss impacts with surrogate neck #3 fixed to head-neck-torso system and head-neck-rail system.

		Peak a (g)	Peak α (rad/s^2)	Peak ω (rad/s)
Torso	Mean±SD	33.9±1.3	3111.5±109.4	20.6±0.4
	95% CI	(33.3, 34.5)	(3060.3, 3162.7)	(20.4, 20.8)
Rail	Mean±SD	27.6±1.9	3324.6±161.5	23.4±0.6
	95% CI	(26.7, 28.5)	(3249.1, 3400.2)	(23.1, 23.6)
	M.D.	6.3	-213.1	-2.8
	P.C.	+22.9%	-6.4%	-12.0%

a = linear acceleration, α = angular acceleration, ω = angular velocity

Table 4.51: Mean±SD, 95% CI, mean difference (M.D.), and percent change (P.C.) values of kinetic impact metrics from front boss impacts with surrogate neck #3 fixed to head-neck-torso system and head-neck-rail system.

		Impact F (N)	Impact M (Nm)	Peak F (N)	Peak M (Nm)
Torso	Mean±SD	500.2±49.6	3.3±0.4	756.0±57.9	12.0±0.8
	95% CI	(477.0, 523.4)	(3.1, 3.5)	(728.9, 783.1)	(11.7, 12.4)
Rail	Mean±SD	501.0±26.6	3.4±0.5	608.6±22.3	17.4±2.1
	95% CI	(488.5, 513.4)	(3.1, 3.6)	(598.2, 619.1)	(16.4, 18.4)
	M.D.	-0.8	-0.1	147.4	-5.4
	P.C.	-0.1%	-1.0%	+24.2%	-30.8%

F = force, M = moment

A statistical difference was seen for all impact metrics except impact force (U = 182.000, z = -0.487, p = 0.640) and impact moment (U = 201.000, z = 0.027, p = 0.999), both of which are almost identical for the head-neck-torso system and the head-neck-rail system. The largest percent change, 30.8%, was seen in peak moment values for the head-neck-torso system (mean rank = 10.65) and the head-neck-rail system (mean rank = 30.35), U = 397.000, z = 5.329, p = 0.000.

Table 4.52: Independent samples two-tailed t-test or Welch t-test results for appropriate impact metrics from front boss impacts with the surrogate neck #3. Significant p-values are shaded in grey.

	t-statistic	df	95% CI of the Difference	p-value
Peak a (g)	12.605	38	5.31, 7.35	p<0.001
Peak α (rad/s^2)	-4.886	38	-301.4, -124.8	p<0.001
Peak ω (rad/s)	-17.496	38	-3.14, -2.49	p<0.001
Peak F (N)*	10.261	24.507	118.7, 175.9	p<0.001

a = linear acceleration, α = angular acceleration, ω = angular velocity, F = force
*Welch t-test

Table 4.53: Mean ranks, U statistics, z-scores, and p-values from a Mann-Whitney U Test for front boss impacts with surrogate neck #3 for all impact metrics. Significant p-values are shaded in grey.

	Mean Rank				
	Head-neck-torso	Head-neck-rail	*U* Statistic	z-score	p-value
Impact F (N)	21.40	19.60	182.000	-0.487	p = 0.640
Impact M (Nm)	20.45	20.55	201.000	0.027	p = 0.999
Peak M (Nm)	10.65	30.35	397.000	5.329	p = 0.000

F = force, M = moment

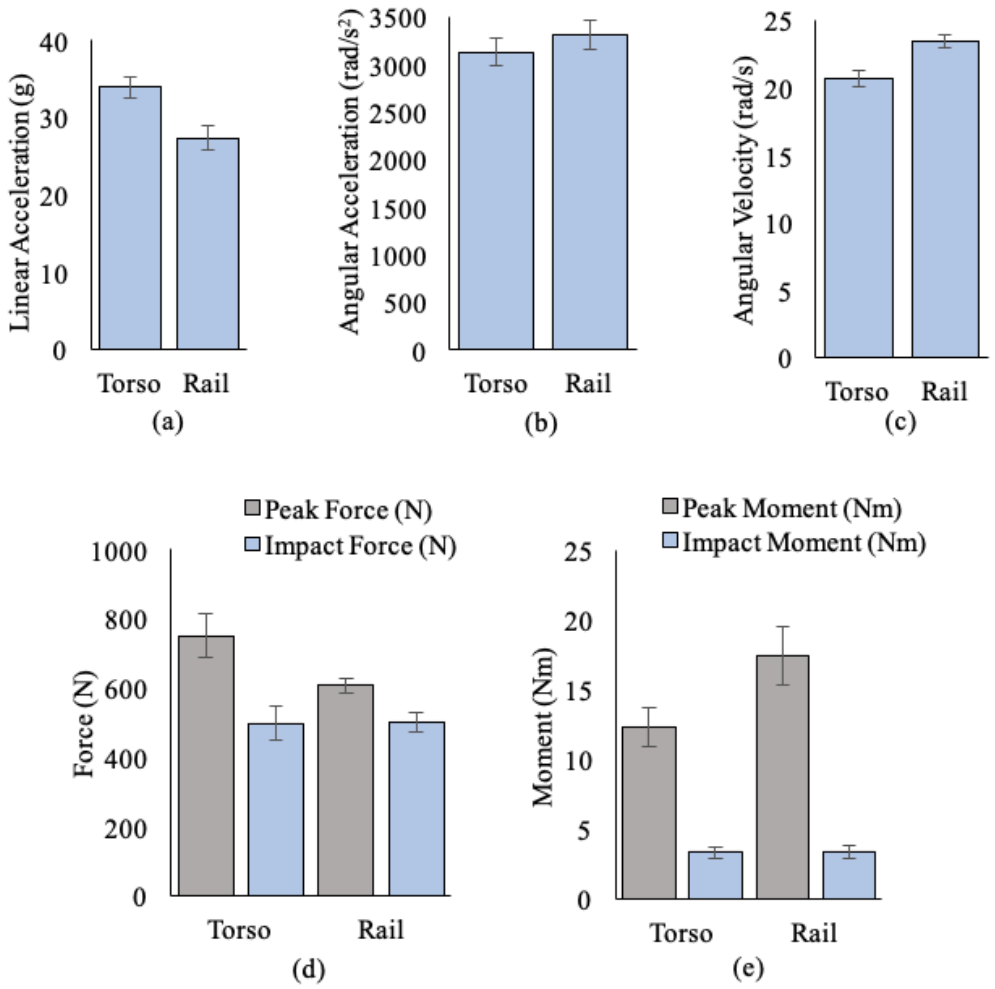

Figure 4.23: Bar charts of means and standard deviations for the head-neck-torso system and the head-neck-rail system for (a) linear acceleration, (b) angular acceleration, (c) angular velocity, (d) peak and impact force, and (e) peak and impact moment from front boss impacts with the surrogate neck #3.

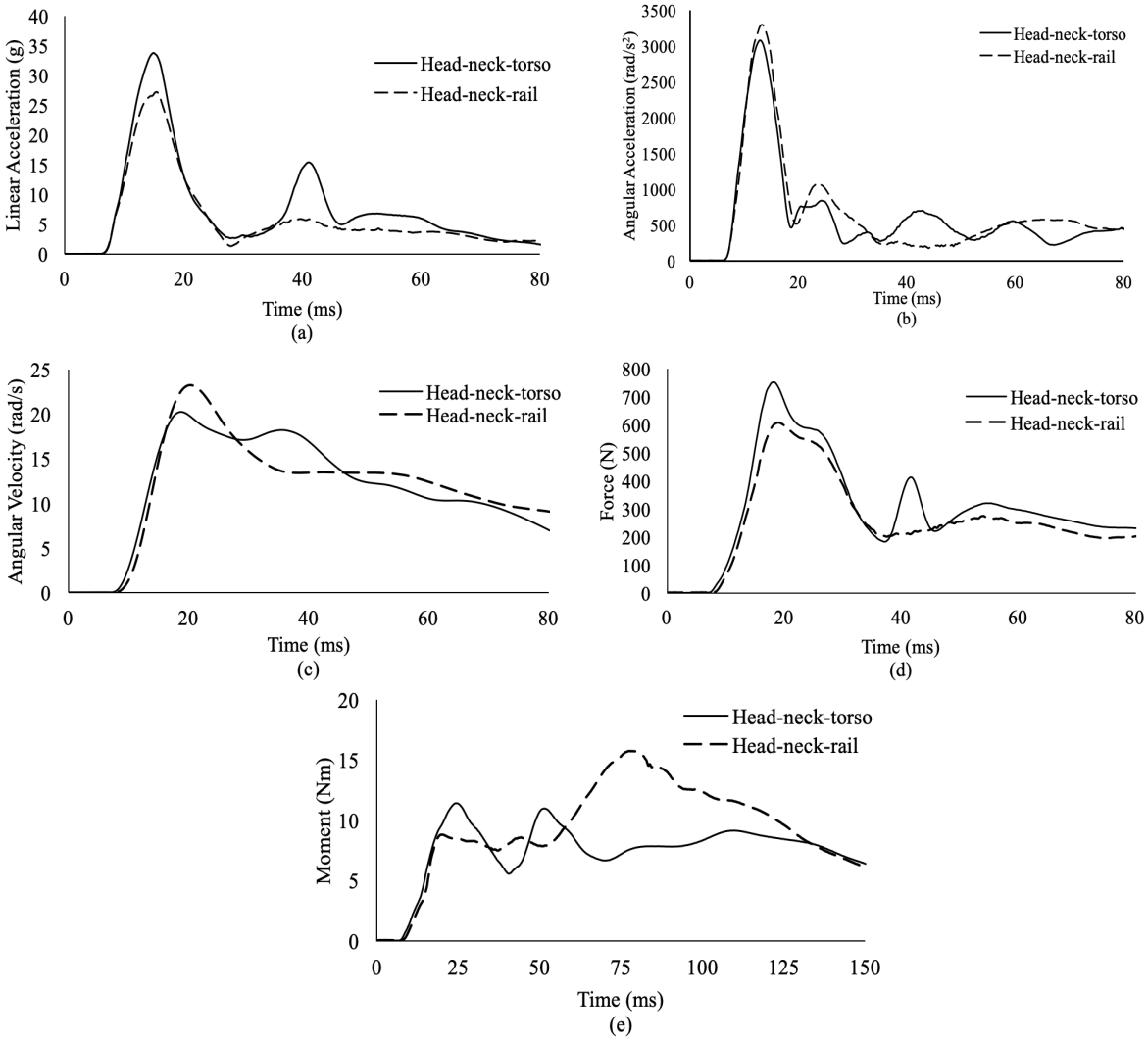

Figure 4.24: Comparison of ensemble averages from front boss impacts with the surrogate neck #3 fixed to the head-neck-torso system and head-neck-rail system for (a) linear acceleration, (b) angular acceleration, (c) angular velocity, (d) force, and (e) moment.

5 DISCUSSION

In this chapter, the repeatability and reproducibility of the modified surrogate neck is summarized and the results are related to the previous modified Phase II model. The surrogate neck is then compared to the Hybrid III neck, followed by a discussion of the implications of the differences between the head-neck-torso and the head-neck-rail system.

5.1 Phase III Neck Repeatability

Because significant modifications were made to the Phase II neck, a repeatability and reproducibility analysis of the Phase III surrogate neck was necessary to confirm the Phase III neck still met performance requirements. It was also important to compare the Phase III neck to the Hybrid III neck. Section 5.1.1 - 5.1.3 summarize these findings, while further detail can be found in a separate original work.

The Phase III surrogate neck demonstrated acceptable within-neck and between-neck repeatability as indicated by CV_W, CV_B, and normalized absolute difference values. The normalized absolute difference values between the Phase III necks and the Hybrid III neck were >20%, and significantly different ANOVA results indicate the surrogate neck and the Hybrid III neck produce differing head kinematics during impact.

5.1.1 Within-Neck Repeatability

Within-neck repeatability CV_W values for linear acceleration, angular acceleration, and angular velocity in all three impact locations were under 10% except for angular velocity in frontal impacts with surrogate neck #2 (17.1%), which indicates repeatability of the Phase III surrogate neck. The overall pooled CV_W, however, is greater than 10% for frontal linear acceleration (10.7%), front boss linear acceleration (11.4%), and frontal angular velocity (12.8%). The remaining impact kinematics CV_W were less than 8%. The largest CV_W values were always seen in surrogate neck #2; for linear acceleration (7.3%), angular acceleration (17.1%), and angular velocity (4.1%). As described in Sections 5.3.1, a limitation of this work is that the three copies of the Phase III neck were molded from two separate containers of silicone at different stages of shelf life. Surrogate neck #2 was molded soon after opening the second container of silicone, which may be a contributing factor in the increased variance in kinematics. The Phase III neck presented in this thesis produced similar CV_W values to previous iterations, but overall, there was no improvement compared to the latest model. This result was expected as the Phase III model underwent major design changes, as outlined in Section 3.1, to allow for attachment to the Hybrid III dummy torso. While the current model did exhibit some unacceptable repeatability measures, the CV_W values did prove more acceptable than the Phase II model; however, the modified Phase II model (Section 2.4.3) remains the most repeatable, although slightly different experimental setups were utilized [29].

5.1.2 Between-Neck Repeatability

Although ≤15% is acceptable for the reproducibility coefficient of variation (CV_B) values, in the three impact locations, all CV_B values were under 10% except for linear acceleration in frontal

(11.4%) and front boss (12.6%) impacts. The CV_B values in the current investigation are comparable to CV_B values calculated for the modified Phase II surrogate neck in helmeted impacts, which concluded all kinematics for frontal and front boss impacts were less than 12% [29]. Additionally, most NAD values were less than 20%, further indicating that the between-neck repeatability of the Phase III surrogate neck is acceptable. Only two metrics had an NAD over 20%; frontal linear acceleration differences between surrogate neck #1 and #2, and front boss linear acceleration differences between surrogate neck #1 and #3. On average, the impact metrics differed by less than 15% between necks except for linear acceleration in front boss impacts (16.8%). The NAD values for the Phase III neck are similar to Wynn's modified Phase II neck in frontal and front boss helmeted impacts [29].

5.1.3 Comparison to Hybrid III Neck

Within-neck repeatability of the Hybrid III is comparable to the Phase III neck CV_W values. The Phase III neck and Hybrid III neck perform similarly in that the variance was typically lowest in angular velocity and greatest in angular acceleration. Generally, both the Phase III neck and Hybrid III neck CV_W values were below 8% for linear acceleration, 7% for angular velocity, and, excluding the CV_W value for surrogate neck #2 of 17.1%, below 6% for angular acceleration.

The NAD values between each of the three Phase III necks and the Hybrid III neck was calculated to investigate the difference of impact metrics between the neck models. Generally, the differences between the Phase III surrogate necks and the Hybrid III neck were larger than the differences seen between the three Phase III surrogate necks. For example, the average NAD between the Phase III

necks was 6.5% for lateral linear acceleration, while the average was 35% between the Phase III necks and Hybrid III neck. The largest difference in NAD was seen in frontal angular velocity, where the average difference in kinematics between the Phase III necks was 12% and the average difference between the Phase III necks and the Hybrid III neck was 77.4%. This trend is seen in all kinematics in frontal, lateral, and front boss impacts except for frontal linear acceleration and front boss angular velocity. Results presented in Wynn, 2022 also followed this trend, although the differences in NAD values were smaller than those in the current thesis [29].

To further investigate differences between the Phase III neck and the Hybrid III neck, an ANOVA was performed. Overall, the ANOVA results showed significant differences between the Hybrid III neck and the Phase III necks for frontal, lateral, and front boss impacts. The ANOVA tables are included in Appendix A: Cases in which there was no statistical difference between the Hybrid III and the Phase III neck were lateral angular acceleration with surrogate neck #3, lateral impact moment with surrogate neck #1 and #2, lateral peak force with surrogate neck #3, front boss angular velocity with surrogate neck #1. A finding outlined in Wynn, 2022 was that the resultant head kinematics from impacts to an unhelmeted head differed between the Hybrid III and the modified Phase II neck. Conversely, when the headform was helmeted, the differences in head kinematics were less clear [29]. Results of the current thesis do not align with that conclusion. Although there were five cases in which no statistical difference was found, overwhelmingly, post-hoc statistical results indicate substantial differences in resultant head kinematics between the Phase III neck and the Hybrid III neck. The current work did not test unhelmeted head impacts, however, so a conclusive decision on the effect of a helmet cannot be made. Additionally,

conclusions made in Wynn, 2022 were based on the modified Phase II neck in slightly lower severity impacts so those results are not directly transferrable to the current investigation.

5.1.4 Summary

A significant challenge with developing ATD neck models is producing a neck that reliably and accurately represents human impact biomechanical responses. The Phase III surrogate neck demonstrated acceptable within-neck and between-neck repeatability and reproducibility, and substantial differences are apparent when compared to the Hybrid III neck. Even as the gold standard in impact research, the Hybrid III neck is limited in that it was designed for indirect, frontal motion and ultimately resists motion in the lateral and front boss planes. While the Hybrid III neck and other ATD neck models have demonstrated acceptable performance requirements and are currently used in impact testing, they have not been designed for use in omni-directional direct head impacts in sports; and recently, significant differences between the performance of the Hybrid III neck and other neck models has been documented, including in the current work. This puts an emphasis on the demand for the continued development, refinement, and biofidelity assessment of neck models such as the Phase III surrogate neck to compare against the Hybrid III neck, to ultimately assist researchers in improving injury assessment effectiveness.

5.2 Comparison of the Head-Neck-Torso and Head-Neck-Rail Systems

To the author's knowledge, a paucity of research exists directly comparing the resultant head dynamics of impacts when an isolated head-neck is fixed to a translating linear rail and when fixed

to an upright ATD dummy torso. Current helmet testing standards and laboratory impact reconstruction methods typically use isolated head-neck assemblies, without justifying the effect of a torso mass. Because of this, there was a need to present quantitative evidence of the head dynamic response of these two systems in direct helmeted head pendulum impacts. These two systems experienced different mechanical behavior after impact, and consequently, different head COG and upper neck response. An investigation into head and neck biomechanical parameters and their relationship to neck injury severity in lateral impacts found statistically significant relationships between resultant head acceleration and neck force and neck injury severity [96]. In the current work, the differences in impact metrics were statistically analyzed between a head-neck-torso and a head-neck-rail system, and in majority of cases, the head-neck-torso system resulted in higher resultant head COG kinematic and upper neck kinetic values, suggesting that the currently used head-neck-rail system may be misrepresenting injury risk.

Out of a combination of 12 impact metric comparisons (3 impact locations x 4 surrogate necks), generally, higher average impact metrics were seen in the head-neck-torso system than the head-neck-rail system. To summarize the kinematic data, all twelve comparisons of average peak linear acceleration showed greater values for the head-neck-torso system than the head-neck-rail system. Additionally, 67% (8 of 12) of average peak angular acceleration comparisons were higher for the head-neck-torso system, while only 33% (4 of 12) averages of angular velocity were higher than the head-neck-rail system. Regarding the kinetic impact metrics, 83% (10 of 12) and 75% (9 of 12) of average peak force and impact moment values, respectively, were higher in the head-neck-torso system. Further, 67% (8 of 12) of impact force averages were higher in the head-neck-torso

system than the head-neck-rail system, while only 33% (4 of 12) of peak moment averages were higher than the head-neck-rail system.

The results of this investigation showed that there is a significant difference between most impact metrics when comparing direct head impacts to a head-neck-rail system and a head-neck-torso system. One of the most important findings was that all average peak linear accelerations were higher in impacts to the head-neck-torso system compared to the head-neck-rail system. Further, all differences were determined to be statistically different except for one; frontal impacts with surrogate neck #2. This result is of great importance considering that one of the NOCSAE requirements for passing helmets is an evaluation of the SI which is a measurement of injury tolerance directly determined by linear acceleration [56]. If greater linear accelerations, and thus, SI values, result from impacting a head-neck fixed to a dummy torso, it questions whether the current pneumatic linear impactor helmet testing method is adequately assessing head injury risk. The consistent differences in linear acceleration and typically higher impact metrics from the head-neck-torso system is likely related to a combination of two mechanical effects. First, the larger mass of the Hybrid III torso compared to the linear rail gimbal assembly. And, second, the different constraining forces at the base of the surrogate neck, referred to in the literature as chest compliance [97]. The biomechanical phenomenon of chest compliance was presented in a study comparing the Hybrid III and THOR full dummies to post mortem human subjects (PMHS) in frontal sled tests [97] . This study reported that the THOR dummy produced biomechanical metrics closer to the PMHS than the Hybrid III dummy because of the greater chest compliance of the THOR as a result of its flexible dorsal spine joints, more anatomical ribcage, and increased softness in the neck and chest structures, when compared to the stiffness of the Hybrid III. This paper

explains that the contrasting motion of the head and torso, because of the lower chest compliance of the rigid Hybrid III, creates significant tensile forces in the neck. A similar, larger-scale scenario in which this occurs is during automotive collisions without head rests, where the torso motion is restrained by the seat and seatbelt while the head continues to accelerate and extend posteriorly. In the head-neck-rail system used in the experiments in this thesis, the base of the surrogate neck is bolted to a gimbal that is fixed to a translating platform on a linear rail. The experimental setup allowed the translating platform to move post-impact linearly along the rail in the direction of impact including, and along with it, the entire head-neck-gimbal assembly. Because the whole system moved linearly away from the impact, the compliance of the assembly was greater at the base of the neck. Additionally, the mass below the surrogate neck of the translating platform and gimbal assembly was notably less than the mass of the Hybrid III torso. Conversely, in the head-neck-torso assembly, high-speed video shows the torso move later compared to the gimbal post-impact, likely because the mass of the Hybrid III torso is considerably larger, and the Hybrid III torso is more rigid and has lower chest compliance.

Torso mass and chest compliance contribute to the head's resultant impact metrics because they affect the biomechanics of the neck. When the head is impacted, a compressive, rearward force is sent from the head through the cervical components of the neck and a frontward reaction force is produced at the boundary condition at the base of the neck, simulating a forward displacement of the torso with the head revolving backward into extension [98]. A greater torso mass would generate a greater reaction force, and subsequently, greater neck extension and upper neck force. If the lower neck and upper torso can translate backwards even slightly, as seen in the head-neck-rail system, the reaction force at the base of the neck lessens, and the force at the upper neck is not

as severe. To summarize, a combination of greater torso mass and lesser chest compliance at the base of the neck would cause greater peak forces at the upper neck. This idea is supported by the upper neck forces and impact moments observed in the impacts. After linear acceleration, the impact metric that produced consistently higher values from the head-neck-torso system compared to the head-neck-rail system was peak force, with 85% (10 of 12) of comparisons being higher with the inclusion of the Hybrid III torso. Further, impact moment was the 3rd most affected impact metric behind linear acceleration and peak force, with 75% (9 of 12) comparisons between the two systems resulting in higher values from the head-neck-torso system. A higher moment at the upper neck is evidence of greater force that could be stemming from increased constraining forces [99].

5.3 Research Limitations

5.3.1 Phase III Neck Manufacturing

The three Phase III surrogate necks were molded with DragonSkin© silicone from two separate one-gallon containers and at different times after the containers had been opened. Surrogate neck #1 was molded from the first container, while surrogate neck #2 and #3 were molded from the second container. The physical properties of the silicone may vary in each container which may result in differences in the performance of the necks. Additionally, surrogate neck #1 was cured after the DragonSkin© container had been opened for three weeks while surrogate neck #2 and #3 were cured within four days of the second container being opened. The exact shelf life of the silicone is unknown, but the product still seemed to be in usable condition when surrogate neck #1 was molded. Further, the temperature and humidity in the lab was not consistently monitored, so

there is a possibility the lab temperature affected the silicone as well as any equipment used in the experiments.

5.3.2 Experimental Setup and Procedure

While the use of a Hybrid III dummy torso aimed to eliminate the unrealistic constraining forces that the head-neck-rail system introduces, it still has limitations. First, the arms and legs of the dummy were removed to isolate the torso mass and avoid the introduction of additional variables. Second, the Hybrid III dummy was positioned seated upright on the ground, which introduces its own unrealistic ground reaction forces. The setup of the seated limbless dummy in this study is a limitation that requires further investigation of biofidelity and validity of use in reconstruction methods. Another limitation of this work is that there was no predetermined wait time in between pendulum impacts; thus, the effects of numerous impacts on the helmet, head, neck, rail, and torso, although likely small, were not quantified. This investigation into the effect of torso mass only tested one mass; that of the Hybrid III 50^{th} percentile male torso and pelvis. The mass changes with the addition of dummy arms and legs and the removal of the pelvis, and the effects of these modifications are not known. Because of this, the results presented in this thesis are only applicable to the 50^{th} percentile male and the effect of torso mass on other weight percentiles and female subjects remains unknown. Finally, while every possible effort was made to conduct accurate repeat impacts, there is still a possibility of user error in the setup of each impact. Laser levels, ground markings, high speed camera, and thorough visual inspections were used to position the Hybrid III dummy and helmet after each impact, however, slight inconsistencies may have occurred.

5.4 Recommendations for Future Work

As previously mentioned, the three copies of the Phase III surrogate neck were made from two separate containers of DragonSkin© silicone, and surrogate neck #1 was cured after the container had been opened for three weeks. Future work with the surrogate necks should re-mold the necks simultaneously and from the same gallon container of silicone to limit the possible effects from differences in physical properties of the silicone and the day-to-day laboratory environment.

Future work further investigating the effect of torso mass in direct head impacts should consider conducting impacts at other impact velocities and torso masses. Only one impact velocity of 4.0 m/s was used in this investigation so these results can only translate to the specific experimental inputs as described. Higher impact velocities would better represent real-life football collisions and helmet testing methods and could further expand on the analysis presented in this thesis and more accurately apply it to those scenarios. Additionally, only one torso mass was tested in this thesis so it is recommended that future work test a range of torso masses so results are applicable to a wider population.

As mentioned in Section 5.3.2, using the Hybrid III dummy torso and pelvis introduced its own unrealistic constraining forces by being positioned upright seated on the ground. Investigations using a dummy torso in the future should consider the effect the ground reaction forces have on the resultant head dynamics. The use of a suspended dummy torso or a torso fixed to a translating rail may be appropriate, although these setups become more difficult to assemble.

Significant differences between the Hybrid III neck and the Phase III surrogate necks provide further reason to investigate biofidelity of the Phase III neck. Possible investigations for determining biofidelity of the surrogate necks could utilize databases such as the Naval Biodynamics Laboratory (NBDL) database to compare the resultant head kinematics to human volunteer data in sled test scenarios. To the author's knowledge, a reference database for direct head impacts similar to the NBDL does not exist, and the only human volunteer data available is collected from single collision events in real-life football games or practice. Further, high severity direct head impacts to human volunteers for comparison to surrogate head and necks would not be safe or ethical to perform.

This thesis showed significant differences in the head kinematics and upper neck kinetics between a head-neck-rail and a head-neck-torso system but it could not conclude which system was more biofidelic. Studies of the effect of torso mass have been conducted with PMHS in sled tests and direct head impacts at low velocity, which could be utilized in future research to investigate biofidelity of a head-neck-rail and a head-neck-torso system; however, these results are not translatable to high severity football collisions, and conducting head impacts at higher impact velocities with human volunteers is not safe, as mentioned above. A reference database of high severity head impacts is needed from PMHS or estimated with computational models for biofidelity assessments of surrogate models and laboratory testing methods to ensure appropriate methods are used to increase player safety.

6 CONCLUSION

In this chapter, a summary of the motivation and main results of this thesis are summarized and the contributions of this work are outlined.

6.1 Summary

Currently common in laboratory impact reconstructions and required in NOCSAE football helmet testing is the use of an isolated head and neck assembly. Because these methods of testing ignore or attempt to estimate the full torso mass and its effects on the resultant head dynamics, an investigation into the differences between the resultant head kinematics and kinetics of the two impact methods was necessary. The overarching goal of comparing the head impact mechanics from a head-neck-rail and head-neck-torso system was to determine if the two impact testing methods produce differing output impact metrics. This thesis provides an overview of the head center of gravity kinematic and upper neck kinetic differences between a head-neck assembly fixed to a linear rail and a Hybrid III dummy torso in frontal, lateral, and front boss impacts. Results showed significant differences between the currently used head-neck-rail system and a head-neck-torso system, suggesting that further research is necessary to determine which system more realistic of human head impact dynamics.

The main results of this thesis were:

1) The repeatability of the Phase III surrogate neck is acceptable;
2) Direct head impacts to the Phase III neck result in differing kinematics compared to the Hybrid III neck;

3) The inclusion of a dummy torso mass in direct head impacts significantly affects the resultant head COG dynamics in frontal, lateral, and front boss impacts, and;
4) Resultant head COG linear acceleration is consistently higher when the head-neck assembly is fixed to a dummy torso.

6.2 Contributions

Further modifications were made to a novel surrogate neck designed for omni-directional head impacts in sports. The need for a surrogate neck of this kind is substantial as the most commonly used surrogate neck in sports impact biomechanics, the Hybrid III neck, was designed for frontal automotive collisions and does not accurately reflect human motion in lateral or off-axis motion. Modifying and further refining this novel surrogate neck will advance human head and neck injury assessment and injury prevention effectiveness to help safeguard against head injury.

Isolated head-neck-rail systems are typically used in laboratory impact reconstructions and helmet testing methods. The results from this investigation show that typically, resultant head COG kinematics and upper neck kinetics are statistically higher with the addition of a Hybrid III torso to the base of the ATD neck. These results suggest that head-neck-rail systems are producing kinematics and kinetics that may be misrepresenting injury risk. If the results of helmet testing and/or injury assessments are being performed to ultimately improve human safety, the comparison between a head-neck-rail system and a head-neck-torso system needs to be further investigated to determine which system is more biofidelic and appropriate for use as the standard for helmet testing and laboratory reconstructions.

References

[1] Chen, M., Maier, K., Ritenour, D., and Sun, C., 2022, "Improving Global TBI Tracking and Prevention: An Environmental Science Approach," Global Journal of Health Science, **14**(3), pp. 1–20.

[2] Honeybul, S., and Kolias, A. G., eds., 2021, *Traumatic Brain Injury: Science, Practice, Evidence and Ethics*, Springer International Publishing, Cham.

[3] "Unintentional Injuries: Magnitude, Prevention, and Control" [Online]. Available: https://www.annualreviews.org/doi/epdf/10.1146/annurev-publhealth-031811-124558. [Accessed: 07-Jul-2022].

[4] 2022, "TBI Data | Concussion | Traumatic Brain Injury | CDC Injury Center" [Online]. Available: https://www.cdc.gov/traumaticbraininjury/data/index.html. [Accessed: 07-Jul-2022].

[5] Miller, G. F., DePadilla, L., and Xu, L., 2021, "Costs of Nonfatal Traumatic Brain Injury in the United States, 2016," Medical Care, **59**(5), pp. 451–455.

[6] 2019, "Global, Regional, and National Burden of Traumatic Brain Injury and Spinal Cord Injury, 1990–2016: A Systematic Analysis for the Global Burden of Disease Study 2016," Lancet Neurol, **18**(1), pp. 56–87.

[7] McCrea, M. A., Shah, A., Duma, S., Rowson, S., Harezlak, J., McAllister, T. W., Broglio, S. P., Giza, C. C., Goldman, J., Cameron, K. L., Houston, M. N., McGinty, G., Jackson, J. C., Guskiewicz, K., Mihalik, J. P., Brooks, M. A., Pasquina, P., and Stemper, B. D., 2021, "Opportunities for Prevention of Concussion and Repetitive Head Impact Exposure in College Football Players: A Concussion Assessment, Research, and Education (CARE) Consortium Study," JAMA Neurol, **78**(3), p. 346.

[8] Jadischke, R., "Biomechanics Of Concussion: The Importance Of Neck Tension," p. 223.

[9] National Football League, 2018, "How the NFL Is Advancing Player Health and Safety."

[10] Vorst, M. J. V., and Chan, P. C., "Biofidelity of Motorcycle Helmet Criteria."

[11] Campbell, S., Elliott, M., Graveline, E., and Rakauskas, P., 2020, "A Dual-Helmet Interpretation of the Virginia Tech STAR Method," Bachelor of Science, Worcester Polytechnic Institute.

[12] Rowson, B., Terrell, E., and Rowson, S., 2018, "Quantifying the Effect of the Facemask on Helmet Performance," Proceedings of the Institution of Mechanical Engineers, Part P: Journal of Sports Engineering and Technology, **232**(2), pp. 94–101.

[13] Andriessen, T. M. J. C., Jacobs, B., and Vos, P. E., 2010, "Clinical Characteristics and Pathophysiological Mechanisms of Focal and Diffuse Traumatic Brain Injury," Journal of Cellular and Molecular Medicine, **14**(10), pp. 2381–2392.

[14] Graham, R., Rivara, F. P., Ford, M. A., Spicer, C. M., Youth, C. on S.-R. C. in, Board on Children, Y., Medicine, I. of, and Council, N. R., 2014, *Neuroscience, Biomechanics, and Risks of Concussion in the Developing Brain*, National Academies Press (US).

[15] Mohan, D., 1993, "Mechanics of Head Injury and Politics of Brain Damage," Current Science, **65**(10), pp. 749–760.

[16] Kleiven, S., 2003, "Influence of Impact Direction on the Human Head in Prediction of Subdural Hematoma," Journal of neurotrauma, **20**, pp. 365–79.

[17] King, A. I., Yang, K. H., Zhang, L., Hardy, W., and Viano, D. C., 2003, "Is Head Injury Caused by Linear or Angular Acceleration?," p. 12.

[18] Forero Rueda, M. A., Cui, L., and Gilchrist, M. D., 2011, "Finite Element Modelling of Equestrian Helmet Impacts Exposes the Need to Address Rotational Kinematics in Future Helmet Designs," Computer Methods in Biomechanics and Biomedical Engineering, **14**(12), pp. 1021–1031.
[19] Post, A., and Blaine Hoshizaki, T., 2015, "Rotational Acceleration, Brain Tissue Strain, and the Relationship to Concussion," Journal of Biomechanical Engineering, **137**(3), p. 030801.
[20] Islam, S. U., "Significance of the Neck in Concussive Head Impacts – A Computational Approach," p. 116.
[21] Streifer, M., Brown, A. M., Porfido, T., Anderson, E. Z., Buckman, J. F., and Esopenko, C., 2019, "The Potential Role of the Cervical Spine in Sports-Related Concussion: Clinical Perspectives and Considerations for Risk Reduction," J Orthop Sports Phys Ther, **49**(3), pp. 202–208.
[22] Bretzin, A. C., Mansell, J. L., Tierney, R. T., and McDevitt, J. K., 2017, "Sex Differences in Anthropometrics and Heading Kinematics Among Division I Soccer Athletes: A Pilot Study," Sports Health, **9**(2), pp. 168–173.
[23] Eckner, J. T., Oh, Y. K., Joshi, M. S., Richardson, J. K., and Ashton-Miller, J. A., 2014, "Effect of Neck Muscle Strength and Anticipatory Cervical Muscle Activation on the Kinematic Response of the Head to Impulsive Loads," Am J Sports Med, **42**(3), pp. 566–576.
[24] Jin, X., Feng, Z., Mika, V., Li, H., Viano, D. C., and Yang, K. H., 2017, "The Role of Neck Muscle Activities on the Risk of Mild Traumatic Brain Injury in American Football," ASME. J Biomech Eng., **139**(10).
[25] "Axial, Coronal, & Sagittal Planes – IPF Radiology Rounds" [Online]. Available: https://www.ipfradiologyrounds.com/hrct-primer/image-reconstruction/. [Accessed: 31-Oct-2022].
[26] Rizzetti, A., Kallieris, D., Schiemann, P., and Mattem, R., 1997, "RESPONSE AND INJURY SEVERITY OF-THE HEAD-NECK UNIT DURING A LOW VELOCITY HEAD IMPACT," p. 14.
[27] Advisory Group for Aerospace Research and Development, ed., 1996, "Anthropomorphic Dummies for Crash and Escape System Testing (Mannequins Anthropométriques Utilisés Lors Des Tests d'impact et d'éjection)."
[28] Wismans, J., Bermond, F., Gertosio, G., Kreuzinger, T., Roberts, A., van Ratingen, M., and Svensson, M., 2001, "Development and Evaluation of the ES-2 Dummy," European Enhanced Vehicle-Safety Committee, p. 36.
[29] Wynn, G. F., 2022, "Repeatability of a Novel Prototype Surrogate Neck Model Developed for Omni-Directional Head Impacts," Master of Science, University of Alberta.
[30] Mertz, H. J., Neathery, R. F., and Culver, C. C., 1973, "Performance Requirements and Characteristics of Mechanical Necks," *Human Impact Response*, W.F. King, and H.J. Mertz, eds., Springer US, Boston, MA, pp. 263–288.
[31] Thunnissen, J., Wismans, J., Ewing, C. L., and Thomas, D. J., 1995, "Human Volunteer Head-Neck Response in Frontal Flexion: A New Analysis," p. 952721.
[32] 2011, "49 Code of Federal Regulations (CFR) Part 572 - Anthropomorphic Test Devices."
[33] MacGillivray, S., 2020, "Design and Characterization of a Novel Mechanical Surrogate Neck Model for Use in Head Impact Applications," Master of Science, University of Alberta.
[34] Foster, J. K., Kortge, J. O., and Wolanin, M. J., 1977, "Hybrid III-A Biomechanically-Based Crash Test Dummy," p. 770938.

[35] Yoganandan, N., Sances, A., and Pintar, F., 1989, "Biomechanical Evaluation of the Axial Compressive Responses of the Human Cadaveric and Manikin Necks," Journal of Biomechanical Engineering, **111**(3), pp. 250–255.
[36] Withnall, C., 2005, "Biomechanical Investigation of Head Impacts in Football," British Journal of Sports Medicine, **39**(Supplement 1), pp. i49–i57.
[37] Cantu, R. C., 2008, "Concussion in Professional Football: Biomechanics of the Struck Player—Part 14," Yearbook of Sports Medicine, **2008**, pp. 20–22.
[38] Pellman, E. J., Viano, D. C., Withnall, C., Shewchenko, N., Bir, C. A., and Halstead, P. D., 2006, "Concussion in Professional Football: Helmet Testing to Assess Impact Performance—Part 11," Neurosurgery, **58**(1), pp. 78–95.
[39] Pellman, E. J., Viano, D. C., Tucker, A. M., Casson, I. R., and Waeckerle, J. F., 2003, "Concussion in Professional Football: Reconstruction of Game Impacts and Injuries," Neurosurgery, **53**(4), pp. 799–814.
[40] Viano, D. C., and Pellman, E. J., 2005, "Concussion in Professional Football: Biomechanics of the Striking Player—Part 8," Neurosurgery, **56**(2), pp. 266–280.
[41] Viano, D. C., Pellman, E. J., Withnall, C., and Shewchenko, N., 2006, "Concussion in Professional Football," Neurosurgery, **59**(3), pp. 591–606.
[42] Giudice, J. S., Park, G., Kong, K., Bailey, A., Kent, R., and Panzer, M. B., 2019, "Development of Open-Source Dummy and Impactor Models for the Assessment of American Football Helmet Finite Element Models," Ann Biomed Eng, **47**(2), pp. 464–474.
[43] Walsh, E. S., Kendall, M., Hoshizaki, T. B., and Gilchrist, M. D., 2014, "Dynamic Impact Response and Predicted Brain Tissue Deformation Comparisons for an Impacted Hybrid III Headform With and Without a Neckform and Torso Masses," p. 7.
[44] Funk, J. R., Jadischke, R., Bailey, A., Crandall, J., McCarthy, J., Arbogast, K., and Myers, B., 2020, "Laboratory Reconstructions of Concussive Helmet-to-Helmet Impacts in the National Football League," Ann Biomed Eng, **48**(11), pp. 2652–2666.
[45] Jadischke, R., Viano, D. C., McCarthy, J., and King, A. I., 2016, "The Effects of Helmet Weight on Hybrid III Head and Neck Responses by Comparing Unhelmeted and Helmeted Impacts," Journal of Biomechanical Engineering, **138**(10), p. 101008.
[46] Karton, C. M., Hoshizaki, T. B., and Gilchrist, M. D., 2014, "The Influence of Impactor Mass on the Dynamic Response of the Hybrid III Headform and Brain Tissue Deformation," *Mechanism of Concussion in Sports*, A. Ashare, and M. Ziejewski, eds., ASTM International, 100 Barr Harbor Drive, PO Box C700, West Conshohocken, PA 19428-2959, pp. 23–40.
[47] Newman, J. A., Beusenberg, M. C., Shewchenko, N., Withnall, C., and Fournier, E., 2005, "Verification of Biomechanical Methods Employed in a Comprehensive Study of Mild Traumatic Brain Injury and the Effectiveness of American Football Helmets," Journal of Biomechanics, **38**(7), pp. 1469–1481.
[48] Ogle, M. K., 2018, "Development and Characterization of a Mechanical Surrogate Neck Prototype for Use in Helmet Certification Applications," Master of Science, University of Alberta.
[49] Panjabi, M. M., Duranceau, J., Goel, V., Oxland, T., and Takata, K., 1991, "Cervical Human Vertebrae. Quantitative Three-Dimensional Anatomy of the Middle and Lower Regions," Spine, **16**(8), pp. 861–869.
[50] Thunert, C., 2017, "CORAplus 4.0.4 User's Manual."
[51] Lissner, H., Lebow, M., and Evans, F., 1960, "Experimental Studies on the Relation between Acceleration and Intracranial Pressure Changes in Man.," Surg. Gynecol. Obstetr.

[52] Hodgson, V. R., Thomas, L. M., and Prasad, P., 1970, "Testing the Validity and Limitations of the Severity Index," p. 700901.
[53] Rush, G. A., Prabhu, R., Rush, G. A., Williams, L. N., and Horstemeyer, M. F., 2017, "Modified Drop Tower Impact Tests for American Football Helmets," J Vis Exp, (120), p. 53929.
[54] "Standards," NOCSAE.
[55] National Operating Committee on Standards for Athletic Equipment (NOCSAE), 2020, "Standard Test Method and Equipment Used in Evaluating the Performance Characteristics of Headgear/Equipment - NOCSAE DOC ND 001-17m20."
[56] National Operating Committee on Standards for Athletic Equipment (NOCSAE), 2021, "Standard Test Method and Equipment Used in Evaluating the Performance Characteristics of Headgear/Equipment - NOCSAE DOC ND 081-18am21."
[57] National Operating Committee on Standards for Athletic Equipment (NOCSAE), 2021, "Standard Performance Specification for Newly Manufactured Football Helmets- NOCSAE DOC ND 002-17m21."
[58] Viano, D. C., Withnall, C., and Halstead, D., "Impact Performance of Modern Football Helmets," p. 15.
[59] Rowson, B., "Hockey STAR: A Methodology for Assessing the Biomechanical Performance of Hockey Helmets," p. 15.
[60] Bailey, A. M., "Development and Evaluation of a Test Method for Assessing the Performance of American Football Helmets," p. 14.
[61] Post, A., Karton, C., Hoshizaki, T. B., and Gilchrist, M. D., 2014, "Analysis of the Protective Capacity of Ice Hockey Helmets in a Concussion Injury Reconstruction," p. 9.
[62] Bina, A. J., Batt, G. S., and DesJardins, J. D., 2018, "A Review of Laboratory Methods and Results Used to Evaluate Protective Headgear in American Football," Proceedings of the Institution of Mechanical Engineers, Part P: Journal of Sports Engineering and Technology, **232**(4), pp. 360–368.
[63] Thorne, B., "Pendulum Based Impact Testing of Athletic Helmets Using the NOCSAE Headform," p. 113.
[64] Campolettano, E. T., and Rowson, S., 2021, "Relating On-Field Youth Football Head Impacts to Pneumatic Ram Laboratory Testing Procedures," Proceedings of the Institution of Mechanical Engineers, Part P: Journal of Sports Engineering and Technology, **235**(1), pp. 62–69.
[65] Elkin, B. S., Gabler, L. F., Panzer, M. B., and Siegmund, G. P., 2019, "Brain Tissue Strains Vary with Head Impact Location: A Possible Explanation for Increased Concussion Risk in Struck versus Striking Football Players," Clinical Biomechanics, **64**, pp. 49–57.
[66] Zanetti, K., Post, A., Karton, C., Kendall, M., Hoshizaki, T. B., and Gilchrist, M. D., 2013, "Identifying Injury Characteristics for Three Player Positions in American Football Using Physical and Finite Element Modeling Reconstructions," p. 11.
[67] Funk, J. R., McIntosh, A. S., Withnall, C., Wonnacott, M., and Jadischke, R., 2022, "Best Practices for Conducting Physical Reconstructions of Head Impacts in Sport," Ann Biomed Eng, **50**(11), pp. 1409–1422.
[68] Post, A., Karton, C., Hoshizaki, T. B., and Gilchrist, M. D., 2014, "Analysis of the Protective Capacity of Ice Hockey Helmets in a Concussion Injury Reconstruction," p. 9.
[69] Hering, A. M., and Derler, S., 2000, "MOTORCYCLE HELMET DROP TESTS USING A HYBRID III DUMMY," p. 15.

[70] Ghajari, M., Galvanetto, U., Iannucci, L., and Willinger, R., 2011, "Influence of the Body on the Response of the Helmeted Head during Impact," International Journal of Crashworthiness, **16**(3), pp. 285–295.
[71] Feist, F., and Klug, C., 2016, "A Numerical Study on the Influence of the Upper Body and Neck on Head Kinematics in Tangential Bicycle Helmet Impact," p. 23.
[72] Beusenberg, M., Schewchenko, N., and Newman, J. A., "Head, Neck, and Body Coupling in Reconstructions of Helmeted Head Impacts," p. 16.
[73] Yu, C., Wang, F., Wang, B., Li, G., and Li, F., 2020, "A Computational Biomechanics Human Body Model Coupling Finite Element and Multibody Segments for Assessment of Head/Brain Injuries in Car-To-Pedestrian Collisions," IJERPH, **17**(2), p. 492.
[74] Ghajari, M., Peldschus, S., Galvanetto, U., and Iannucci, L., 2013, "Effects of the Presence of the Body in Helmet Oblique Impacts," Accident Analysis & Prevention, **50**, pp. 263–271.
[75] Hynčík, L., and Bońkowski, T., 2019, "Helmet to Head Coupling by Multi-Body System," ACM, **13**(1).
[76] Dymek, M., "Design and Virtual Testing of American Football Helmets–A Review," p. 13.
[77] Decker, W., "Development and Multi-Scale Validation of a Finite Element Football Helmet Model," p. 13.
[78] 2018, "Hybrid III 50th Male Humanetics ATD."
[79] "SAE J211-1: Instrumentation for Impact Test," p. 25.
[80] Padgaonkar, A. J., Krieger, K. W., and King, A. I., 1975, "Measurement of Angular Acceleration of a Rigid Body Using Linear Accelerometers," Journal of Applied Mechanics, **42**(3), pp. 552–556.
[81] Crisco, J. J., Wilcox, B. J., Beckwith, J. G., Chu, J. J., Duhaime, A.-C., Rowson, S., Duma, S. M., Maerlender, A. C., McAllister, T. W., and Greenwald, R. M., 2011, "Head Impact Exposure in Collegiate Football Players," Journal of Biomechanics, **44**(15), pp. 2673–2678.
[82] Pellman, E. J., Viano, D. C., Tucker, A. M., and Casson, I. R., 2003, "Concussion in Professional Football: Location and Direction of Helmet Impacts—Part 2," Neurosurgery, **53**(6), pp. 1328–1341.
[83] Rowson, S., Duma, S. M., Beckwith, J. G., Chu, J. J., Greenwald, R. M., Crisco, J. J., Brolinson, P. G., Duhaime, A.-C., McAllister, T. W., and Maerlender, A. C., 2012, "Rotational Head Kinematics in Football Impacts: An Injury Risk Function for Concussion," Ann Biomed Eng, **40**(1), pp. 1–13.
[84] McIntosh, A. S., Patton, D. A., Fréchède, B., Pierré, P.-A., Ferry, E., and Barthels, T., 2014, "The Biomechanics of Concussion in Unhelmeted Football Players in Australia: A Case–Control Study," BMJ Open, **4**(5), p. e005078.
[85] Duma, S. M., Manoogian, S. J., Bussone, W. R., Brolinson, P. G., Goforth, M. W., Donnenwerth, J. J., Greenwald, R. M., Chu, J. J., and Crisco, J. J., 2005, "Analysis of Real-Time Head Accelerations in Collegiate Football Players:," Clinical Journal of Sport Medicine, **15**(1), pp. 3–8.
[86] Brooks, J. S., Redgrift, A., Champagne, A. A., and Dickey, J. P., 2021, "The Hammer and the Nail: Biomechanics of Striking and Struck Canadian University Football Players," Ann Biomed Eng, **49**(10), pp. 2875–2885.
[87] Fukuda, T., Koike, S., Miyakawa, S., Fujiya, H., and Yamamoto, Y., 2017, "Impact on the Head during Collisions between University American Football Players - Focusing on the Number of Head Impacts and Linear Head Acceleration -," JPFSM, **6**(4), pp. 241–249.

[88] Rowson, S., Brolinson, G., Goforth, M., Dietter, D., and Duma, S., 2009, "Linear and Angular Head Acceleration Measurements in Collegiate Football," Journal of Biomechanical Engineering, **131**(6), p. 061016.
[89] Beckwith, J. G., Greenwald, R. M., Chu, J. J., Crisco, J. J., Rowson, S., Duma, S. M., Broglio, S. P., Mcallister, T. W., Guskiewicz, K. M., Mihalik, J. P., Anderson, S., Schnebel, B., Brolinson, P. G., and Collins, M. W., 2013, "Head Impact Exposure Sustained by Football Players on Days of Diagnosed Concussion," Medicine & Science in Sports & Exercise, **45**(4), pp. 737–746.
[90] Broglio, S. P., Eckner, J. T., and Kutcher, J. S., 2012, "Field-Based Measures of Head Impacts in High School Football Athletes," Current Opinion in Pediatrics, **24**(6), pp. 702–708.
[91] Broglio, S. P., Sosnoff, J. J., Shin, S., He, X., Alcaraz, C., and Zimmerman, J., "Head Impacts During High School Football: A Biomechanical Assessment," p. 8.
[92] Broglio, S. P., Schnebel, B., Sosnoff, J. J., Shin, S., Feng, X., He, X., and Zimmerman, J., 2010, "Biomechanical Properties of Concussions in High School Football," Medicine & Science in Sports & Exercise, **42**(11), pp. 2064–2071.
[93] Brolinson, P. G., Manoogian, S., McNeely, D., Goforth, M., Greenwald, R., and Duma, S., 2006, "Analysis of Linear Head Accelerations from Collegiate Football Impacts:," Current Sports Medicine Reports, **5**(1), pp. 23–28.
[94] Yoganandan, N., Pintar, F. A., Moore, J., Rinaldi, J., Schlick, M., and Maiman, D. J., 2012, "Upper and Lower Neck Loads in Belted Human Surrogates in Frontal Impacts," Ann Adv Automot Med, **56**, pp. 125–136.
[95] Rhule, D., Rhule, H., and Donnelly, B., 2005, "The Process of Evaluation and Documentation of Crash Test Dummies for Part 572 of the Code of Federal Regulations."
[96] McIntosh, A. S., Kallieris, D., and Frechede, B., 2007, "Neck Injury Tolerance under Inertial Loads in Side Impacts," Accident Analysis & Prevention, **39**(2), pp. 326–333.
[97] Yoganandan, N., Pintar, F. A., Schlick, M., Moore, J., and Maiman, D. J., 2011, "Comparison of Head-Neck Responses in Frontal Impacts Using Restrained Human Surrogates," **55**, p. 11.
[98] Swartz, E. E., Floyd, R. T., and Cendoma, M., "Cervical Spine Functional Anatomy and the Biomechanics of Injury Due to Compressive Loading."
[99] Yoganandan, N., Pintar, F., Maiman, D., Phillippens, M., and Wismans, J., 2008, "Head Kinematics, Neck Loads, and Injuries in Side Impact Sled Tests," p. 15.

Appendix A: Surrogate Neck Repeatability

FRONTAL

Table A.1: Mean differences and ANOVA p-values with and without outliers for all head kinematics and kinetics for all datasets of frontal impacts on the linear rail. Differences in p-values are highlighted in green. Differences in statistical significance are highlighted in yellow.

		With Outliers		Without Outliers	
		Mean Difference	p-value	Mean Difference	p-value
Peak a (g)	ANOVA	-	$p < 0.001$*	-	$p < 0.001$*
	Neck 1-Neck 2	-6.75	$p < 0.001$†	-6.75	$p < 0.001$†
	Neck 1-Neck 3	-1.88	$p < 0.001$†	-1.88	$p < 0.001$†
	Neck 2-Neck 3	4.88	$p < 0.001$†	4.88	$p < 0.001$†
Peak α (rad/s^2)	ANOVA	-	$p < 0.001$*	-	$p < 0.001$*
	Neck 1-Neck 2	-100.69	$p = 0.746$†	-100.69	$p = 0.746$†
	Neck 1-Neck 3	237.55	$p < 0.001$†	249.89	$p < 0.001$†
	Neck 2-Neck 3	338.24	$p = 0.120$†	350.58	$p = 0.008$†
Peak ω (rad/s)	ANOVA	-	$p < 0.001$	-	$p < 0.001$
	Neck 1-Neck 2	2.81	$p < 0.001$	2.74	$p < 0.001$
	Neck 1-Neck 3	1.31	$p < 0.001$	1.16	$p < 0.001$
	Neck 2-Neck 3	-1.50	$p < 0.001$	-1.58	$p < 0.001$
Impact Force (N)	ANOVA	-	$p < 0.001$*	-	$p < 0.001$*
	Neck 1-Neck 2	-409.86	$p < 0.001$†	-409.86	$p < 0.001$†
	Neck 1-Neck 3	-131.14	$p < 0.001$†	-116.20	$p < 0.001$†
	Neck 2-Neck 3	278.72	$p < 0.001$†	293.66	$p < 0.001$†
Impact Moment (Nm)	ANOVA	-	$p < 0.001$*	-	$p < 0.001$*
	Neck 1-Neck 2	-5.06	$p < 0.001$†	-5.35	$p < 0.001$†
	Neck 1-Neck 3	-2.12	$p < 0.001$†	-1.53	$p < 0.001$†
	Neck 2-Neck 3	2.93	$p < 0.001$†	3.82	$p < 0.001$†
Peak Force (N)	ANOVA	-	$p < 0.001$*	-	$p < 0.001$*
	Neck 1-Neck 2	-452.96	$p < 0.001$†	-457.26	$p < 0.001$†
	Neck 1-Neck 3	-200.30	$p < 0.001$†	-180.04	$p < 0.001$†
	Neck 2-Neck 3	252.66	$p < 0.001$†	277.22	$p < 0.001$†
Peak Moment (Nm)	ANOVA	-	$p < 0.001$*	-	$p < 0.001$*
	Neck 1-Neck 2	-0.30	$p = 0.295$†	-0.27	$p = 0.671$†
	Neck 1-Neck 3	-2.01	$p < 0.001$†	-1.8	$p < 0.001$†
	Neck 2-Neck 3	-1.71	$p < 0.001$†	-1.55	$p < 0.001$†

a = linear acceleration, α = angular acceleration, ω = angular velocity
‡Cohen's f; *Welch's ANOVA; †Games-Howell

Table A.2: Mean differences, ANOVA p-values with outliers, and Cohen's d values for all impact metrics for all necks from frontal impacts on the linear rail.

		Mean Difference	p-value	Cohen's d
Peak a (g)	ANOVA	-	p<0.001*	2.21‡
	Hybrid III-Neck 1	-1.34	p<0.001†	2.18
	Hybrid III-Neck 2	-8.10	p<0.001†	4.50
	Hybrid III-Neck 3	-3.22	p<0.001†	4.03
Peak α (rad/s^2)	ANOVA	-	p<0.001*	9.29‡
	Hybrid III-Neck 1	1766.53	p<0.001†	15.70
	Hybrid III-Neck 2	1665.83	p<0.001†	5.44
	Hybrid III-Neck 3	2004.08	p<0.001†	18.55
Peak ω (rad/s)	ANOVA	-	p<0.001	3.46‡
	Hybrid III-Neck 1	7.00	p<0.001	25.63
	Hybrid III-Neck 2	9.80	p<0.001	25.48
	Hybrid III-Neck 3	8.30	p<0.001	18.03
Impact Force (N)	ANOVA	-	p<0.001*	7.02‡
	Hybrid III-Neck 1	1081.91	p<0.001†	18.90
	Hybrid III-Neck 2	672.05	p<0.001†	9.69
	Hybrid III-Neck 3	950.77	p<0.001†	12.55
Impact Moment (Nm)	ANOVA	-	p<0.001*	3.77‡
	Hybrid III-Neck 1	9.12	p<0.001†	21.24
	Hybrid III-Neck 2	4.06	p<0.001†	4.92
	Hybrid III-Neck 3	6.99	p<0.001†	6.82
Peak Force (N)	ANOVA	-	p<0.001*	11.50‡
	Hybrid III-Neck 1	1457.41	p<0.001†	59.12
	Hybrid III-Neck 2	1004.45	p<0.001†	17.27
	Hybrid III-Neck 3	1257.11	p<0.001†	28.47
Peak Moment (Nm)	ANOVA	-	p<0.001*	24.28‡
	Hybrid III-Neck 1	42.88	p<0.001†	51.54
	Hybrid III-Neck 2	42.58	p<0.001†	54.05
	Hybrid III-Neck 3	40.87	p<0.001†	42.94

a = linear acceleration, α = angular acceleration, ω = angular velocity
‡Cohen's f; *Welch's ANOVA; †Games-Howell

Table A.3: Normalized absolute difference between surrogate necks and Hybrid III neck for frontal impacts on the linear rail.

	Δ*a* (%)	Δα (%)	Δω (%)	ΔIm. F (%)	ΔIm. M (%)	ΔPk. F (%)	ΔPk. M (%)
Neck 1-Hybrid III	4.4	44.8	75.4	174.8	141.2	180.5	248.3
Neck 2-Hybrid III	26.5	62.8	71.1	108.6	62.9	124.4	146.6
Neck 3-Hybrid III	10.5	53.2	85.6	153.6	108.3	155.7	236.7
Average	13.8	53.6	77.4	145.6	104.1	153.5	243.9

a = linear acceleration, α = angular acceleration, ω = angular velocity, Im. F = impact force, Im. M = impact moment, Pk. F = peak force, Pk. M = peak moment

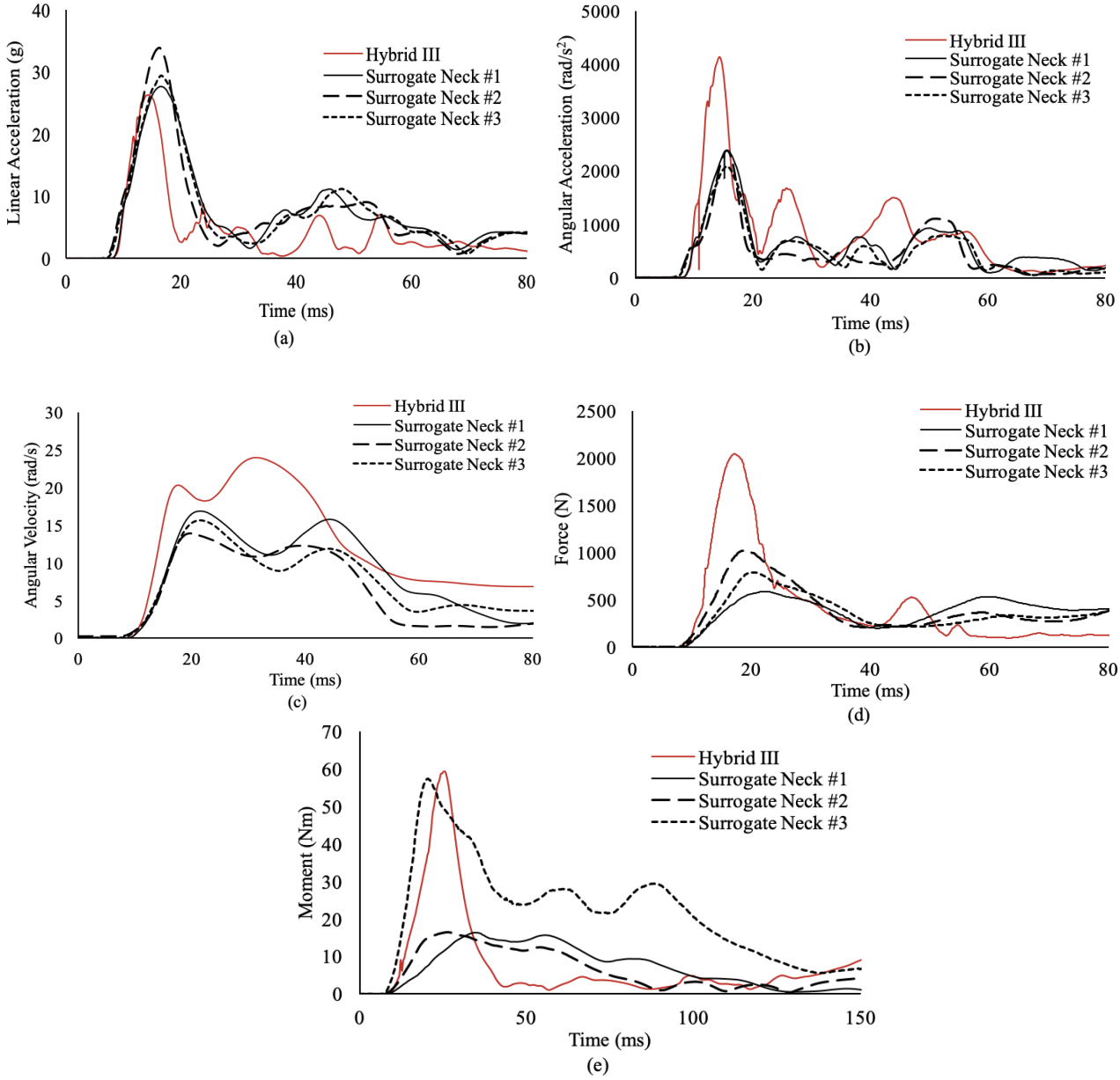

Figure A.1: Comparison of ensemble averages of all surrogate necks from frontal impacts for (a) linear acceleration, (b) angular acceleration, (c) angular velocity, (d) force, and (e) moment.

LATERAL

Table A.4: Mean differences and p-values with and without outliers for all head kinematics and kinetics for all datasets of lateral impacts on the linear rail. Differences in p-values are highlighted in green. Differences in statistical significance are highlighted in yellow.

		With Outliers		Without Outliers	
		Mean Difference	p-value	Mean Difference	p-value
Peak a (g)	ANOVA	-	$p < 0.001$*	-	$p < 0.001$*
	Neck 1-Neck 2	0.78	$p = 0.310$†	0.78	$p = 0.310$†
	Neck 1-Neck 3	-3.49	$p < 0.001$†	-3.49	$p < 0.001$†
	Neck 2-Neck 3	-4.27	$p < 0.001$†	-4.27	$p < 0.001$†
Peak α (rad/s^2)	ANOVA	-	$p < 0.001$*	-	$p < 0.001$*
	Neck 1-Neck 2	61.65	$p = 0.099$†	61.65	$p = 0.099$†
	Neck 1-Neck 3	-384.17	$p < 0.001$†	-384.17	$p < 0.001$†
	Neck 2-Neck 3	-445.82	$p < 0.001$†	-445.82	$p < 0.001$†
Peak ω (rad/s)	ANOVA	-	$p < 0.001$*	-	$p < 0.001$
	Neck 1-Neck 2	0.87	$p < 0.001$†	0.78	$p = 0.008$
	Neck 1-Neck 3	-2.04	$p < 0.001$†	-2.04	$p < 0.001$
	Neck 2-Neck 3	-2.91	$p < 0.001$†	-2.82	$p < 0.001$
Impact Force (N)	ANOVA	-	$p < 0.001$*	-	$p < 0.001$*
	Neck 1-Neck 2	-3.06	$p = 0.745$†	-3.06	$p = 0.745$†
	Neck 1-Neck 3	-28.11	$p < 0.001$†	-28.11	$p < 0.001$†
	Neck 2-Neck 3	-25.05	$p < 0.001$†	-25.05	$p < 0.001$†
Impact Moment (Nm)	ANOVA	-	$p < 0.001$*	-	$p < 0.001$*
	Neck 1-Neck 2	0.82	$p < 0.001$†	0.81	$p < 0.001$†
	Neck 1-Neck 3	1.85	$p < 0.001$†	1.95	$p < 0.001$†
	Neck 2-Neck 3	1.03	$p < 0.001$†	1.14	$p < 0.001$†
Peak Force (N)	ANOVA	-	$p < 0.001$	-	$p < 0.001$
	Neck 1-Neck 2	194.49	$p < 0.001$	202.79	$p < 0.001$
	Neck 1-Neck 3	122.53	$p < 0.001$	130.83	$p < 0.001$
	Neck 2-Neck 3	-71.97	$p < 0.001$	-71.97	$p < 0.001$
Peak Moment (Nm)	ANOVA	-	$p < 0.001$	-	$p < 0.001$
	Neck 1-Neck 2	3.13	$p < 0.001$	2.94	$p < 0.001$
	Neck 1-Neck 3	0.20	$p = 0.661$	0.20	$p = 0.608$
	Neck 2-Neck 3	-2.93	$p < 0.001$	-2.74	$p < 0.001$

a = linear acceleration, α = angular acceleration, ω = angular velocity
‡Cohen's f; *Welch's ANOVA; †Games-Howell

Table A.5: Mean differences, ANOVA p-values with outliers, and Cohen's d values for all impact metrics for all necks from lateral impacts on the linear rail.

		Mean Difference	p-value	Cohen's d
Peak a (g)	ANOVA	-	p<0.001*	1.29‡
	Hybrid III-Neck 1	-2.34	p<0.001†	1.42
	Hybrid III-Neck 2	-1.57	p=0.002†	1.25
	Hybrid III-Neck 3	-5.84	p<0.001†	2.96
Peak α (rad/s^2)	ANOVA	-	p<0.001*	1.61‡
	Hybrid III-Neck 1	469.16	p<0.001†	3.37
	Hybrid III-Neck 2	530.81	p<0.001†	3.60
	Hybrid III-Neck 3	84.98	p=0.508†	0.44
Peak ω (rad/s)	ANOVA	-	p<0.001*	2.57‡
	Hybrid III-Neck 1	-1.87	p<0.001†	2.31
	Hybrid III-Neck 2	-1.01	p<0.001†	1.18
	Hybrid III-Neck 3	-3.92	p<0.001†	4.55
Impact Force (N)	ANOVA	-	p<0.001*	2.27‡
	Hybrid III-Neck 1	78.37	p<0.001†	5.55
	Hybrid III-Neck 2	75.32	p<0.001†	5.92
	Hybrid III-Neck 3	50.26	p<0.001†	2.85
Impact Moment (Nm)	ANOVA	-	p<0.001*	0.86‡
	Hybrid III-Neck 1	-0.52	p=0.394†	0.51
	Hybrid III-Neck 2	0.30	p=0.772†	0.31
	Hybrid III-Neck 3	1.33	p=0.003†	1.24
Peak Force (N)	ANOVA	-	p<0.001	2.19‡
	Hybrid III-Neck 1	-136.69	p<0.001	4.56
	Hybrid III-Neck 2	57.80	p<0.001	2.05
	Hybrid III-Neck 3	-14.17	p=0.534	0.42
Peak Moment (Nm)	ANOVA	-	p<0.001	8.51‡
	Hybrid III-Neck 1	9.75	p<0.001	16.99
	Hybrid III-Neck 2	12.88	p<0.001	20.67
	Hybrid III-Neck 3	9.95	p<0.001	18.10

a = linear acceleration, α = angular acceleration, ω = angular velocity
‡Cohen's f; *Welch's ANOVA; †Games-Howell

Table A.6: Normalized absolute difference between surrogate necks and Hybrid III neck for lateral impacts on the linear rail.

	Δa (%)	$\Delta\alpha$ (%)	$\Delta\omega$ (%)	ΔIm. F (%)	ΔIm. M (%)	ΔPk. F (%)	ΔPk. M (%)
Neck 1-Hybrid III	2.7	3.9	5.5	8.3	27.9	8.3	2.1
Neck 2-Hybrid III	18.6	20.2	22.3	18.5	28.7	6.6	16.1
Neck 3-Hybrid III	83.7	77.4	85.1	85.0	290.1	85.8	77.4
Average	35.0	33.8	37.7	37.2	115.6	33.6	31.9

a = linear acceleration, α = angular acceleration, ω = angular velocity, Im. F = impact force, Im. M = impact moment, Pk. F = peak force, Pk. M = peak moment

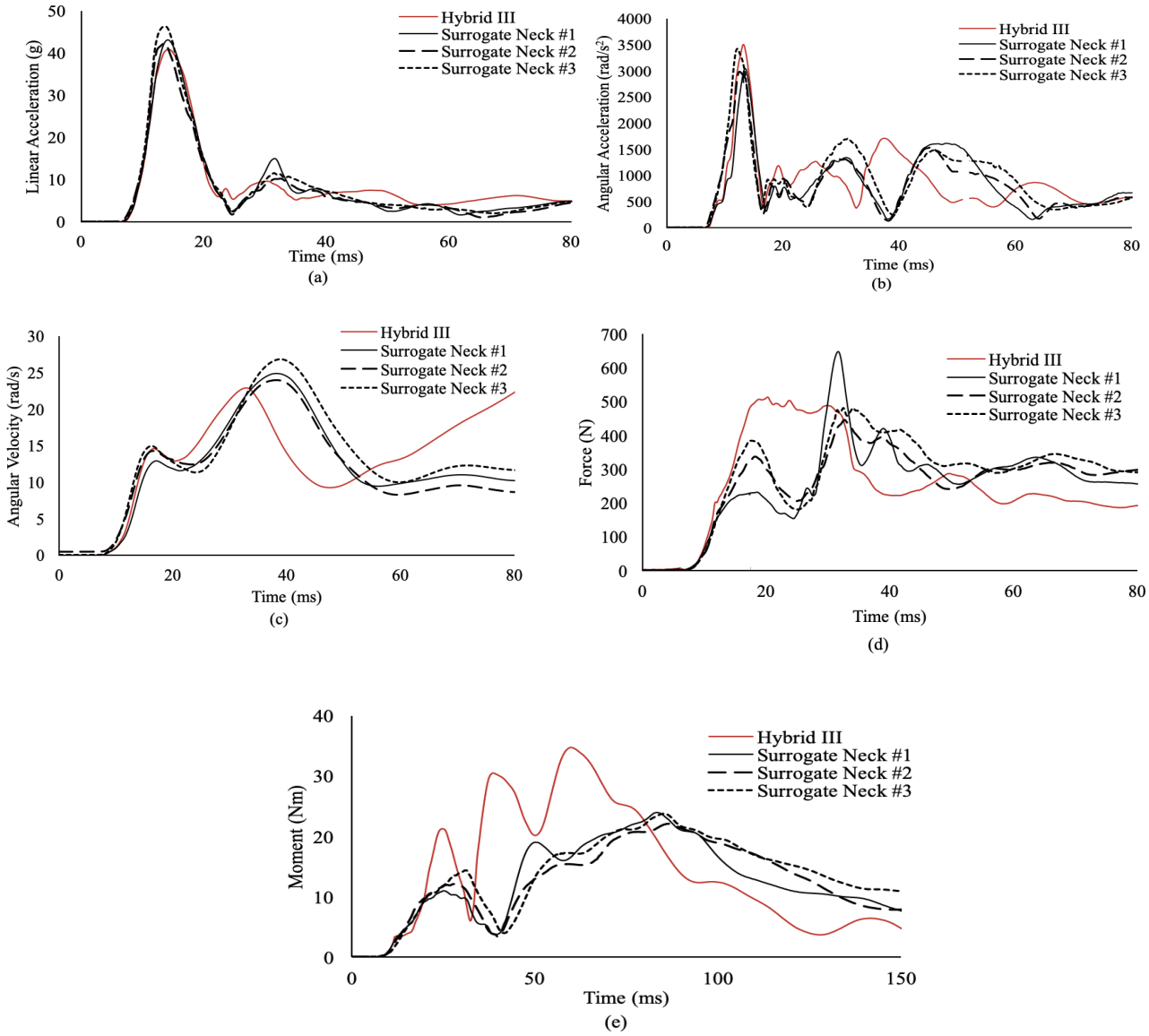

Figure A.2: Comparison of ensemble averages of all surrogate necks from lateral impacts for (a) linear acceleration, (b) angular acceleration, (c) angular velocity, (d) force, and (e) moment.

FRONT BOSS

Table A.7: Mean differences and p-values with and without outliers for all head kinematics and kinetics for all datasets of front boss impacts on the linear rail. Differences in p-values are highlighted in green. Differences in statistical significance are highlighted in yellow.

		With Outliers		Without Outliers	
		Mean Difference	p-value	Mean Difference	p-value
Peak a (g)	ANOVA	-	$p < 0.001$	-	$p < 0.001$*
	Neck 1-Neck 2	3.91	$p < 0.001$	3.36	$p < 0.001$†
	Neck 1-Neck 3	7.98	$p < 0.001$	8.22	$p < 0.001$†
	Neck 2-Neck 3	4.07	$p < 0.001$	4.86	$p < 0.001$†
Peak α (rad/s^2)	ANOVA	-	$p < 0.001$*	-	$p < 0.001$*
	Neck 1-Neck 2	-421.31	$p < 0.001$†	-434.96	$p < 0.001$†
	Neck 1-Neck 3	-145.25	$p = 0.004$†	-158.91	$p = 0.002$†
	Neck 2-Neck 3	276.05	$p < 0.001$†	276.05	$p < 0.001$†
Peak ω (rad/s)	ANOVA	-	$p < 0.001$*	-	$p < 0.001$*
	Neck 1-Neck 2	-1.96	$p < 0.001$†	-1.96	$p < 0.001$†
	Neck 1-Neck 3	-3.74	$p < 0.001$†	-3.74	$p < 0.001$†
	Neck 2-Neck 3	-1.78	$p < 0.001$†	-1.78	$p < 0.001$†
Impact Force (N)	ANOVA	-	$p < 0.001$*	-	$p < 0.001$*
	Neck 1-Neck 2	-310.08	$p < 0.001$†	-321.96	$p < 0.001$†
	Neck 1-Neck 3	-249.10	$p < 0.001$†	-250.15	$p < 0.001$†
	Neck 2-Neck 3	60.99	$p < 0.001$†	71.82	$p < 0.001$†
Impact Moment (Nm)	ANOVA	-	$p < 0.001$*	-	$p < 0.001$*
	Neck 1-Neck 2	-1.40	$p < 0.001$†	-1.41	$p < 0.001$†
	Neck 1-Neck 3	-1.23	$p < 0.001$†	-1.23	$p < 0.001$†
	Neck 2-Neck 3	0.17	$p = 0.458$†	0.19	$p = 0.388$†
Peak Force (N)	ANOVA	-	$p < 0.001$	-	$p < 0.001$
	Neck 1-Neck 2	-355.60	$p < 0.001$	-362.28	$p < 0.001$
	Neck 1-Neck 3	-238.96	$p < 0.001$	-241.63	$p < 0.001$
	Neck 2-Neck 3	116.64	$p < 0.001$	120.66	$p < 0.001$
Peak Moment (Nm)	ANOVA	-	$p < 0.001$*	-	$p < 0.001$*
	Neck 1-Neck 2	5.51	$p < 0.001$†	5.51	$p < 0.001$†
	Neck 1-Neck 3	5.95	$p < 0.001$†	5.95	$p < 0.001$†
	Neck 2-Neck 3	0.44	$p = 0.827$†	0.44	$p = 0.827$†

a = linear acceleration, α = angular acceleration, ω = angular velocity
‡Cohen's f; *Welch's ANOVA; †Games-Howell

Table A.8: Mean differences, ANOVA p-values with outliers, and Cohen's d values for all impact metrics for all necks from front boss impacts on the linear rail.

		Mean Difference	p-value	Cohen's d
Peak a (g)	ANOVA	-	p<0.001*	5.25‡
	Hybrid III-Neck 1	6.83	p<0.001†	8.50
	Hybrid III-Neck 2	10.74	p<0.001†	7.89
	Hybrid III-Neck 3	14.81	p<0.001†	10.06
Peak α (rad/s^2)	ANOVA	-	p<0.001*	2.15‡
	Hybrid III-Neck 1	692.68	p<0.001†	7.90
	Hybrid III-Neck 2	271.37	p<0.001†	2.07
	Hybrid III-Neck 3	547.42	p<0.001†	4.15
Peak ω (rad/s)	ANOVA	-	p<0.001*	1.88‡
	Hybrid III-Neck 1	0.06	p=0.997†	0.04
	Hybrid III-Neck 2	-1.91	p<0.001†	1.27
	Hybrid III-Neck 3	-3.69	p<0.001†	2.60
Impact Force (N)	ANOVA	-	p<0.001*	4.76‡
	Hybrid III-Neck 1	374.94	p<0.001†	11.44
	Hybrid III-Neck 2	64.85	p<0.001†	1.66
	Hybrid III-Neck 3	125.84	p<0.001†	3.40
Impact Moment (Nm)	ANOVA	-	p<0.001*	1.92‡
	Hybrid III-Neck 1	2.09	p<0.001†	4.74
	Hybrid III-Neck 2	0.69	p<0.001†	1.47
	Hybrid III-Neck 3	0.86	p<0.001†	1.51
Peak Force (N)	ANOVA	-	p<0.001	9.50‡
	Hybrid III-Neck 1	634.28	p<0.001	26.70
	Hybrid III-Neck 2	278.68	p<0.001	9.81
	Hybrid III-Neck 3	395.32	p<0.001	15.48
Peak Moment (Nm)	ANOVA	-	p<0.001*	4.13‡
	Hybrid III-Neck 1	8.30	p<0.001†	7.04
	Hybrid III-Neck 2	13.82	p<0.001†	10.20
	Hybrid III-Neck 3	14.26	p<0.001†	7.79

a = linear acceleration, α = angular acceleration, ω = angular velocity
‡Cohen's f; *Welch's ANOVA; †Games-Howell

Table A.9: Normalized absolute difference between surrogate necks and Hybrid III neck for front boss impacts on the linear rail.

	Δa (%)	$\Delta\alpha$ (%)	$\Delta\omega$ (%)	ΔIm. F (%)	ΔIm. M (%)	ΔPk. F (%)	ΔPk. M (%)
Neck 1-Hybrid III	21.6	0.3	20.6	86.0	70.5	111.7	42.5
Neck 2-Hybrid III	34.0	8.9	8.1	15.2	23.3	49.1	70.7
Neck 3-Hybrid III	46.8	17.1	16.3	28.8	27.2	69.6	73.0
Average	34.1	8.8	15.0	43.3	40.3	76.8	62.1

a = linear acceleration, α = angular acceleration, ω = angular velocity, Im. F = impact force, Im. M = impact moment, Pk. F = peak force, Pk. M = peak moment

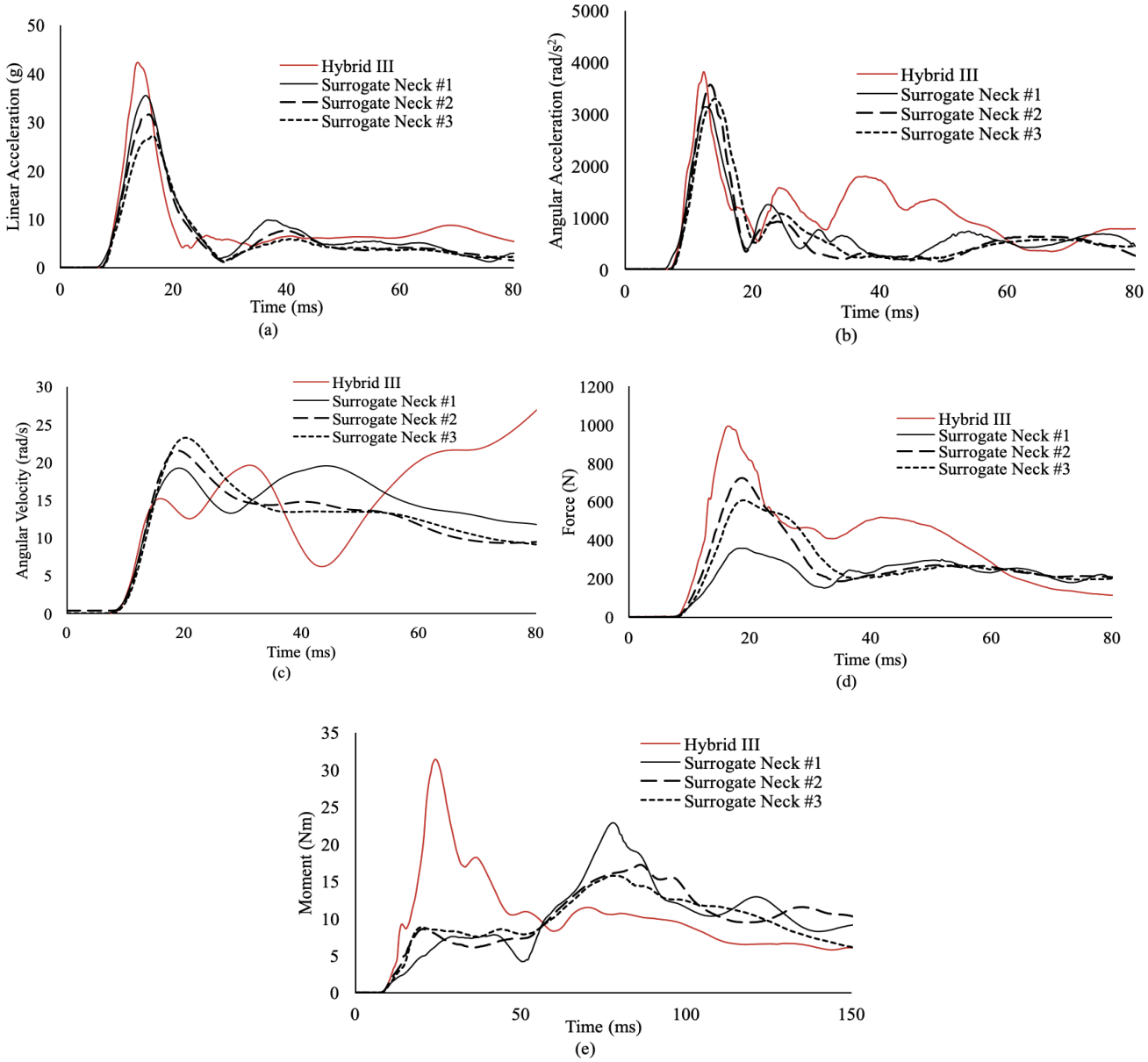

Figure A.3: Comparison of ensemble averages of all surrogate necks from front boss impacts for (a) linear acceleration, (b) angular acceleration, (c) angular velocity, (d) force, and (e) moment.